UNIVERSITY OF CALIFORNIA, SAN DIEGO

Impact Generated Pulses in Strongly Nonlinear Dissipative Metamaterial

A dissertation submitted in partial satisfaction of the
requirements for the degree of Doctor of Philosophy

in

Engineering Sciences (Mechanical Engineering)

by

Yichao Xu

Committee in charge:

Professor Vitali F. Nesterenko, Chair
Professor Yuri Bazilevs
Professor Renkun Chen
Professor Hyonny Kim
Professor Vlado Lubarda

2016

This dissertation of Yichao Xu is approved, and it is acceptable in quality and form for publication on microfilm and electronically:

_____

_____

_____

_____

_____

Chair

University of California, San Diego

2016

DEDICATION

This work is lovingly dedicated to my parents.

TABLE OF CONTENTS

LIST OF FIGURES

LIST OF TABLES

ACKNOWLEDGEMENTS

This work has been carried out at the University of California, San Diego, in the Department of Mechanical and Aerospace Engineering under the supervision of Professor Vitali F. Nesterenko. Firstly, I would like to acknowledge and extend my heartfelt gratitude to Professor Vitali F. Nesterenko for his support, encouragement and systematic guidance. During my whole PhD track, through the countless instructive and insightful discussions about my research, Vitali's deep knowledge, rigorous scholarship as well as his patience, deeply inspired me. It has been a pleasure and honor for me being able to learn from him. His enthusiasm and love for the science and academic research is contagious. I hope that someday I will be as enthusiastic, energetic and knowledgeable as him.

I am also grateful for the support from Professor Vlado Lubarda, and I still vividly remember my first thermodynamic class with him. I have been working as his Teaching Assistant for more than four years during my graduate school career, and in him I see all the characteristics of a great teacher. He is sincere, knowledgeable and joyful while teaching and really caring about his students.

I also would like to thank the members of my dissertation committee, Professor Yuri Bazilevs, Professor Renkun Chen, Professor Hyonny Kim and Professor Vlado Lubarda for their helpful comments and suggestions.

I am very thankful and will not forget the support from the Department of Mechanical and Aerospace Engineering that have granted me the ability to study and survive in La Jolla.

I would like to thank Siyin Wang and Dr. Po-Hsun Chiu for including me in many fruitful discussions on either the academic research or the graduate life here at UCSD.

I also wish to acknowledge the helpful advices of Nicholas Busan and Thomas W. Chalfant who provided to me a valuable support on the design and manufacturing of some experimental equipment used in my study.

I want to acknowledge a special debt to Linda Ellis who reviewed several drafts of chapters of my dissertation and provided me invaluable comments on my writing and grammar.

Many thanks go also to Brandy Carrasco for her kind help, generous support and the fun time we spent together.

Finally, I offer my sincere and earnest thankfulness to my parents for their selfless support, encouragement and tolerance during my long experience abroad. Without them all this would have not been possible.

Some of the Chapters are, in whole or part, published or submitted or being prepared for publication. Chapter 1 contains part of the materials that have been published in the paper *Philosophical Transactions of the Royal Society A*, **372**, art. 20130186, pp 1-14 by Yichao Xu and Vitali F. Nesterenko and in *Journal of Applied Physics*, **117**, art. 11430, pp. 1-12 by Yichao Xu and Vitali F. Nesterenko. The dissertation author was the primary investigator and author of above papers.

Part of Chapter 2 has been published in *Philosophical Transactions of the Royal Society A*, **372**, art. 20130186, pp 1-14 by Yichao Xu and Vitali F. Nesterenko. The dissertation author was the primary investigator and author of this paper.

Part of the Chapter 3 has been published in the *Journal of Applied Physics*, **117**, art. 11430, pp. 1-12 by Yichao Xu and Vitali F. Nesterenko. The dissertation author was the primary investigator and author of this paper.

Chapter 4 contains material currently being prepared for publication with the tentative title "Waves generated by impacts on dissipative sonic vacuum" by Yichao Xu and Vitali F. Nesterenko. The dissertation author was the primary investigator and author of this paper.

Chapter 5 contains material currently being prepared for publication with the tentative title "Waves generated by impacts on dissipative sonic vacuum" by Yichao Xu and Vitali F. Nesterenko. Section 2 in Chapter 5, is been in press in the *AIP Conference Proceedings,* with the title "Strongly nonlinear stress waves in dissipative metamaterials" authored by Yichao Xu and Vitali F. Nesterenko. The dissertation author was the primary investigator and author of this paper.

VITA

Education

2009 Bachelor of Engineering, Southeast University, Nanjing, China

2010 Master of Engineering, University of California, San Diego

2016 Doctor of Philosophy, University of California, San Diego

Honors and Awards

Ovshinsky Student Honorable Mention Award, January 2016

APS/SCCM travel award recipient, February 2015

Mechanical and Aerospace Engineering Department Distinguished Fellowship, UCSD (2015)

Presidential Award, Southeast University (2006-2007)

Research Experience

UCSD – University of California, San Diego (Winter 2011 to present)

Advisor: Professor Vitali F. Nesterenko

Teaching Experience

Teaching Assistant, Dept. of Mechanical and Aerospace Engineering, UCSD (2011-2016).

"*Mechanics I-III: Statics/Dynamics/Vibrations*" MAE 130A/B/C (undergraduate upper level)

"*Mechanical Engineering Lab: Material testing*" MAE 171A (undergraduate upper level)

"*Mechanics of Nanomaterial*" NANO 150 (undergraduate upper level)

"*Engineering Computation Using Matlab*" NANO 15 (undergraduate level)

Publications

Refereed Journal

Yichao Xu and Vitali F. Nesterenko. (2016) Waves generated by impacts on dissipative sonic vacuum (in preparation).

Yichao Xu and Vitali F. Nesterenko. (2015) Attenuation of short stress pulses in strongly nonlinear dissipative metamaterial, *Journal of Applied Physics*, **117**, art. 114303, pp. 1-12.

Yichao Xu and Vitali F. Nesterenko. (2014) Propagation of short stress pulses in discrete strongly nonlinear tunable metamaterials, *Philosophical Transactions of the Royal Society A*, **372**, art. 20130186, pp. 1-14.

Refereed Conference Proceedings

Vitali F. Nesterenko, Siyin Wang and Yichao Xu (2016) Strongly nonlinear waves generated by impact in weakly and strongly dissipative sonic vacuum, *XXIV International Congress on Theoretical and Applied Mechanics* (submitted).

Yichao Xu and Vitali F. Nesterenko. (2015) Strongly nonlinear stress waves in dissipative metamaterials, *AIP Conference Proceedings*, in press.

Conference Presentations

IUTAM – XXIV International Congress of Theoretical and Applied Mechanics, Montreal, Canada (August, 2016) *Strongly nonlinear waves generated by impact in weakly and strongly dissipative sonic vacuum*. Vitali F. Nesterenko, Siyin Wang and Yichao Xu.

APS – APS March Meeting, Baltimore, ML (March, 2016) *Impacts on dissipative sonic vacuum*. Yichao Xu and Vitali F. Nesterenko.

ASME – Applied Mechanics and Materials Conference, Seattle, WT (June 2015) *Experiments and modeling of short stress waves propagation in dissipative Metamaterials.* Yichao Xu and Vitali F. Nesterenko.

APS – Shock Compression of Condensed Matter, Tampa, FL (June, 2015) *Strongly nonlinear stress waves in dissipative Metamaterials*. Yichao Xu and Vitali F. Nesterenko.

DYMAT – Hopkinson Centenary Conference, Cambridge, UK (September, 2014) *Propagation of short stress pulses in discrete strongly nonlinear tunable metamaterials*. Yichao Xu and Vitali F. Nesterenko.

UCSD – Research Expo., San Diego, CA (April 2014) *Strongly nonlinear dynamic deformation of toroidal rubber elements and their application in dissipative metamaterials*. Yichao Xu (Advisor Vitali F. Nesterenko).

UCSD – Research Expo., San Diego, CA (April 2013) *Propagation of short pulses in discrete strongly nonlinear dissipative granular chains.* Yichao Xu (Advisor Vitali F. Nesterenko).

Professional Memberships

APS – Applied Physics Society, Topical Group of Shock Compression and Condensed Matter (SCCM).

ASME – The American Society of Mechanical Engineers.

ABSTRACT OF THE DISSERTATION

Impact Generated Pulses in Strongly Nonlinear Dissipative Metamaterials

by

Yichao Xu

Doctor of Philosophy in Engineering Sciences (Mechanical Engineering)

University of California, San Diego, 2016

Professor Vitali F. Nesterenko, Chair

This research is conducted to study the propagation of stress pulses with wave length comparable to the size of a unit cell in an one-dimensional chain composed of steel cylinders alternating with toroidal Nitrile rubber O-rings under different levels of precompression or without precompression force by using experiments, numerical simulations and theoretical analysis. Nitrile O-rings are making the system more tunable than the traditional metamaterials composed of steel spherical particles and this

metamaterial has better dissipative properties especially for high energy repeatable impact loading. This strongly nonlinear discrete metamaterial can be potentially useful for acoustic and shock/impact mitigating applications.

Investigated metamaterial is strongly nonlinear system with unique properties, where the strong nonlinearity arises from the Hertzian contact interaction or from more general double power interaction law under large compression. If the initial precompression is zero, such a system cannot support a classical sound waves and for this reason it is called a "sonic vacuum".

The static force-displacement relationship for toroidal O-ring is described by a combination of two power-law terms being in satisfactory agreement with experimental observations. This suggests unique tunability and it was demonstrated that the pulse speed indeed is strongly tunable with applied static stress. A strong attenuation of stress pulse was observed at a relatively short distances from the entrance. It is attributed to the viscous dissipation during dynamic deformation of strongly nonlinear viscoelastic O-rings, its dependence on the initial precompression was studied. Several models for this nonlinear metamaterial were numerically investigated to clarify the mechanism of the observed strongly nonlinear dissipation by representing O-rings in the frame of Kelvin-Voigt model: strongly nonlinear massless spring with parallel dashpot with nonlinear damping coefficient being function of initial precompression. Single bell shape waves of different durations and amplitudes were generated in the system without precompression by an impact of strikers with different masses. The viscous dissipation prevents the incoming pulse from splitting into trains of solitary waves typical for non-dissipative strongly nonlinear discrete systems. Very unusual behavior of strikers with

relatively large masses in comparison with mass of steel cylinders in the metamaterial was observed in experiments – strikers did not recoil after impact with investigated metamaterial. Results of numerical modeling were in agreement with speed of stress pulses, their attenuation and strikers behavior observed in experiments.

CHAPTER 1

INTRODUCTION

1.1 A New Type of Strongly Nonlinear Metamaterial

There is always a continued need and interest in investigating the complex dynamic behavior of heterogeneous metamaterials, and in such a broad and developing area, the experimental, theoretical and numerical investigations reveal new and interesting properties and phenomenon that may be useful to practical application. Their strongly nonlinear dynamic response is affected by the geometry and topology of metamaterial, geometry of the contacting elements which determine the strongly nonlinear contact forces between adjacent elements (e.g., the contact interaction between linear elastic spherical grains described by the Hertz law [1]). Extensive research has been done to investigate the transmission of waves in granular based low-dimensional metamaterials. One of the exciting discoveries was observation of the strongly nonlinear solitary waves which are qualitatively different from weakly nonlinear waves [2-13]. The nature of waves in these materials is also of general interest because they represent the dynamic response strongly affected by the mesostructure [14].

The term *metamaterial* is used to describe the types of materials which are not found in nature. They usually assembled from multiple elements with dramatically different properties. Metamaterials investigated in this research provide an example of media where linear and even weakly nonlinear descriptions of force-displacement relation fail. They are highly nonlinear materials with a qualitatively new behavior

according to some physically inner properties, such as nonlinearity of the force interaction law between neighboring particles, structural rearrangements under an applied load, and inevitable dissipation between particles. It is well known that metamaterials can reduce damage caused by impact or explosion due to their ability to absorb significant energy and transform high amplitude short pulse into a longer ramped pulse with significantly smaller amplitude [8,15]. For example, heterogeneous metamaterials could be good buffers for shock loads, and the thorough understanding of pulse propagation in these materials can lead to development of barriers for attenuation of high amplitude pulse valuable for example in medical applications, like disintegration of kidney stones [16]. The study of mechanics of strongly nonlinear metamaterials provide a natural step from linear, weakly nonlinear to strongly nonlinear wave dynamics which is of substantial interest for science and engineering.

The idealized one-dimensional metamaterial has a simple structure, and thus provide direct comparison between theoretical description and experimental observations. This idealized structure is able to provide an unexpected result which enlighten our understanding of the materials in real life. Although the practical applications of granular based metamaterials involve wave propagation in higher dimensional granular assemblies, the study of a one dimensional granular chain is a logical step forward to lay the groundwork for our understanding of strongly nonlinear wave dynamics in metamaterials with more complex mesostructure.

Most of the earlier studies about granular materials were focused on rather elastically rigid systems composed from steel beads. Sound waves can propagate in these systems only if they are precompressed and the sound speed increases relatively

fast with increase in applied precompression [8]. Tunability of these strongly nonlinear systems represents their important difference from the perfectly linear elastic materials, giving the possibility for qualitatively new phenomena, e,g., 'acoustic diode' effect [17]. It should be mentioned that elastic modulus of the system composed from spherical particles in case of zero precompression is zero – "sonic vacuum" [8]. Later linear chains composed of other metal [7] and polymer beads such as Teflon [10,11] or steel beads coated with soft polymer layer [11,12] were also investigated. It was demonstrated that strongly nonlinear solitary waves exist in these metamaterials even in case of polymer (or polymer coated) beads. The one dimensional chains composed of spherical particles made from stainless steel, brass, glass, Nylon, Teflon [2,6,7,9-12], steel particles coated by Parylene-C [11,12], and Homalite-100 circular cylinders [4], were shown to support solitary waves in experiments in agreement with numerical calculations and analytical analysis.

The Hertz type of contact interaction at the contact point is an acceptable approximation though with significantly larger elastic moduli than their static values for Teflon and Parylene-C [10-12]. New type of strongly nonlinear chains composed from toroidal elements, e.g., Teflon O-rings was proposed and investigated in [18-21]. The advantage of this system is based on its stronger nonlinearity than the Hertzian type nonlinearity of interaction force and potential for high energy absorption which is a basis for the current extensive applications of O-rings in heavy machinery [22].

This work focuses on the nonlinear behavior of the strongly nonlinear dissipative metamaterial composed of alternating stainless steel cylinders and toroidal Nitrile O-ring, which are much softer than Teflon O-rings. This results in a smaller speed of signal

propagation and with a better potential for higher energy absorption [23-25]. Nitrile is the most popular O-ring elastomer, with a wide application in the seal industry. It has high resistance to oil. But the circular shape of O-ring and the viscoelasticity of Nitrile O-ring strongly affect the dynamic behavior of these metamaterials and make the analysis of wave propagation more difficult. Compared with traditional metamaterials composed from elastic spherical particles, this system with toroidal Nitrile O-rings can be more tunable, because they exhibit highly nonlinear, double power law dependence of force on deformation in static loading [26-28]. Compressive solitary waves in the lattices with O-rings as strongly nonlinear elements placed between steel cylinders were investigated in [18-21].

It was demonstrated that the introduction of Nitrile O-rings in drop weight machine allowed to conduct "soft" drop weight test effectively reducing the high amplitude parasitic oscillations typical for standard drop weight tests which is especially important for the dynamic testing of low strength samples [29-31]. The behavior of O-rings under static deformation is well known [26-28] and the corresponding properties are used in the design of heavy machinery. But the dynamic behavior of these most common and important elements of machine design is not well investigated and understood. Only few papers were published where the complex dynamic behavior of Nitrile O-rings under low velocity impact (expected in some heavy machinery) were investigated [32-33].

Each part of this dissertation deals with the dynamic behavior of metamaterials composed of steel cylinders and Nitrile O-rings which could support the propagation of energy in the form of different types of waves. Wave propagation in these one-

dimensional nonlinear metamaterials presents dramatic dependence on the application of compressive forces, practically without the changes to the geometry of the system. Different types of waves in metamaterial may be classified by the degree of nonlinearity in the system.

The first part of this work (chapters 2-3) is focused on the weakly nonlinear dynamic behavior of the precompressed metamaterial composed of alternating steel cylinders and Nitrile O-rings. Chapter 2 presents results related to the properties of the metamaterial composed of Nitrile O-rings and steel cylinders, specifically the effect of the static compression force on the speed of the short-duration stress waves. The mechanism of strongly nonlinear dissipation in this metamaterial is discussed in chapter 3, and its corresponding detailed numerical analysis and simulations are described in Appendix A.

The second part of this work (chapters 4-5) presents results related to the strongly nonlinear dynamic behavior of this metamaterial under zero precompression force. This investigation is directed toward clarification of the effects of viscous dissipation accompanying dynamic deformation of Nitrile O-ring and its effects on the stress wave attenuation.

1.2 Weakly Nonlinear Behavior of Metamaterials

Unique properties of strongly nonlinear metamaterials are attributed to the completely nonlinear interaction forces between adjacent particles. For example, the force-displacement between neighboring steel cylinders in a chain composed of altering steel cylinders and Nitrile O-rings is described by a double power-law without linear

part [26-28].

Depending on the specific static loading and impact conditions the nature of a wave propagating in metamaterials varies. A low velocity impact may result in short duration small amplitude weakly nonlinear waves or even sound waves in a precompressed system. An impact on sonic vacuum may generate solitary wave (or their train) or a single bell shape pulse depending on the striker mass and dissipative properties of the system.

In this section of the dissertation, the weakly nonlinear dynamic response of the metamaterial composed of steel cylinders and O-rings is discussed. Consider a periodic chain of N steel cylinders separated by O-rings and statically compressed by static force F_0. Its unit cell contains a stainless steel cylinder and one O-ring having the initial size a (a=h+d, where h is the height of steel cylinders, and d is the cross section diameter of O-ring), as showed in Fig. 1.1. The initial static forces between neighboring cylinders are due to the nonlinear elastic deformation of O-rings caused by decreasing their height by x_0. The quasi-static elastic forces between cylinders (F_{el}) are represented by double power-law equation and depend on their geometric parameters, elastic properties and ratio (x_0/d) [26-28],

$$F_{el} = \pi D_m d E_0 [1.25 \left(\frac{x_0}{d}\right)^{3/2} + 50 \left(\frac{x_0}{d}\right)^{6}], \tag{1.1}$$

where D_m is a mean diameter, and E_0 is quasi-static Young's modulus of the Nitrile rubber. Thus, O-rings represent a strongly nonlinear elastic element with nonlinearity stronger than Hertzian law at relatively large x_0, when the second term in Eq. (1.1) dominates.

The deformation of soft O-ring in contact with rigid steel cylinder is confined to a very small region near the contact point. As a first approximation, one can consider that deformation of an O-ring during a dynamic process obeys a static Eq. (1.1), because its strong nonlinearity is due mainly to geometrical effects, with possible change in the elastic modulus E_0 accounting for strain-rate effects. The steel cylinders are practically not deformed, and it is assumed that the duration of the pulse is much longer than the characteristic time for wave propagation inside steel cylinders, which allows simplifying them as point masses. The mass of steel cylinder (m=3.065g) was about 50 times larger than O-rings (mass 0.0625g). Thus, to a first approximation, the O-rings can be considered as massless viscoelastic springs.

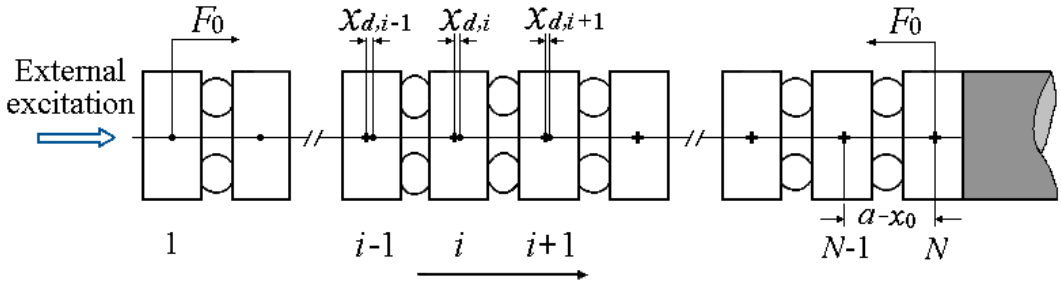

Figure 1.1: A schematic representation of a one–dimensional chain composed of steel cylinders and Nitrile O-rings with a large static compression force F_0 causing an initial displacement x_0 between neighboring centers of cylinders. And $x_{d,i}$ is the displacement of the i-th cylinder from its equilibrium position in the statically compressed chain and a is a distance between centers of neighboring cylinders without precompression. The right end of the chain is fixed and the external excitation is applied to the left end. The crosses show the initial equilibrium position of cylinder centers in a statically compressed chain. The black circles correspond to the position of the cylinder centers in the wave.

When the external excitation applied to the chain, the equations of cylinder

motion without considering dissipation is described as

$$\ddot{u}_i = A_0[(x_0 - x_{d,i} + x_{d,i-1})^{\frac{3}{2}} - (x_0 - x_{d,i+1} + x_{d,i})^{\frac{3}{2}}] + B_0\left[(x_0 - x_{d,i} + x_{d,i-1})^6 - (x_0 - x_{d,i+1} + x_{d,i})^6\right], \quad (1.2)$$

where $x_{d,i}$ $(2 \le i \le N-1)$ denote the displacement of the *i*-th cylinder from its static equilibrium positions in the initially compressed chain and the O-rings remain compressed during the wave propagation. *N* is the number of steel cylinder and *m* is a mass of steel cylinders. If the behavior of O-ring obeys static dependence of force on their height reduction then $A_0 = 1.25\pi D_{\mathrm{m}}\, E_0/md^{1/2}$, $B_0 = 50\pi D_{\mathrm{m}}\, E_0/md^5$ [26-28]. The dot denotes a derivative with respect to *t*.

Since the system is "strongly compressed" by static precompression force, the discrete anharmonic approximation (i.e. considering $|x_{d,i-1} - x_{d,i}| \ll x_0$) of Eq. (1.2) in a long wave limit ($L \gg a_1 = a - x_0$, where *L* is a characteristic spatial size of the wave perturbation) can be derived using the continuum variable replacement resulting in the Boussinesq's wave equation [8]

$$u_{tt} = {c_0}^2 u_{xx} + 2\gamma c_0 u_{xxxx} - \sigma u_x u_{xx}, \quad (1.3)$$

where the subscripts *t* or *x* denote the partial derivatives with respect to *t* or *x*.

For short pulses, the regularized Boussinesq wave equation is more suitable [8]

$$u_{tt} = {c_0}^2 u_{xx} + \frac{2\gamma}{c_0} u_{ttxx} - \sigma u_x u_{xx}, \quad (1.4)$$

where the corresponding parameters are:

$${c_0}^2 = \left(3A_0 {x_0}^{\frac{1}{2}}/2 + 6B_0 {x_0}^5\right) a_1^2,\ \gamma = c_0 a_1^2/24,$$

and $$\sigma = \left(3A_0 {x_0}^{-\frac{1}{2}}/4 + 30B_0 {x_0}^4\right) a_1^3.$$

All the higher-order terms are omitted, and the convective derivative in acceleration is ignored assuming that speed of the pulse is much larger than the particle velocity.

The long-wave sound speed c_0 in this precompressed metamaterial can be expressed as

$$c_0{}^2 = a_1^2 \left|\frac{3}{2}A_0(a_1\xi_0)^{1/2} + 6B_0(a_1\xi_0)^5\right|, \tag{1.5}$$

where ξ_0 is the static initial global strain in the metamaterial, defined as x_0/a_1. It is assumed that the dynamic behavior of the O-ring is similar to its static response.

It should be mentioned that sound speed c_0 in Eq. (1.5) is not the sound speed in the steel cylinder or Nitrile O-ring. It is a long-wave sound speed in the whole metamaterial. It can be significantly smaller than the bulk sound speed in the materials of the steel cylinder or O-ring and can be tuned by precompression. Apparently, the sound speed c_0 not only depends on the initial strain, but also can be affected by the elastic modulus of O-rings, their geometric parameters and the mass of steel cylinders.

The dispersion relations for linearized Eqs. (1.3) and (1.4) are, correspondingly,

$$\omega^2 = c_0{}^2k^2 - 2c_0\gamma k^4 \tag{1.6}$$

and

$$\omega^2 = c_0{}^2k^2\left(1 + \frac{2\gamma}{c_0}k^2\right)^{-1}. \tag{1.7}$$

Here k is the wave vector $(2\pi/\lambda)$, and λ is the wave length. Based on the above dispersion relations, the group velocity c_g of a pulse propagating through the chain is given by the following equation for the Boussinesq's and regularized Boussinesq's wave equations, correspondingly:

$$c_g \equiv \frac{d\omega}{dk} = c_0\left(1 - \frac{a_1^2k^2}{6}\right)\left(1 - \frac{a_1^2k^2}{12}\right)^{-1/2}, \tag{1.8}$$

$$c_g \equiv \frac{d\omega}{dk} = c_0 \left(1 + \frac{a^2k^2}{12}\right)^{-3/2}. \quad (1.9)$$

Equation (1.3) could be transformed into Korteweg-de Vries (KdV) equation under the same assumptions [8, 34]:

$$\xi_t + c_0\xi_x + \gamma\xi_{xxx} + \frac{\sigma}{2c_0}\xi\xi_x = 0,\ \xi = -u_x. \quad (1.10)$$

According to KdV equation [Eq. (1.10)], a stationary solitary wave and shock wave (if dissipation is included) can propagate in an initially compressed weakly nonlinear system [8, 35]. This Eq. (1.10) could be used to analyze the behavior of the investigated metamaterial for the weakly nonlinear case, when the force amplitude of the localized pulse is significantly smaller than the initial precompression force. A solitary wave speed *V*s for the solitary wave stationary solution to Eq. (1.10) is given by

$$V_s = c_0 + \frac{\sigma(\xi_m - \xi_0)}{6c_0}, \quad (1.11)$$

where ξ_m is the maximum strain in the solitary wave.

It is evident that the speed of this wave has a linear dependence on the maximum strain and in weakly nonlinear case ($\xi_m - \xi_0 \ll \xi_0$), V_s is close to the sound speed c_0. This equation can be used to estimate the role of nonlinearity on the value of the pulse speed for the short compression pulses observed in the experiments. It should be mentioned that only compression solitary waves are supported by nonlinear systems with elastic stiffening under compression.

1.3 Strongly Nonlinear Behavior of Metamaterial

One very interesting feature of the investigated metamaterial is that it behaves quite differently in the presence or absence of precompression. For a system composed

of elastic spherical particles, the zero precompression will lead to a complete absence of linear wave dynamic and zero velocity of sound in these media (characterized as "sonic vacuum" by Nesterenko [8]), and the corresponding wave equation supports a qualitatively new strongly nonlinear Nesterenko solitary wave [2,3].

This section is devoted to the analysis of the strongly nonlinear dynamic response of the metamaterial. Consider a one-dimensional metamaterial composed of N steel cylinders alternated by Nitrile O-rings in the state of sonic vacuum (zero precompression force) (Fig. 1.2). The Nitrile O-rings are considered as massless nonlinear springs based on the large ratio of mass of steel cylinder (with mass m = 3.065 g) to the mass of Nitrile O-ring (0.0625 g) and steel cylinders as point masses.

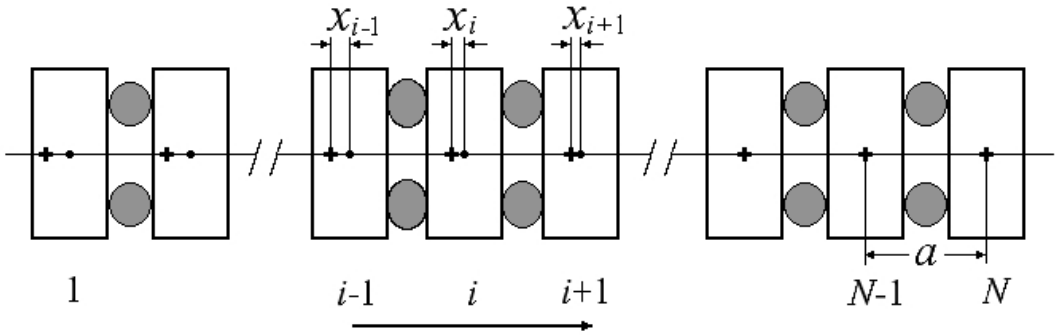

Figure 1.2: A schematic representation of wave propagation in one-dimensional metamaterial composed of N steel cylinders alternated by Nitrile O-rings without initial compression force. The value of a is the distance between centers of neighboring steel cylinders in the uncompressed chain in front of propagating wave and x_i is the displacement of the i-th steel cylinder from its position in the uncompressed chain caused by wave propagation. The crosses show the initial positions of cylinder centers in the uncompressed chain. The solid dots correspond to the position of the cylinder centers in the wave. At the bottom the arrow shows the direction of impulse propagation, the left part of the chain is unloaded but first and second cylinders are still in contact (depending on the impact conditions they can be separated) and the right part is not loaded yet.

The non-dissipative equations of steel cylinder motion in this strongly nonlinear system, using double power law similar to the quasi-static force between the contact particles (quasi-static law), is presented below:

$$\ddot{u}_i = A[(x_{i-1} - x_i)^{\frac{3}{2}} - (x_i - x_{i+1})^{\frac{3}{2}}] + B[(x_{i-1} - x_i)^6 - (x_i - x_{i+1})^6], \qquad (1.12)$$

where x_i denotes the displacement of the i-th cylinder from its equilibrium positions in the system without precompression, and $A = 1.25\pi D_{\mathrm{m}}\, E_{\mathrm{imp}}/md^{1/2}$, $B = 50\pi D_{\mathrm{m}}\, E_{\mathrm{imp}}/md^5$. The equivalent elastic modulus of Nitrile rubber O-ring in the propagating wave generated by impact (E_{imp}) on the uncompressed system may be different than its static value E_0 due to a possible frequency dependence of properties of the dynamically deformed O-ring. It also can be different than the effective elastic modulus E_{eff} used for the precompressed chain [23,24] and related to the elastic behavior of O-ring in the vicinity of statically precompressed state.

According to Ref. [23], the dependence of force on the deformed height of Nitrile O-ring obeys Hertzian behavior [first term on right in Eq. (1.12) with exponent 3/2] at relatively small strains (less than 0.3). The dynamic response of metamaterial in sonic vacuum under investigated impact conditions is within the "Hertzian zone". Then the speed of the solitary wave V_{s} in a non-dissipative metamaterial without precompression ("sonic vacuum") in the long wave approximation is determined by the amplitude of the dynamic force (F_{m}) [8]:

$$V_{\mathrm{s}} = \frac{2}{\sqrt{5}} a A^{1/3} m^{-1/6} F_{\mathrm{m}}^{1/6}, \qquad (1.13)$$

where a (=h+d, and h is the height of steel cylinder) is the distance between the centers of neighboring cylinders.

The above analysis neglects the dissipation effect, but due to the nature of Nitrile rubber O-ring, the inevitable presence of dissipation strongly influences the behavior of the metamaterial composed of steel cylinders and Nitrile O-rings. To include the dissipation, the viscous term should be added to Eq. (1.12). The presence of dissipation allows the propagation of another shock-like stress wave with speed different than the speed of the solitary wave. The speed of the stationary shock like stress wave with force F_{sh} in the equilibrium state has the following expression (independent on the type of dissipation):

$$V_{\mathrm{sh}} = aA^{1/3}m^{-1/6}F_{\mathrm{sh}}^{1/6}. \tag{1.14}$$

The above Eqs. (1.13) and (1.14) describe speeds of different type of strongly nonlinear waves in a non-compressed metamaterial ("sonic vacuum"). It is interesting that in case of $F_{\mathrm{m}} = F_{\mathrm{sh}}$, $V_{\mathrm{s}} < V_{\mathrm{sh}}$, so the metamaterial behavior in solitary wave is "softer" than in a shock wave with the same amplitude. Equations (1.13) and (1.14) are based on the assumption that the elastic properties of the O-ring and the Hertzian nonlinearity are the same during the whole cycle of O-rings dynamic deformation including loading and unloading.

If this metamaterial is statically precompressed then its static deformation is determined by the elastic modulus E_0, which can be significantly different from its values characterized for dynamic deformation E_{d} [23,24] and E_{imp}. Moreover, the last two elastic moduli even at the same level of overall global strains can be different due to the difference in the corresponding loading paths [33]: elastic modulus E_{d} is related

to small dynamic strains about statically precompressed state and E_{imp} is describing the elastic behavior of an initially uncompressed O-ring.

1.4 Viscous Dissipation in Metamaterial

Most of the previous publications related to the wave propagation in metamaterials neglect the dissipation effect, since the discrete nature of metamaterials and strong nonlinearity play the major role and the dissipation may be neglected when waves travel relatively short distances. The first example of strongly nonlinear metamaterials [2,3] was based on the Hertz law, a well-known non-dissipative quasi-static interaction law [1], acting between adjacent linear elastic spherical particles.

However, the presence of dissipation will strongly influence the dynamic response of the metamaterial. According to [8, 36-39], it is known that the presence of dissipation strongly influences the behavior of media within the shock front and determines the shape of shock profile and even qualitative outcome of the impact. For example, in a weakly nonlinear system described by Korteweg-de Vries (KdV) equation or in a strongly nonlinear system, two different shock profiles exist depending on the value of viscosity, i.e. oscillatory if viscosity is below the critical value and monotonic if it is above the critical value [35].

It is well known that rubber O-rings have dissipative properties which are also presumably nonlinear with respect to the strain and strain rate and exhibit hysteresis due to the viscoelastic nature of elastomers. Thus it is would be no surprise to see that the metamaterials composed of steel cylinders alternating with toroidal Nitrile O-rings show significant attenuation of compression pulses due to dissipation in the

experimental setting of this work (see also [18,19]) for both strongly nonlinear and weakly nonlinear regimes. Thus the viscous dissipation must be included to model a real system to account for pulse attenuation in this metamaterial.

Due to the complexity of the geometry of O-rings and the viscoelastic properties of Nitrile rubber, there is no clear and well established physical model to describe the energy dissipation during wave propagation through this discrete metamaterial composed of alternating steel cylinders and Nitrile O-rings. In this work, the commonly used Kelvin-Voigh model (KV) (Fig. 1.3) is applied to model the viscoelastic interaction force between neighboring particles in the system with precompression or in sonic vacuum condition.

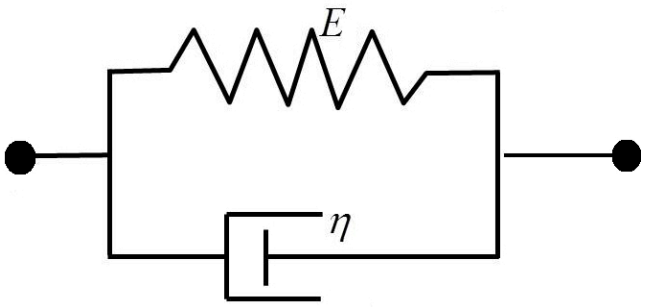

Figure 1.3: Viscoealstic Kelvin-Voigt mechanical model.

For a K-V model the additional dissipative term is represented by a dashpot connected in parallel to the spring. The viscous force is based on the relative velocity between particles. The total stress is given by:

$$\sigma(t) = E\varepsilon(t) + \eta\frac{d\varepsilon(t)}{dt}, \tag{1.15}$$

where E is elasticity modulus of spring and η is the viscosity of dashpot.

Chapter 1 contains part of the material that has been published in the paper *Philosophical Transactions of the Royal Society A*, 372, art. 20130186, pp 1-14 by Yichao Xu and Vitali F. Nesterenko and in *Journal of Applied Physics*, 117, art. 11430, pp. 1-12 by Yichao Xu and Vitali F. Nesterenko. The dissertation author was the primary investigator and author of above papers.

References

[1] H. Hertz, J. Reine Angew, Math. **92**, 156 (1881).

[2] V. F. Nesterenko, Prikl. Mekh. Tekh. Fiz. **24**, 136 (1983) [J. Appl. Mech. Tech. Phys. 24, 733 (1984)].

[3] A. N. Lazaridi, and V.F. Nesterenko, Prikl. Mekh. Tekh. Fiz. **26**, 115 (1985) [J. Appl. Mech. Tech. Phys. 26, 405 (1985)].

[4] A. Shukla, M. H. Sadd, Y. Xu, and Q.M. Tai, J. Mech. Phys. Solids **41**, 1795 (1993).

[5] E. J. Hinch and S. Saint-Jean, Proc. R. Soc. London A **455**, 3201 (1999).

[6] C. Coste, E. Falcon, and S. Fauve, Phys. Rev. E **56**, 6104 (1997).

[7] C. Coste and B. Gilles, Eur. Phys. J. B **7**, 155 (1999).

[8] V. F. Nesterenko, *Dynamics of Heterogeneous Materials* (Springer, NY, 2001), Chapter 1, pp. 1-53.

[9] S. Job, F. Melo, A. Sokolow, and S. Sen, Phys. Rev. Lett. **94**, 178002 (2005).

[10] C. Daraio, V. F. Nesterenko, E. B. Herbold and S. Jin, Phys, Rev, E **72**, 016603 (2005).

[11] C. Daraio, V. F. Nesterenko, E. B. Herbold and S. Jin, J. Phys. IV France **134**, 473 (2006).

[12] C. Daraio and V. F. Nesterenko, Phys. Rev. E **73**, 026612 (2006).

[13] S. Sen, J. Hong, J. Bang, E. Avalos, and R. Doney, Phys. Rep. **462**, 21(2008).

[14] M. S. Kushwaha, Int. J. Mod. Phys. B **10**, 977 (1996).

[15] V. F. Nesterenko, in *Proceedings of Granular Material-Based Technologies,* 2003, edited by S. Sen, M.L. Hunt, and A. J. Hurd (MRS, Pittsburgh, PA, 2003), pp. MM4.3.1- 4.3.12.

[16] M. Thiel, Clin. Orthop. Relat. Res. **387**, 18 (2001).

[17] V. F. Nesterenko, C. Daraio, E. B. Herbold and S. Jin, Phys. Rev. Lett. **95**, 158702 (2005).

[18] E. B. Herbold and V. F. Nesterenko, Appl. Phys. Lett. **90**, 261902 (2007).

[19] E. B. Herbold and V. F. Nesterenko*,* in *Shock Compression of Condensed Matter-2007*, edited by M. Elert, M. D. Furnish, R. Chau, N. Holmes, and J. Nguyen, AIP Conf. Proc. No. 955 (AIP, Melville, New York, 2007), pp. 231.

[20] I. L. D. Pinto, A. Rosas, A. H. Romero and K. Lindenberg, Phys. Rev. E **82**, 031308 (2010).

[21] A. Spadoni, C. Daraio, W. Hurst and M. Brown, Appl. Phys. Lett. **98**, 161901 (2011).

[22] P. K. Freakley and A. R. Payne, 1978 *Theory and Practice of Engineering with Rubber* (Applied Science, London, UK, 1978), pp. 146-165.

[23] Y. Xu and V. F. Nesterenko, Phil. Trans. R. Soc. A **372**, 20130186 (2014).

[24] Y. Xu and V. F. Nesterenko, J. Appl. Phys. **117**, 114303 (2015).

[25] Y. Xu and V. F. Nesterenko, APS Proceeding, in print.

[26] P. B. Lindley, J. Inter. Rubber Inst. **1**, 202(1967).

[27] P. B. Lindley, J. Strain Anal. **1**, 190 (1966).

[28] P. W. Allen, P. B. Lindley and A. R. Payne, *Use of rubber in engineering*. (Maclaren and Sons, London, UK, 1966), Chap. 1, pp. 1-23.

[29] J. Addiss, J. Cai, S. M. Walley, W. G. Proud, and V. F. Nesterenko, in *Shock Compression of Condensed Matter-2007*, edited by M. Elert, M. D. Furnish, R. Chau, N. Holmes, and J. Nguyen, AIP Conf. Proc. No. 955 (AIP, Melville, New York, 2007), pp. 773.

[30] J. Cai and V. F. Nesterenko, et al., Appl. Phys. Lett. **92**, 031903 (2008).

[31] E. B. Herbold, V. F. Nesterenko, D. J. Benson, et al., J. Appl. Phys. **104**, 103903(008).

[32] C. Lee and V. F. Nesterenko, J. Appl. Phys. **114**, 083509 (2013).

[33] C. Lee and V. F. Nesterenko, J. Appl. Phys. **116**, 083512 (2014).

[34] V. Karpman, *Nonlinear waves in dispersive Media.* (PergamonPress, New York, 1975), Chap. 1, pp. 1-65.

[35] E. B. Herbold and V. F. Nesterenko, Phys. Rev. E **75**, 021304 (2007).

[36] A. Rosas, A. H. Romero, V. F. Nesterenko and K. Lindenberg, Phys. Rev. Lett. **98**, 164301 (2007).

[37] A. Rosas, A. H. Romero, V. F. Nesterenko and K. Lindenberg, Phys. Rev. E **78**, 051303(2008).

[38] E. B. Herbold, V. F. Nesterenko. and C Daraio, *in Proceedings of the Conference of the American Physical Society Topical Group on Shock Compression of Condensed Matte 2005*, edited by M. D. Furnish, M. Elert, T.P. Russel, and C. T. White (AIP, Melville, New York, 2006), pp. 1523.

[39] E. B. Herbold.and V. F. Nesterenko, Phys. Procedia **3**, 465 (2010).

[40] A. Palermo and A. Marzani, ASME J. Vib. Acoust. **138**, 011022 (2016).

CHAPTER 2

TUNABILITY OF SHORT STRESS PULSES IN THE STRONGLY NONLINEAR METAMATERIAL

This chapter is devoted to study the propagation of short stress pulses with wavelength comparable to the size of a unit cell in a one-dimensional discrete metamaterial composed of steel discs alternating with toroidal Nitrile O-rings under different levels of precompression using experiments, numerical simulations and theoretical analysis. This strongly nonlinear metamaterial is more tunable than granular chains composed of linear elastic spherical particles and has better potential for attenuation of dynamic loads. Based on the experimental data the elastic modulus of Nitrile O-rings in quasi-static and dynamic loading are found. Numerical results will be provided and compared with experimental data to help identifying the mechanism of strong tunability and attenuation. It is demonstrated that the double power-law system allows a dramatic change of pulse speed with a moderate force.

In this chapter, I will focus on the following aspects of behavior of the periodic discrete metamaterial composed of steel cylinders and O-rings: (a) their ability to support propagation of short pulses with wavelength comparable to the cell size of the metamaterial, (b) relevance of strongly nonlinear static force–displacement relations to the dynamic behavior of O-rings, and (c) tunability of metamaterial pulse speed caused by compressive force.

2.1 Experimental Procedure and Results

One-dimensional metamaterial was assembled filling a polymethyl methacrylate (PMMA) hollow cylinder with chains composed of 18 Nitrile O-rings (N70-008, supplied by O-ring West) and 19 stainless steel cylinders (AISI 314). O-rings in experiments had initial cross section diameter d=1.78 mm, mean diameter D_m=6.22 mm and the mass m_0=0.0625 g. They were placed between steel cylinders with a height h=5.0 mm, diameter 10.0 mm and mass m=3.065 g, respectively.

The behavior of the O-rings under static deformation was investigated by loading the one-dimensional chain using a weight attached to the top (Fig. 2.1). For measurements of displacements caused by smaller forces (3.13 N and 8.16 N), four cylinders and three O-rings were used to minimize the influence of gravitational force due to weight of steel cylinders and O-rings.

Two slight slots were made in the PMMA tube to provide air escape from the spaces between cylinders during deformation. Measurements of displacements of top cylinder was performed 4 min later after load application when their final displacements were reached. The level of force induced by the top mass was significantly larger than mass of the steel cylinders thus we neglected the difference of forces between various cylinders cause by their weights.

Figure 2.2 presents the results of measurements of relative displacements x_0 at different static compression forces compared with the theoretical value obtained using Eq. (1.1). Owing to the viscoelastic behavior, the saturation of the deformation of O-rings after about 4 min following the application of load is observed. The measurements were repeated four times for each static load in the range 3.1–193.0 N, and the average values of the multiple measurements are shown in Fig. 2.2 with standard deviation in

the range of 2–4% for loads 70.3–193.0 N and 5–9% for smaller static loads 3.1–52.2 N.

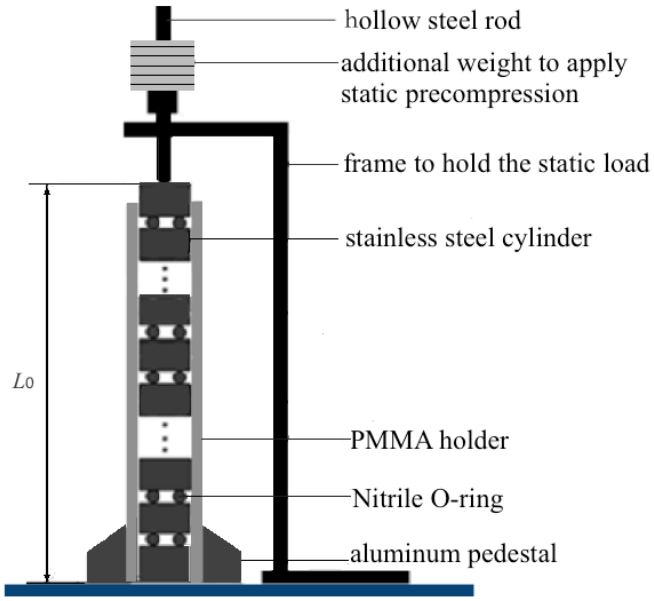

Figure 2.1: Experimental setup with O-rings placed between 19 stainless steel cylinders to test static force-displacement relation under applied static load.

A very good fit between experimental and calculated data using a double power law with corresponding exponents 3/2 and 6 [Eq. (1.1)] and elastic modulus E_0=7.6 MPa (which is close to the value 9 MPa reported for Nitrile [1]) was obtained for the investigated range of forces. This is in agreement with experimental and theoretical data for O-rings made from different materials up to x_0/d=0.5 [2]. It is important that the functional dependence of the force on x_0/d is significantly different from the Hertzian behavior at x_0/d>0.3 (Fig. 2.2). Thus we may expect significant deviations in sound speed in this system calculated based on Hertzian law starting at strains about 0.25 where derivatives to two corresponding curves starts to deviate significantly.

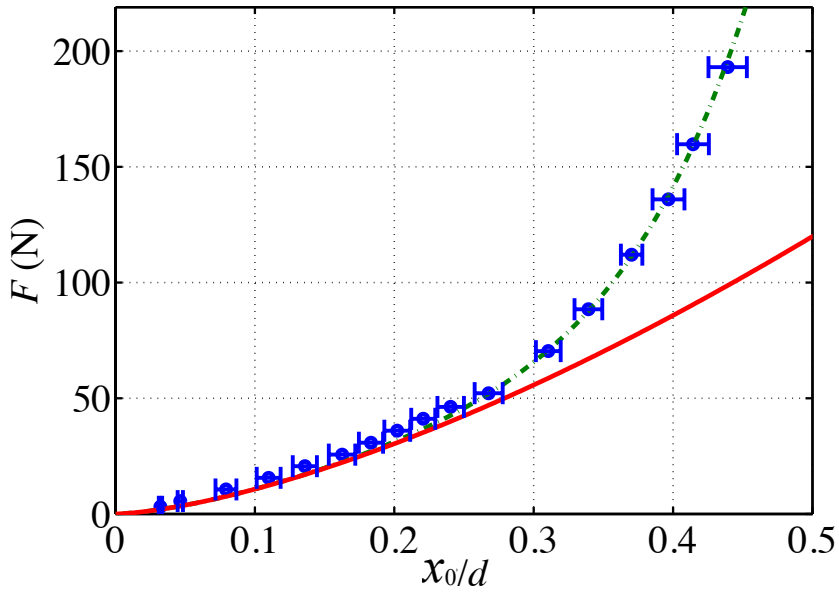

Figure 2.2: Experimental and theoretical values of global strain in O-ring as function of static forces. The dashed line represents the theoretical curve corresponding to Eq. (1.1) with E_0=7.6 MPa, and the solid line denotes the corresponding Hertzian part (n=3/2) of the force at E_0= 7.6 MPa. The experimental values are shown by blue circles.

Stress wave propagation in this metamaterial was investigated using a set-up similar to that shown in Fig. 2.1. Two piezo-sensors (supplied by Piezo Systems, Inc.; 6 mm side plates with 0.267 mm thickness, *RC* of the electrical circuit approx. 5.24 ms) were embedded in the fifth and the ninth cylinders (from the top) similar to the study of Daraio *et al*. [3]. Sensors were calibrated using conservation of linear momentum in separate impact experiments. Signals from these gauges were detected using a digital Tektronix oscilloscope (TDS 2014). Small-amplitude pulses (with positive and negative amplitudes being less than 10% of the precompression force), whose speed can be identified with the sound speed under various precompression forces, were generated by impacts of a steel sphere (0.455 g) dropped from the same height (350 mm) moving inside a hollow steel rod under various precompression conditions.

The shapes of these pulses (with the amplitude of the positive pulse in the range of 0.48 – 1.82 N) and their corresponding Fourier frequency spectra are presented in Fig. 2.3. The zero time in Fig. 2.3 is arbitral.

In experiments, the pulse speeds for positive and negative pulses were obtained by dividing the distance between the sensors $4(a\text{-}x_0)$ by the measured peak-to-peak time interval. The accuracy of speed measurement was within 10% or better (depending on the precompression force) and within this limit the speeds of positive and negative pulses were close, demonstrating weak dispersion. The speed data, duration of positive and negative pulses and their normalized widths were calculated (Table 2.1 and 2.2).

Accuracy of the measurements of amplitude of waves was in the range of 7% for large value of small preloading force (F_0 = 50 – 193 N) and 12% for small preload F_0 = 10 – 30 N. The measurement of speed has an accuracy within 12% mainly due to the uncertainty of the impact condition (the steel sphere striker impact velocity and impact location) and the measurement error of x_0.

The recorded pulses change their shape [e.g. ramping of leading fronts, total length of pulse increased from 500 to 700 μs in Fig. 2.3(a)], and this was mainly caused by dissipation. The spatial widths of positive and negative phases of pulses ($L_{exp,+}$, Table 2.1 and $L_{exp,–}$, Table 2.2) were calculated based on their speeds and durations as detected by the gauge in the fifth cylinder. It is evident that these pulses have width comparable to the cell size thus we may expect considerable dispersion effects on the pulse shape and speed especially at larger precompression.

The velocity of negative pulse is also increasing with precompression having values lower than values for positive pulse. This comparison indicates that system

experiences a “softer” behavior in negative pulse than for positive pulse despite that negative pulse runs not only on statically compressed system, but also on the *in situ* compressed material in the preceding positive pulse. It indicates that curvature in force-displacement curve has significant changes in the vicinity of static force. It is obvious that there is a large difference between the experimental data and predicted speed of sound based on Eq. (1.5) with static value of elastic modulus E_0=7.6 MPa.

One of the distinguishing features of the investigated highly nonlinear metamaterial is the strong tunability of pulse speed using initial precompression. Because the amplitude of the pulses was much smaller than the initial precompression, the speed of pulses was close to the sound speed in the continuum limit based on Eq. (1.11). Thus, we may use the equation for sound speed to estimate the theoretical speed of these pulses. The comparison of experimental results and theoretical values for the sound speed using Eq. (1.5), assuming that the dynamic behavior of the O-rings obeys the static dependence of force on x_0/d with E_0=7.6 MPa, is shown in Fig. 2.4.

From Fig. 2.4 we can see that the values of pulse speed are significantly larger than the predicted values based on the static elastic modulus E_0=7.6 MPa. It should be mentioned that the theoretical calculations do take into account the strong nonlinearity, resulting in the increase of sound speed, as is evident from the behavior of curve 1, but the calculated numerical values are too low. It is also evident that the behavior of the experimental data does not reflect even qualitatively the sound speed behavior based on Hertz's law (Fig. 2.4, curve 2). Rather, it demonstrates a more pronounced dependence of signal speed on initial precompression, characteristic of the behavior of sound speed for a double power-law interaction. It should be mentioned that the dynamic rigidity of

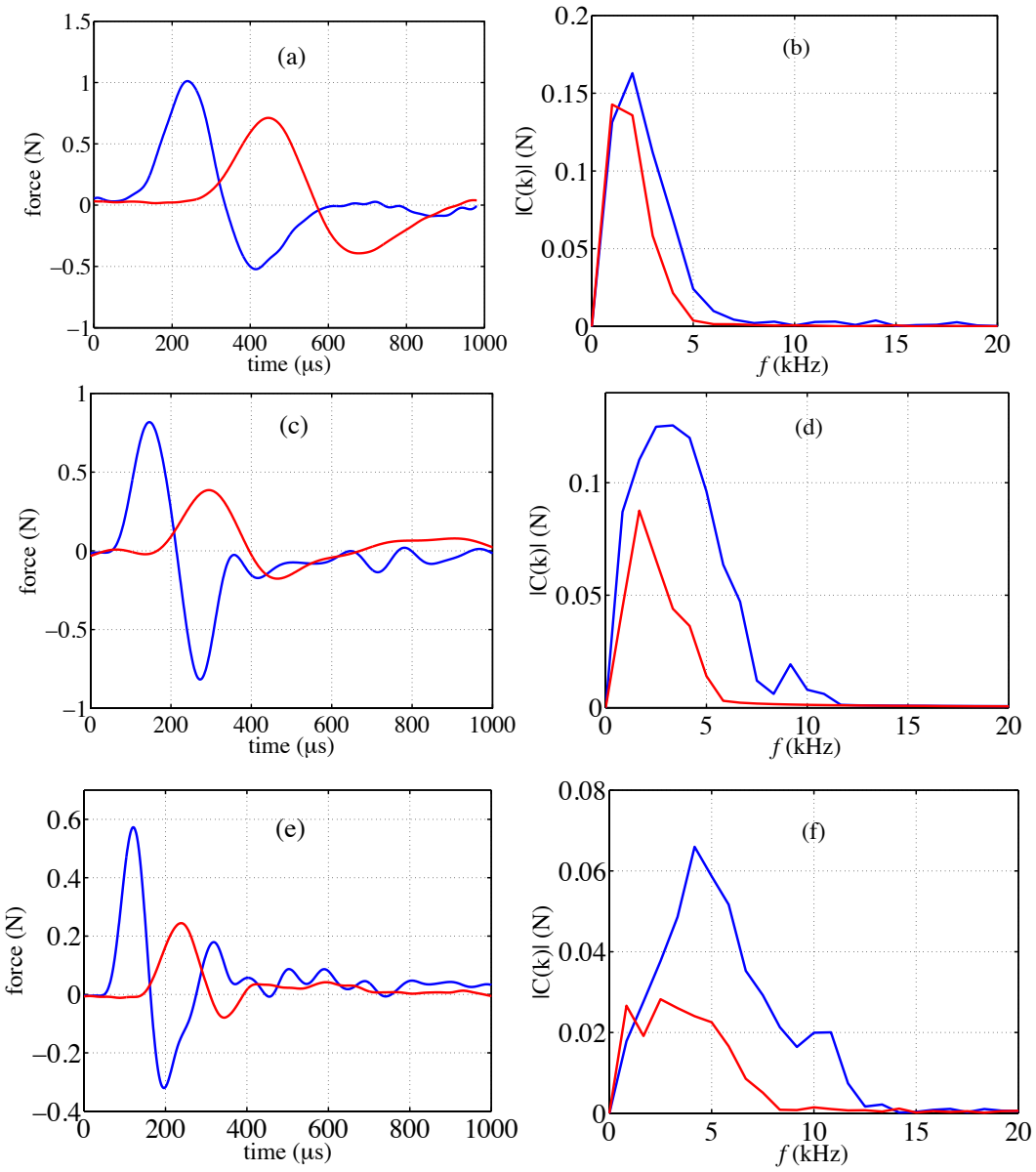

Figure 2.3: Shape of stress pulses and their Fourier spectra propagating in a chain of nitrile O-rings and stainless steel cylinders with various precompression forces generated by a steel striker (0.455 g) with an initial velocity of 2.62 m/s. Left column: average dynamic force in experiments recorded in sensors placed in the fifth and ninth cylinder, respectively. Right column: corresponding Fourier spectra. The static load of each case is (a), (b) F_0 = 10 N; (c), (d) F_0 = 30 N; (e), (f) F_0 = 50 N; (g), (h) F_0 = 74 N; (i), (j) F_0 = 106 N; (k), (l) F_0 = 193 N.

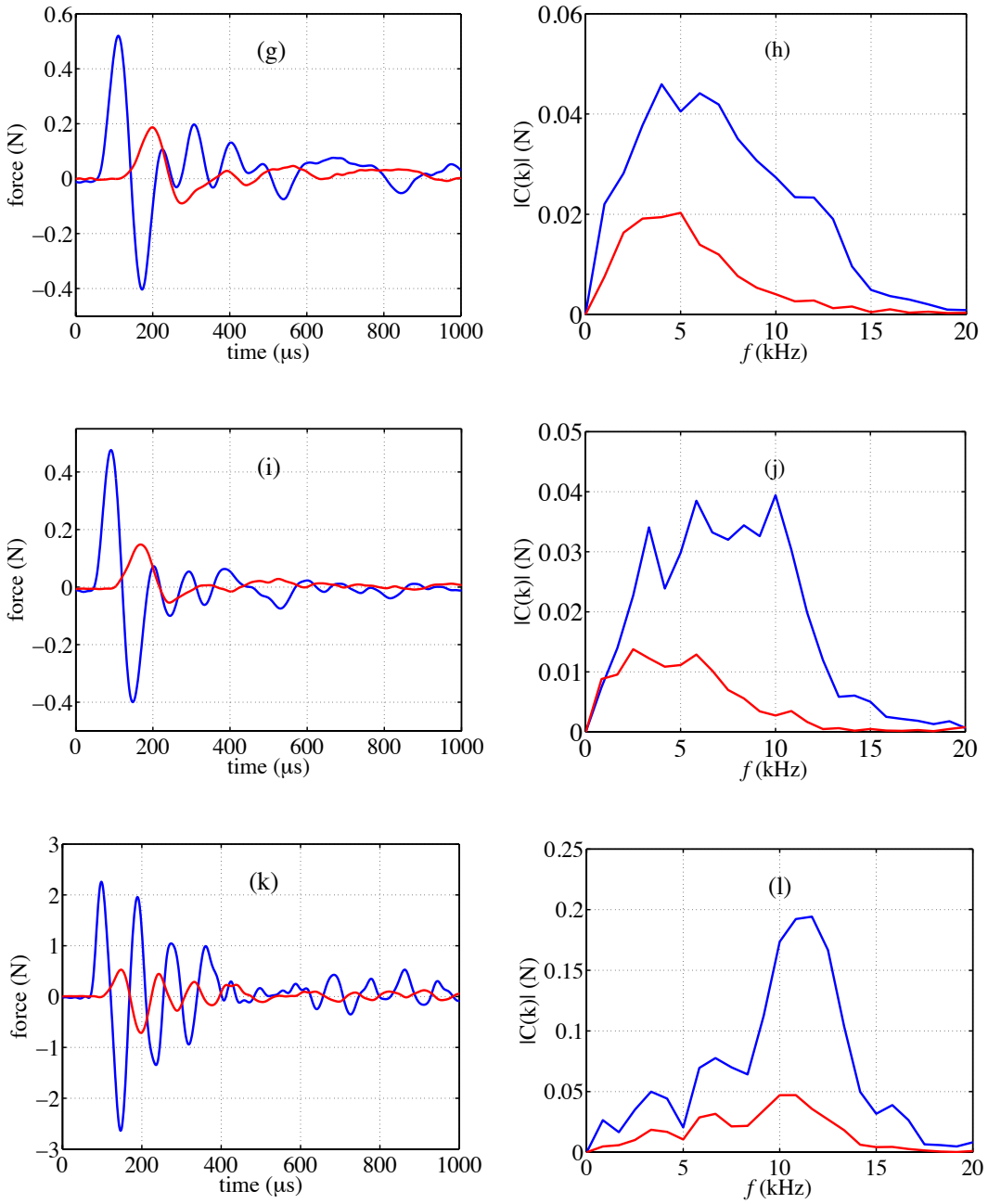

Figure 2.3: Shape of stress pulses and their Fourier spectra propagating in a chain of nitrile O-rings and stainless steel cylinders with various precompression forces generated by a steel striker (0.455 g) with an initial velocity of 2.62 m/s, continued.

Table 2.1: Speeds of positive pulses (V_+) and widths of positive pulses ($L_{exp,+}$) for different precompression forces detected in experiments corresponding to the signal recorded by gauges embedded in the fifth and the ninth cylinders. Normalized width of positive pulse using initial cell size $a_1=a-x_0$.

F_0 (N)	duration (μs)	V_+ (m/s)	$L_{exp,+}/(a-x_0)$
10	260	128±13	4.9
30	162	165±12	4.0
50	115	210±9	3.6
74	87	270±9	3.5
106	74	310±9	3.4
193	48	468±28	3.3

Table 2.2: Speeds of negative pulses (V_-)) and widths of negative pulses ($L_{exp,-}$) for different precompression forces detected in experiments corresponding to the signal recorded by gauges embedded in the fifth and the ninth cylinders. Normalized width of negative pulse using initial cell size $a_1=a-x_0$.

F_0 (N)	duration (μs)	$V-$ (m/s)	$L_{exp,-}/(a-x_0)$
10	270	101	4.0
30	144	135	2.7
50	113	172	2.7
74	74	230	2.5
106	65	254	2.4
193	49	444	3.2

this system may be significantly influenced by viscoelastic behavior, as is evident from the pulse attenuation especially in the case of a large precompression force [Fig. 2.3 (k)].

We can also see that a Hertzian-type interaction is responsible for the tuning of sound speed only for a low range of initial strain. The part of the interaction law with exponent equal to 6 makes metamaterials more tunable at larger strains (this transition of qualitative behavior of sound speed with precompression happens for values of $\xi_0>0.06$; Fig. 2.4).

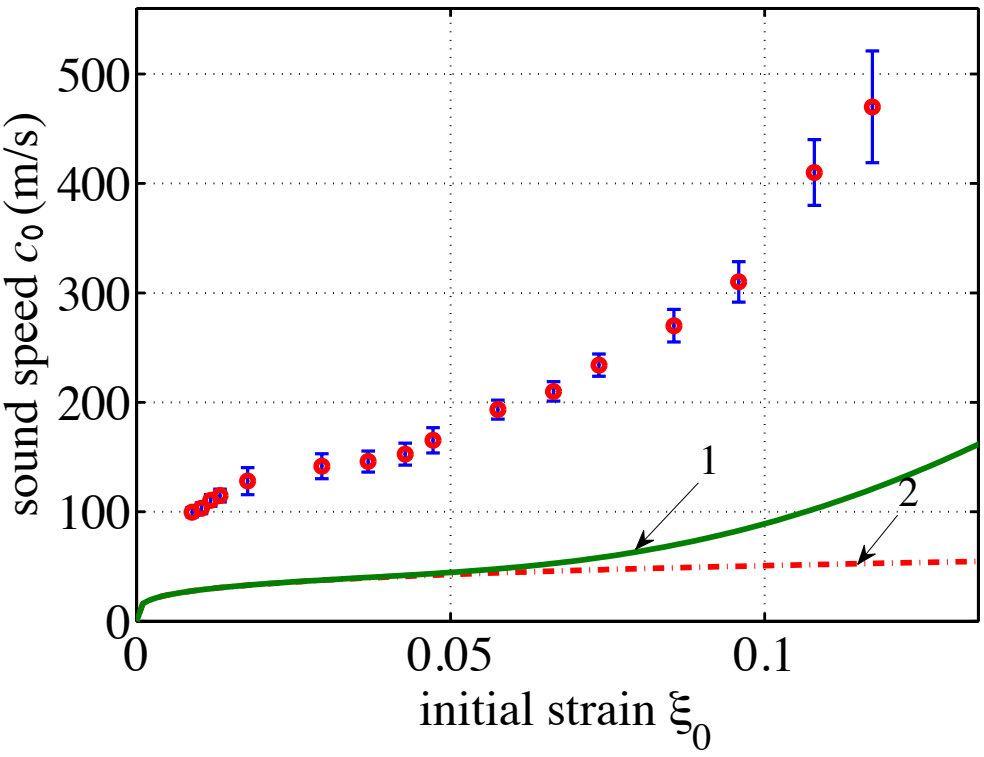

Figure 2.4: Experimental and theoretical dependence of sound speed on initial strain for double power-law system. The experimental values of pulse speed are shown by red circular dots. Curve 1 represents the long-wave sound speed [Eq. (1.5)] with E_0=7.6 MPa. Curve 2 (dashed) represents sound speeds corresponding to the Hertzian part of the interaction law with single exponents 3/2 at E_0=7.6 MPa.

Thus, we apparently need to take into account that O-rings behave differently under dynamic deformation by waves in comparison with static deformation.

To clarify the dynamic behavior of the metamaterial investigated, we proceed with the analysis using numerical calculations of the discrete system. Equations of particle motion for numerical model with different modulus of elasticity of O-ring under dynamic deformation will be introduced in section 2.2.

2.2 Numerical Calculations

Numerical calculations representing the experimental set-up shown in Fig. 2.1 were performed using MATLAB. The steel cylinders were treated as rigid bodies connected by massless nonlinear springs representing the O-rings, with deformation behavior following a strongly nonlinear double power law (dissipation was not included). To model the static precompression force, we introduced gravitational forces applied to the large top mass (hollow steel rod plus additional weight). It is assumed that there is a Hertzian-type interaction at the contact of the hollow steel rod (connected to the precompression mass) and the top cylinder in the chain. Gravitational force was also applied to all particles, simulating conditions in the experiment, though results of numerical modelling demonstrated that gravitational forces acting on particles did not affect the speed of the signals in the investigated range of precompression forces and pulse amplitudes. The pulses were excited by a steel striker and we assume Hertzian-type elastic interaction between the striker and the top steel cylinder in the chain.

In the numerical calculations, it is considered that the displacement x between neighboring cylinders relative to their positions in the undeformed chain is equal to the initial value x_0 plus an additional small change during dynamic deformation x_d. In the experimental conditions, the system is initially strongly compressed and the dynamic part x_d of the decrease in the height of the O-rings is much smaller than x_0. Thus, we can approximate the dynamic contribution to the force by a linear function of x_d, so that total force due to the deformation of an O-ring becomes

$$F_{el} = A_0 m {x_0}^{3/2} + B_0 m {x_0}^{6} + K x_d, \tag{2.1}$$

where $A_0 = 1.25\pi D_\mathrm{m}\, E_0/md^{1/2}$, $B_0 = 50\pi D_\mathrm{m}\, E_0/md^5$, which are related to the initial deformation or initial static force. It is observed in experiments that speed of the

signals is increasing with precompression (Fig. 2.3 and Tables 2.1 and 2.2). Thus the coefficient K should have a nonlinear dependence on the initial precompression. It should be mentioned that effective elastic moduli have been successfully used for the dynamic contact behavior of viscoelastic beads (PTFE [3], nylon [4]), or beads coated with a polymer layer [5]. It is assumed that this coefficient also can be found based on double power-law relationship (which is of geometrical origin), with effective elastic modulus E_{eff} reflecting dynamic deformation of viscoelastic O-rings. Thus I introduce the following dependence of this coefficient on static precompression, which is linearized version of double power law [Eq. (1.1)] in the vicinity of x_0, but with effective dynamic value of elastic modulus E_{eff},

$$K = 1.5(1.25\pi D_{\text{m}}\, E_{\text{eff}} d^{-1/2}) x_0^{1/2} + 6(50\pi D_{\text{m}} E_{\text{eff}} d^{-5}) x_0^{5}. \tag{2.2}$$

The coefficient K depends on both the dynamic modulus (E_{d}) of Nitrile O-rings and on the system's initial deformation x_0. As illustrated in Fig. 2.5, the dynamic force at a given x_{d} may deviate significantly from the static curve depending on the selected value of E_{d}. The value of dynamic modulus of O-rings E_{d} is a fitting parameter, which includes increased stiffness due to elastic and viscous behavior to match the speed of signals detected in experiments with the results of numerical calculations. To accomplish this match in numerical calculation we choose E_{d}=105 MPa.

A chain of 40 elements is used in numerical calculations. The second-order differential equations without considering dissipation for particles inside the chain were reduced to first order equations [6]:

$$\dot{x}_i = F_i(\bar{x}),\ \bar{x} = (x_1, x_2, \dots, x_{2N}),\quad i = 1, \dots, 2N; \tag{2.3}$$

$$F_i(\bar{x}) = x_{N+i},\quad i = 1, \dots, N-1; \tag{2.4a}$$

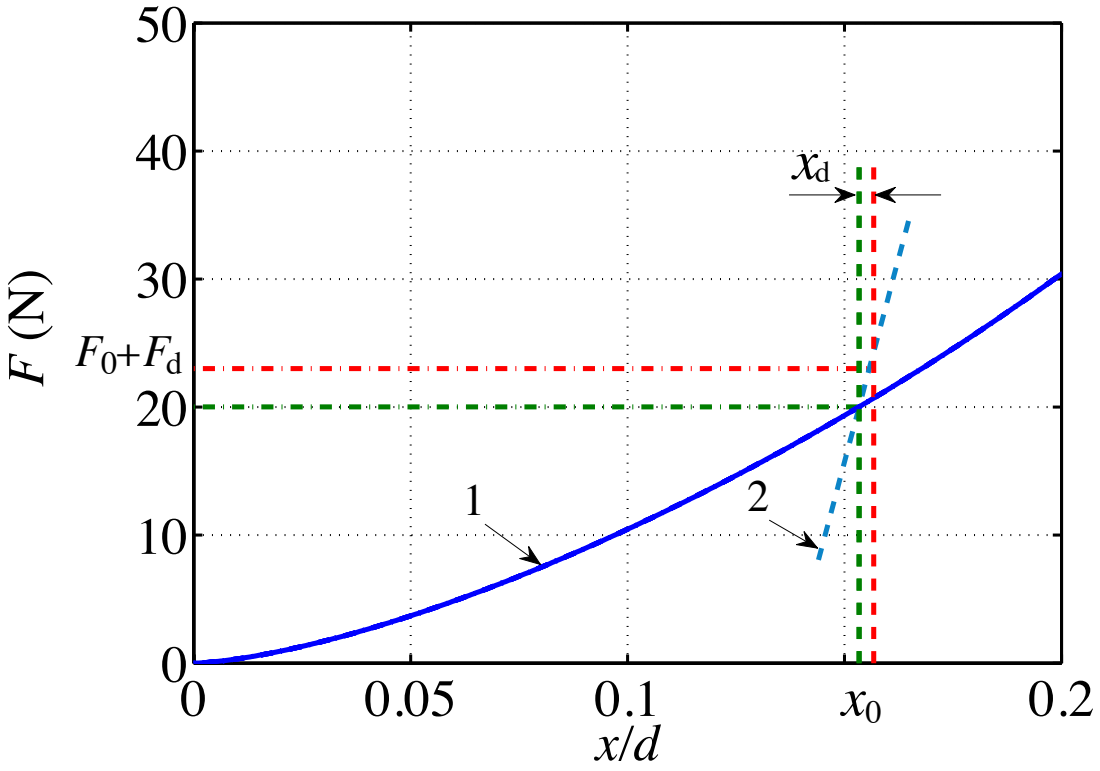

Figure 2.5: The difference in dynamic behavior of O-ring in comparison with static conditions. Curve 1 (blue) represents a relationship according to a double power law at E=7.6 MPa. The initial relative displacement of neighboring steel cylinders is x_0, and its small change during dynamic deformation is x_d. Curve 2 (dashed blue) corresponds to linear dynamic part in Eq. (2.1) with coefficient K represented by Eq. (2.2), which includes dependence on x_0.

$$F_i(\bar{x}) = \varphi_i(\bar{x}) - \psi_i(\bar{x}) + g,\ i = N+1, \dots, 2N-1; \quad (2.4b)$$

$$\varphi_i(\bar{x}) = 0,\ i = N+1, N+2; \quad (2.5a)$$

$$\varphi_i(\bar{x}) = \frac{C}{m}\delta_{i-2-N,i-N}^{\frac{3}{2}} H(\delta_{i-2-N,i-N}) + \frac{D}{m}\delta_{i-1-N,i-N}^{\frac{3}{2}} H(\delta_{i-1-N,i-N}), i = N+3; \quad (2.5b)$$

$$\varphi_i(\bar{x}) = [A_0\left(x_{0,i-1-N}\right)^{\frac{3}{2}} + B_0\left(x_{0,i-1-N}\right)^6 + \frac{K_{i-1-N}}{m}\left(\delta_{i-1-N,i-N} - x_{0,i-1-N}\right)]H(\delta_{i-1-N,i-N}),\ \ i = N+4, \dots, 2N-1; \quad (2.5c)$$

$$\psi_i(\bar{x}) = \frac{C}{M}\delta_{i-N,i+2-N}^{\frac{3}{2}} H\left(\delta_{i-N,i+2-N}\right),\ \ i = N+1; \quad (2.6a)$$

$$\psi_i(\bar{x}) = \frac{D}{m_{imp}}\delta_{i-N,i+1-N}^{\frac{3}{2}} H\left(\delta_{i-N,i+1-N}\right),\ i = N+2; \quad (2.6b)$$

$$\psi_i(\bar{x}) = [A_0\left(x_{0,i-N}\right)^{\frac{3}{2}} + B_0\left(x_{0,i-N}\right)^6 + \frac{K_{i-N}}{m}\left(\delta_{i-N,i+1-N} - x_{0,i-N}\right)]H\left(\delta_{i-N,i+1-N}\right),\ \ i = N+3, \dots, 2N-1; \quad (2.6c)$$

and $\delta_{i-2-N,i-N} = x_{i-2-N} - x_{i-N}$. (2.7)

Boundary conditions are:

$F_i(\bar{x}) = 0,\ i = N, 2N$ (Specify the 'wall'). (2.8)

Initial conditions corresponding to gravitationally loaded chain are:

$$x_N(t=0) = 0, x_{N-i}(t=0) = x_{N-i+1}(t=0) + x_{0,N-i},\ \ i = 1, \dots, N-2,$$

$$x_1(t=0) = x_3 + x_{0,1}; \quad (2.9a)$$

$$x_{N+1}(t=0) = 0,\ x_{N+2}(t=0) = 2.62,\ x_{N+i}(t=0) = 0, 2 < i \leq N, \quad (2.9b)$$

where

$$x_{0,1} = (\frac{Mg}{C})^{2/3},\ x_{0,2} = 0,\ x_{0,N} = 0, \quad (2.10a)$$

$$Mg + (i-3)mg = A_0(x_{0,i})^{3/2} + B_0(x_{0,i})^6,\ i = 3, \dots, N-1. \quad (2.10b)$$

And

$K_{i-1-N} = 1.5(1.25\pi D_m E_{\text{eff}} d^{-\frac{1}{2}}) x_{0,i-1-N}^{\frac{1}{2}} + 6(50\pi D_m E_{\text{eff}} d^{-5}) x_{0,i-1-N}^{5}$, $i = N + 4, \ldots, 2N$.

The value of x_i for i=1,…,N is a displacment of the i-th particle from equlibrium position (corresponding to the chain before it was deformed by gravitational forces, g=9.81 m/s^2 is the gravitational acceleration) assumed due to static loading and dynamically, while x_i for i=N+1, ...,2N is the the velocity of the i-th particle. The Heaviside function $H(\delta)$ ensure that interactions exis only when the grains are in contact (δ>0). The coefficients $C = \frac{2E_{\text{steel}}}{3(1-\nu^2)} R_{\text{rod}}^{1/2}$ and $D = \frac{2E_{\text{steel}}}{3(1-\nu^2)} R_{\text{striker}}^{1/2}$ represent nonlinear Hertzian type interaction between the precompressing mass (particle 1) and the top steel cylinder (particle 3) and between the striker (particle 2) and the top cylinder, where ν, E_{steel} and R_{striker} are the poison ratio, elastic modulus and radius of the steel sphere striker, respectively, and R_{rod} is the radius of the hollow steel rod. The precompressing weight and striker have mass M and m_{imp}, respectively.

It should be noticed that $x_{0,1}$ is the initial displacement of precompressing mass with respect to the first cylinder assuming gravitational loading, while $x_{0,2} = 0$ and $x_{0,i}$ (i=3,…,N-1) are the change of the initial height of the O-ring between the i-th and (i+1)-th cylinder inroduced by graviation. The values of initial displacements produced by gravitational loading are calculated by using Eq. (1.1) with the static modulus of O-ring E_0=7.6 MPa.

Results of numerical calculation modeling dynamic experiments are presented in Tables 2.3 and 2.4.

The corresponding pulses are shown in Fig. 2.6 for elastic modulus E_{eff}=105

MPa providing the best fit of the experimental data and the results of numerical calculations (Fig. 2.7). The zero time in numerical calculations corresponds to the moment of impact.

Table 2.3: Speeds of positive pulses (V_+) and normalized widths of positive pulses ($L_{num,+}$) for different precompression forces detected in numerical calculations corresponding to the dynamic forces on the fifth and the ninth cylinders. The initial cell size in the precompressed chain is $a_1=a-x_0$.

F_0 (N)	V_+ (m/s)	$L_{num,+}/(a-x_0)$
10	127	4.2
30	156	3.9
50	189	3.8
74	237	3.7
106	286	3.7
193	390	3.5

Table 2.4: Speeds of negative pulses (V_-) and normalized widths of negative pulses ($L_{num,-}$) for different precompression forces detected in numerical calculations corresponding to the dynamic forces on the fifth and the ninth cylinders. The initial cell size in the precompressed chain is $a_1=a-x_0$.

F_0 (N)	V_- (m/s)	$L_{num,-}/(a-x_0)$
10	120	2.7
30	133	1.9
50	169	1.9
74	203	2.0
106	253	2.2
193	330	2.3

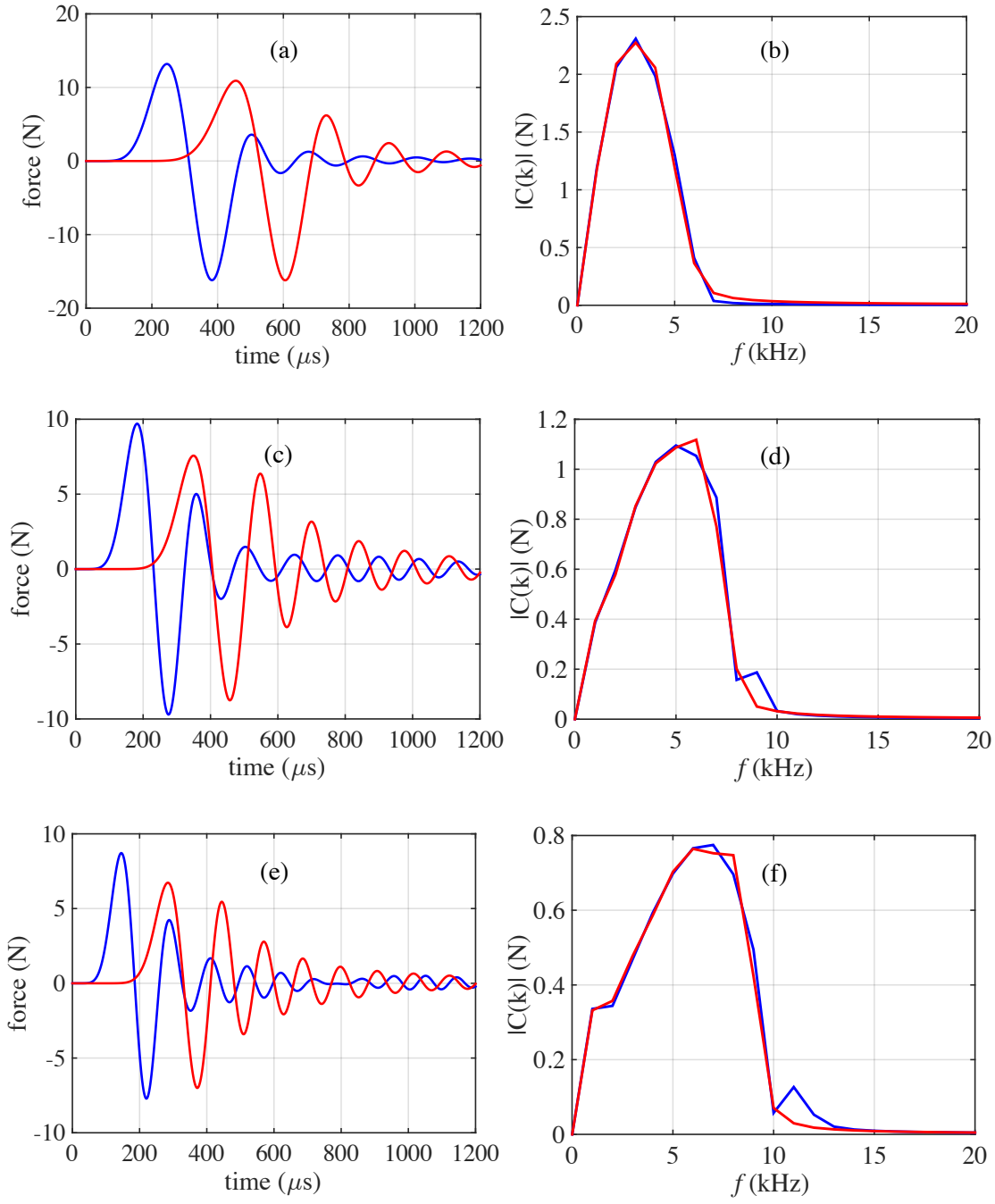

Figure 2.6: Stress pulses obtained in numerical calculations (using non-dissipative model and with E_{eff} = 105 MPa) and their corresponding Fourier spectra in a double power-law system under various preload conditions: (a), (b) F_0 = 10 N; (c), (d) F_0 = 30 N; (e), (f) F_0 = 50 N; (g), (h) F_0 = 74 N; (i), (j) F_0 = 106 N; (k), (l) F_0 = 193 N. The curve represents average dynamic force in the 5th (top curve) and 9th cylinder from the top. Left column: dynamic force in numerical calculation. Right column: corresponding Fourier spectra.

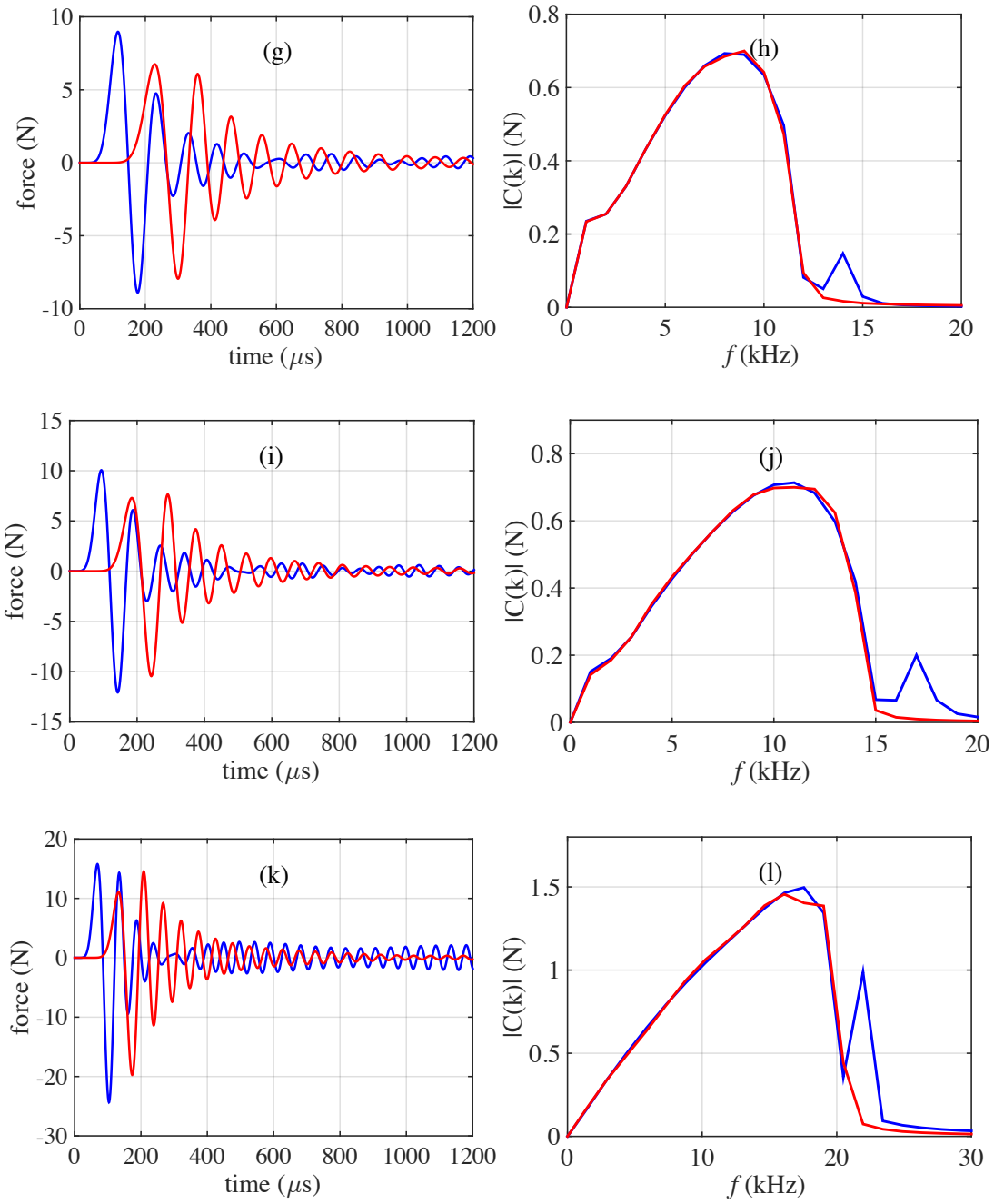

Figure 2.6: Stress pulses obtained in numerical calculations (using non-dissipative model and with E_{eff}=105MPa) and their corresponding Fourier spectra in a double power-law system under various preload conditions, continued.

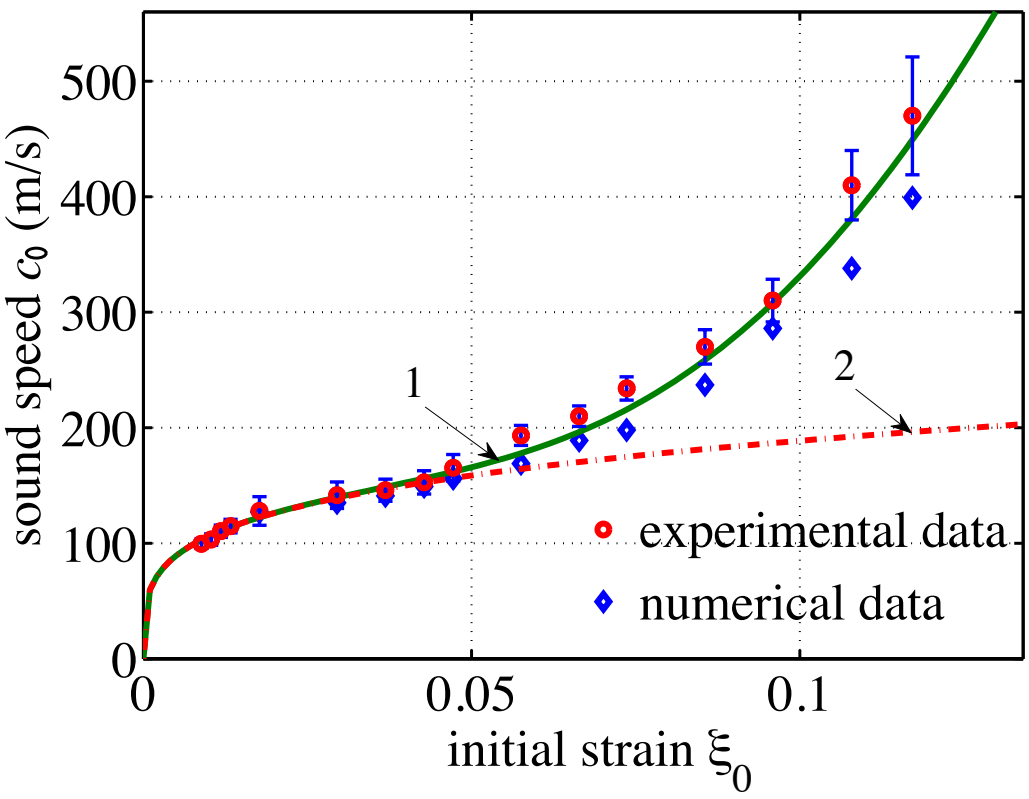

Figure 2.7: Experimental (circles) and numerical (diamonds) dependence of pulse speed on initial strain for investigated metamaterial. Curve 1 represents the long-wave sound speed [Eq. (1.5)] at E_{eff} = 105 MPa. Curve 2 represents sound speeds corresponding to the Hertzian part of the interaction law with single exponent 3/2 at E_{d} = 105 MPa.

The speeds of positive and negative pulses in the numerical calculations were close (the speeds of negative pulses were smaller by about 6–17% for small and large values of compression forces) demonstrating a weak dispersion. The dispersion effects are evident in Fig. 2.6, but they did not dramatically change amplitude and shape of pulses at the investigated distances, and this is consistent with the expected weak dispersion based on Eqs. (1.8) and (1.9). Fourier spectra of propagated pulses, detected in corresponding locations, were similar.

The cause of the negative phase of the pulses (similar to observed [7, 8]) is the

reduction of the initial static precompression force due to the motion of the first cylinder with respect to the hollow steel rod attached to the precompressing mass.

It is interesting to compare the theoretical value of the sound speed [Eq. (1.5)] based on the assumed effective modulus of the O-ring E_{eff}=105 MPa with the results of numerical calculations, as well as with experimental data. The corresponding data are shown in Fig. 2.7.

2.3 Discussion

Experimental data for static deformation of Nitrile O-rings confirmed their strongly nonlinear behavior, with elastic modulus E_0=7.6 MPa being consistent with reported results for these elements [9-11].

Experiments have shown that this metamaterial is highly tunable – the static force increases from 10 N to 193 N resulted in the increase of signal speed by more than a factor of 4 with a decrease in pulse duration and spatial length under the same method of pulse excitation (Fig. 2.3, Table 2.1).

There is a large difference between experimental data and predicted speed of sound based on Eq. (1.5), if we use a static value of elastic modulus E_0=7.6 MPa (figure 2.4). The spatial length of our signals is comparable to the cell size. Thus, we can expect the influence of linear dispersion on phase speed. But according to Eq. (1.9) linear dispersion can only insignificantly reduce (not increase) signal speed to $0.91c_0$ at smallest wave length in the experiments close to $6.5a_1$ (combined width of the pulse at F_0=193 N). Thus, we cannot attribute the difference between the predicted values of c_0 and measurements as being due to dispersion.

From another point of view, we measure the velocity of signals with finite amplitude, thus nonlinearity may increase the speed of propagation in comparison with the sound speed. The role of nonlinearity can be estimated based on the speed of solitary wave at a given amplitude (a solitary wave represents a balance of dispersion and nonlinearity). Based on this estimate, nonlinearity can increase the speed of propagation to at most $1.03c_0$ (at an initial precompression force F_0=10N) assuming that the positive phase of the pulse is approximated by a solitary wave [Eq. (1.11)]. Clearly, effect of the weak nonlinearity is not able to explain the large discrepancy between experimental data and the theoretical value of c_o based on the extension of the quasi-static behavior of O-rings (E_0 = 7.6 MPa) into the dynamic regime.

From the numerical data, it is clear that, despite the short length of pulses, the dispersion effects did not dramatically change the amplitude, shape and spectrum of propagating pulses at the investigated distances in agreement with estimates based on the continuum approximation [Eqs. (1.8) and (1.9)]. Changes of shape and amplitudes of pulses in experiments are mostly due to dissipation, which will be considered in chapter 3. The speeds of pulses in numerical calculations for E_{eff}=105 MPa are close to the corresponding experimental values (Fig. 2.7). A continuum equation for long-wave sound speed [Eq. (1.5)] with elastic modulus E_{eff}=105 MPa satisfactorily describes the speed of pulses in experiments and in numerical calculations (Fig. 2.7). The slight difference in Fig. 2.7 between numerical data and theoretical values based on Eq. (1.5) might be due to the dispersion effects.

The value of this effective dynamic modulus E_{eff}=105 MPa is considerably higher than the value obtained from static loading experiment (approx. 7.6 MPa), which

is qualitatively similar to the dynamic behavior of Teflon and Parylene-C [3-5,7]. I did not separate inputs of elastic and viscous components in this increased stiffness, though the role of dissipation is significant in experiments. The increased value of the effective elastic modulus may be due to the material strain-rate sensitivity of Nitrile rubber, and the selected value of E_{eff} is characteristic only for the conditions of experiments in section 2.1. In this study, the local static strains in the O-rings in the experiments were up to 0.44, the global dynamic strains in our numerical calculations lay in the interval 1.9×10^{-3} to $4.1\times10^{-4}$and the corresponding strain rates were approximately 51–45 s^{-1}.

The deformation behavior of polymer toroidal O-rings is path-sensitive and, in high strain, strain-rate dynamic deformation (without initial precompression) can be successfully described by a strongly nonlinear viscoelastic model [12], also demonstrating increase of stiffness in dynamic conditions.

The detailed explanation of dramatic increase of dynamic stiffness of O-rings requires investigation of their dynamic contact deformation concentrated in a very small area with large local strains and their gradients.

2.4 Conclusions

The speed of small amplitude stress pulses (considered as sound waves) in metamaterial was used to measure the dynamic properties of strongly nonlinear elements (O-rings). Such measurements can be difficult to conduct for very small elements, like very small O-rings or thin layers of nanofoams. At the same time, the measurements of the sound speed related to the dynamic stiffness of deformed elements in the system (in this dissertation O-rings) can be accomplished irrespective of their size,

because it is based on the measurements of wave speed on macroscopic distances.

Propagation of small amplitude short duration pulses in this one-dimensional strongly nonlinear metamaterial was investigated for different conditions of static preloading in experiments and numerical calculations. Experimental results demonstrated that the static deformation of O-rings obeys double power law with elastic modulus 7.6 MPa being in the reported range for this material. The short duration signals with positive and negative phases having spatial length about 6 – 9 cells size have a speeds which significantly exceeds the speed of sound estimated based on the quasi-static behavior of O-rings with elastic modulus 7.6 MPa. Effects of dispersion and weak nonlinearity can't explain this difference. This large discrepancy is explained by a dramatic increase of effective stiffness of precompressed O-rings under dynamic deformation in the wave. This demonstrates that the design of O-rings, which are very important elements with widespread use in machinery, should take into account their dramatic increase of rigidity under dynamic conditions even at low velocity of impact.

It was shown that signal speed in this double power-law metamaterial is a few times more tunable at higher preload than sound speed in granular chains of linear elastic spherical particles obeying the Hertz interaction law. These results provide a background for designing strongly nonlinear tunable metamaterials with the ability to increase the sound speed and acoustic impedance by a factor of 3–4 times at very moderate static precompression (10-193N). This is unattainable for existing solid materials.

Part of Chapter 2 has been published in *Philosophical Transactions of the Royal Society A*, **372**, art. 20130186, pp 1-14 by Yichao Xu and Vitali F. Nesterenko. The

dissertation author was the primary investigator and author of this paper.

References

[1] M. S. Paterson, J. Appl. Phys. **35**, 176 (1964).

[2] A. N. Gent, *Engineering with rubber* (Hanser, New Yor, 2012).

[3] C. Daraio, V. F. Nesterenko, E. B. Herbold and S. Jin, Phys. Rev. E. **72**, 016603 (2005).

[4] C. Coste and B. Gilles, Eur. Phys. J. B **7**, 155 (1999).

[5] C. Daraio and V. F. Nesterenko, Phys. Rev. E **73**, 026612 (2006).

[6] V. F. Nesterenko, *Dynamics of Heterogeneous Materials* (Springer, New York, 2001), Ch.1, pp. 1-53.

[7] C. Coste, E. Falcon and S. Fauve, Phys. Rev. E **56**, 6104 (1997).

[8] G. Huillard, X. Noblin and J. Rajchenbach, Phys. Rev. E **84**, 016602 (2011).

[9] P. B. Lindley, J. Inter. Rubber Inst. **1**, 202(1967).

[10] P. B. Lindley, J. Strain Anal. **1**, 190 (1966).

[11] P. W. Allen, P. B. Lindley and A. R. Payne, *Use of rubber in engineering* (Maclaren and Sons, London, UK, 1975), Ch. 1, pp. 1-65.

[12] C. Lee and V. F. Nesterenko, J. Appl. Phys. **114**, 083509 (2013).

CHAPTER 3

ATTENUATION OF SHORT STRESS PULSES IN STRONGLY NONLINEAR DISSIPATIVE METAMATERIAL

This chapter deals with the attenuation of short stress pulses in strongly nonlinear dissipative metamaterial assembled using alternating steel cylinders and toroidal Nitrile O-rings under static precompression. The modeling of the observed strongly nonlinear attenuation in experiments was performed with the help of numerical simulation. The dispersion behavior caused by the periodic arrangement of elements is contributing to the attenuation of stress pulses, but could not explain the experimental observations. It was explained by taking into account the nonlinear viscous behavior of O-rings. The numerical simulations were able to predict the dependence of the signal speed on the precompression force, a significant decrease of the pulse width with the precompression and the attenuation of the leading positive pulse, the latter of major significance in the protection against impact.

3.1 Introduction

Most of the previous publications related to the wave transmission in metamaterials neglect the dissipation effect, since the discrete nature of metamaterials and strong nonlinearity play the major role when waves travel relatively short distances. However, the dissipation plays a significant role on wave shape and attenuation in experiments when “soft” toroidal elements are introduced [1-5], like Nitrile rubber O-

ring [5]. These Nitrile toroidal elements (O-rings) are widely used in the automotive and aeronautical industry and their quasi-static elastic properties are well known [6-9].

In contrast to the commonly used Hertz contact law between spherical grains [10], toroidal O-rings obey a more complicated force-displacement interaction law – double power law [$F \propto (\delta^{3/2}+\delta^{6})$] under compression [6-8]. At relatively large deformation (when the second term with exponent n=6 dominates) this relationship ensures significantly stronger nonlinearity than the Hertz law. Additionally, due to the strain rate sensitivity the dynamic behavior of the toroidal Nitrile O-rings is significantly different from the static response [5,11,12].

In this chapter, the experimental results related to the attenuation of traveling short stress pulses in a chain composed of alternating steel cylinders and Nitrile O-rings are reported. Numerical simulations were used to explore the role of dispersion and viscous dissipation and explain the experimental data. The dissipative model was introduced with strongly nonlinear dependence of viscous force on the precompression and linear dependence on the relative velocity following the approach proposed by Kuwabara and Kono [13], Brilliantov *et al.*[14,15], and Morgado and Oppenheim [16]. It is observed that this approach allowed description of the attenuation of the amplitude of leading short compression pulse depending on the system precompression as well as the strong tenability of pulse speed.

3.2 Theoretical Analysis

The one-dimensional metamaterial composed form steel cylinders and Nitrile O-rings under static precompression (F_0) as shown schematically in Fig. 1.2. Each cell

of the system includes a stainless steel cylinder and O-ring. It has an initial size a (a=h+d, where h is the height of the steel cylinder, and d is the cross sectional diameter of an undeformed O-ring). For statically loaded chain the cell size is equal to the height of the steel cylinder plus a height of deformed O-ring. For the theoretical treatment, we consider O-rings as massless viscoelastic springs intermittent by the rigid steel cylinders, since the mass of O-rings (0.0625g) is much smaller than that of steel cylinders (m = 3.065 g), and the steel cylinders are practically not deformed at investigated amplitudes of stress pulses. In the initial conditions the forces between neighboring cylinders are due to nonlinear elastic deformation of O-rings having a value of x, the empirical form of the quasi-static force-displacement relationship is a strongly nonlinear double power law [6-8],

$$F_{el} = A_0 m(x)^{3/2} + B_0 m(x)^6, \tag{3.1}$$

where $A_0 = 1.25\pi D_{\mathrm{m}}\, E_0/md^{1/2}$, $B_0 = 50\pi D_{\mathrm{m}}\, E_0/md^5$, and D_{m} is the mean diameter of O-ring (defined as the inside diameter plus cross sectional diameter of the O-ring). A quasi-static Young's modulus of Nitrile rubber is equal to E_0 = 7.6 MPa [5]. The quasi-static force-displacement relationship described by Eq. (3.1) is in a good agreement with experimental data for O-rings made from different materials up to x/d equal 0.5 [6-8]. Its strongly nonlinear nature is caused by the geometry of the contact deformation. During the dynamic process we may assume that this geometric origin of strong nonlinearity will be also present. At the same time due to the viscoelastic behavior of Nitrile rubber we may expect that the value of elastic modulus can be different than its static value.

In our experiments, the system is initially strongly compressed, which means

that the wave amplitude is much smaller than the forces caused by initial precompression, so we assume that the relative displacement between neighboring cylinders relative to their positions in the undeformed chain x is equal to the initial value x_0 plus additional much smaller change during dynamic deformation x_d (Fig. 1.2). Thus we approximate the linearized response of O-rings by the following equation:

$$F_{el} = F_s + F_d = A_0 m {x_0}^{3/2} + B_0 m {x_0}^6 + K x_d, \quad (3.2)$$

where F_s is a static compression force and F_d is dynamic force acting between the particles, and $K = 1.5(1.25\pi D_{\mathrm{m}}\, E_{\mathrm{eff}} d^{-1/2}) x_0^{1/2} + 6(50\pi D_{\mathrm{m}} E_{\mathrm{eff}} d^{-5}) x_0^5$. The coefficient K in the dynamic component of the force was introduced based on the linearization of nonlinear expression for the force [Eq. (3.1)], but assuming that the dynamic deformation may change the elastic properties of O-rings without changing the nonlinear dependence of displacement coming from the geometry of deformed contact. As a result of this approach a coefficient K is nonlinearly dependent on the initial precompression providing the dependence of sound speed on initial strain in agreement with the experimental data [5]. The coefficient E_{eff} can be different than the elastic moduli of Nitrile O-rings and reflects viscoelastic property of the dynamically deformed O-ring in a wave, akin to the effective values of elastic modulus successfully used for the dynamic contact behavior of viscoelastic beads (Polytetrafluoroethylene [17,18]) or beads coated with polymer layer [19].

The coefficient K was selected to match observed experimental data on the speed of stress pulse, in Ref. [5] E_{eff} is chosen to be 105 MPa. It allowed us to associate the speed of this pulse with sound speed based on the analysis of contribution of dispersion and weak nonlinearity [5]. Thus this coefficient was effectively representing the total

input of elastic and viscoelastic mechanisms.

The equations of motion in a vertical chain composed of *N* steel particles and *N*-1 O-rings without considering dissipation is:

$$\ddot{x}_i = \frac{K}{m}(x_{d,i-1} - 2x_{d,i-1} + x_{d,i+1}), \tag{3.3}$$

where $x_{d,i} - x_{d,i+1}$ (i=1,…,N-1) is the change of the height of O-ring between the i-th and (i+1)-th cylinder during the propagation of stress pulse in the precompressed system. The gravitational forces acting on the particles is neglected, which negligibly affect the experimental results at a given value of precompression

Compared to the commonly used elastically stiff steel beads, soft toroidal elements – Nitrile O-rings exhibit a dramatic dissipation effect resulting in the shape and amplitude change of signal in the experiments. To account for the dissipative properties of O-rings, it is necessary to separate the elastic part in the force from viscoelastic part, which was combined in the paper [5] in one coefficient K in the Eqs. (3.2) and (3.3).

In this chapter, I attempt to separate the elastic and viscous contributions to the forces acting between metal cylinders due to the dynamic deformation of O-rings. Motivated by the results reported in Ref. [5], where the level of attenuation was increasing with the initial static compression force, it is anticipated that the dissipation term should has a dependence on the precompression strain. A possible approach to the viscoelastic deformation of the Hertzian contact was proposed by Kuwabara and K. Kono [13], Brilliantov et al.,[14,15], and Morgado and Oppenheim [16]. I modified this approach by introducing the dissipative force (F_{dis}) on the static precompression of O-rings following the approach proposed by Brilliantov *et al*. [14,15],

$$F_{dis} = \alpha \dot{x} \frac{\partial}{\partial x} F_{el}(x). \tag{3.4}$$

Here α is the dissipative constant. In the current paper the nonlinear elastic force F_{el} is taken following Eq. (3.1) with dynamic elastic modulus E_{d}, replacing constant E_0, to consider a possible frequency dependence of the elastic properties of O-rings. It should be emphasized that Eq. (3.4) is based on a quasi-static approach requiring that characteristic time of dynamic deformation being much larger than the relaxation time for the dissipative processes in the material [14,15].

Thus following the approach of Refs. [13-16], which was successfully applied to the behavior of O-rings under heavy impact [11], F_{dis} is equal to

$$F_{dis} = \alpha \dot{x} K_1, \tag{3.5}$$

$$K_1 = 1.5(1.25\pi D_{\mathrm{m}}\, E_d d^{-1/2}) x_0^{1/2} + 6(50\pi D_{\mathrm{m}} E_d d^{-5}) x_0^5. \tag{3.6}$$

The total force due to the elastic and viscoelastic deformation of O-rings at the contact with a separation of elastic and viscous terms is

$$F = F_{el} + F_{dis} = A_0 m {x_0}^{3/2} + B_0 m {x_0}^6 + K_1 x_d + \alpha \dot{x} K_1. \tag{3.7}$$

So besides the geometric properties of steel cylinders and O-rings, adjustable parameters (K_1 and μ) were also used to calculate the dynamic component of the force between neighboring particles in the numerical analysis. The dissipative constant α is related to the viscoelastic, dissipative properties of O-rings in the condition of contact deformation with high strain rate and gradient of strain in the contact area. It is not a property of bulk of the Nitrile rubber and used as adjustable parameters to match the results of calculations and experimental data with respect to the speed of the pulse and attenuation of its amplitude. The viscous term has a nonlinear dependence on the initial

deformation (x_0) following the approach proposed in Refs. [14,15], which is necessary to explain the dependence of attenuation on the initil precompression in experiments as we will see later.

If K_1 will be close to K then the speed of the pulses is determined mainly by the elastic behavior and the viscous term does not contribute significantly to the rigidity (and the speed of stress pulse) only causing dissiaption. In other case, it may be seen that K_1 is a relatively small and the viscosity significantly contribute to the system rigidity and the speed of the signal.

The equations of motion for the chain of alternating steel cylinders and O-rings considering dissipation term is given by,

$$\ddot{x}_i = \frac{K_1}{m}(x_{d,i-1} - 2x_{d,i-1} + x_{d,i+1}) + \frac{K_1\alpha}{m}(\dot{x}_{i-1} - 2\dot{x}_{i-1} + \dot{x}_{i+1}). \quad (3.8)$$

It should be mentioned that the dissipative term in this simplified approach does not depend on the amplitude of pulses and depends linearly on the strain rate. It is a nonlinear function of precompression strain in an attempt to explain the dependence of dissipation on the precompression force observed in the experiments.

3.3 Experimental Procedure, Results and Discussion

To study the viscous dissipation effect, the experiments were carried out in a vertical PMMA tube filled with 19 steel cylinders (with a height h = 5 mm, diameter 10 mm) alternated by 18 Nitrile O-rings (with a cross sectional diameter d = 1.78 mm, and a mean diameter D_m = 6.22 mm) shown in Fig. 3.1. Three Piezo gauges (6 mm side plates with 0.267 mm thickness, RC of the electrical circuit ~5.24 ms) were placed

inside the fifth, ninth, and thirteenth steel particles to measure the averaged compression forces between the corresponding two contacts. The static precompression force due to additional weight placed on the top of the chain ranges from 10 to 193 N.

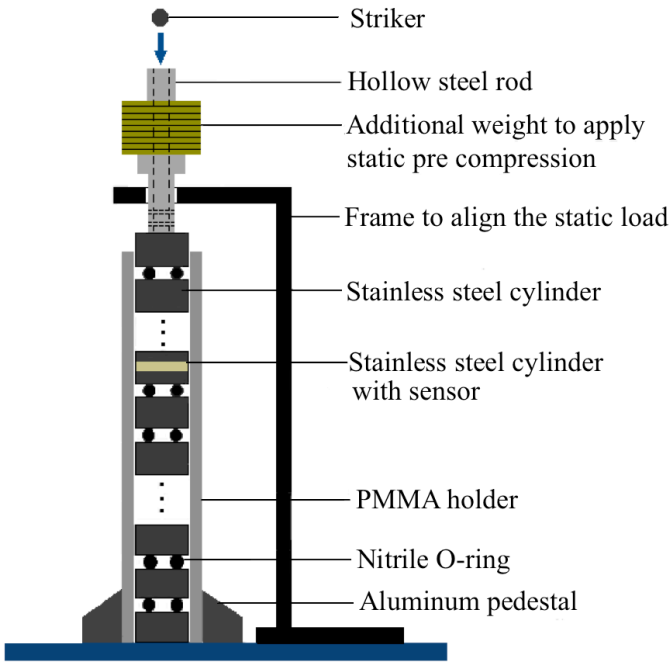

Figure 3.1: Experimental setup composed of alternating stainless steel cylinders and Nitrile O-rings for testing of the stress pulse propagation in a strongly nonlinear 1D chain. Three piezo gauges are placed in the fifth, ninth and thirteenth steel cylinders from the top. The frame with a hole inside its upper part keeps hollow steel rod aligned in the vertical direction. There are two thin slots near the end of hollow steel rod, which were used to measure the velocity of spherical striker by high-speed camera.

The pulses with different durations and amplitudes were generated by the impact of a steel sphere (mass 0.455 g, with a diameter of 4.76 mm) onto the top steel cylinder dropped from a height of 350 mm. We used a high-speed camera (Phantom V12) in order to get the accurate velocity of the steel striker just before the collision, witch was measured to be 2.24 ± 0.01 m/s slightly lower than the theoretical calculated velocity

2.62 m/s, mostly due to the friction between the striker and the inner wall of hollow rod.

A Tektronix TDS2014 oscilloscope was used to record signals from the piezo gauges caused by these stress pulses. Some of the experimental results of pulse propagating under various compression forces (10 N, 30N, 50 N, 74N, 106 N and 193 N) are presented in Fig. 3.2. The zero time in the figures is arbitrary.

The corresponding force amplitude in the stress pulses was found based on the measurements of the electric signals from gauges embedded inside the particles using a calibration factor. The amplitude of pulses was measured with the accuracy of 9%.

From Fig. 3.2 we see that in a relative short distances (from the fifth steel cylinder to the ninth), the fronts of the positive and negative signals are ramped and their amplitudes decreased. For example, in Fig. 3.2(a) the total length of pulse (positive and negative phases combined) increased from 550 microseconds to 1000 microseconds after it propagated through only four cells. With increased precompression the pulse dispersion is smaller [compare Figs. 3.2(a) and 3.2(e)]. The Fourier spectra of these stress waves demonstrate that higher frequencies of the signal decayed faster.

The speed of propagation of the positive and negative stress pulses in the chain was calculated dividing the distance $4(a\text{-}x_0)$ between the sensors embedded in the fifth and ninth steel cylinders by the peak-to-peak time interval of corresponding signals (x_0 denotes the initial reduction of O-rings height due to the static precompression). The spatial widths of positive and negative phases ($L_{\exp,+}$ and $L_{\exp,-}$) of stress pulses were calculated based on their speeds and durations detected by the gauges in the fifth cylinder. All the data are shown in Tables 3.1 and 3.2.

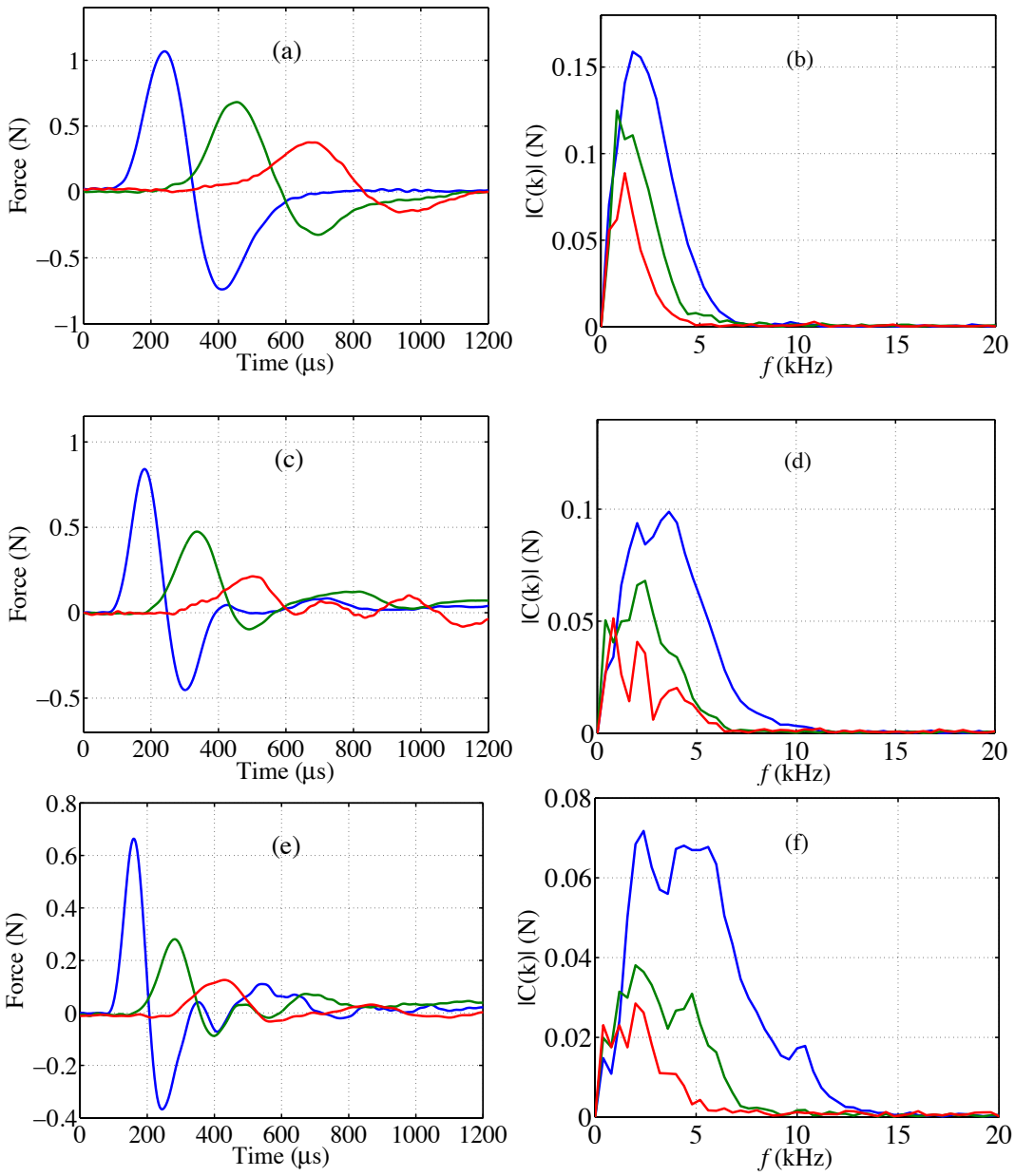

Figure 3.2: Stress pulses (left column) generated in a chain of stainless steel cylinders and Nitrile O-rings by a steel striker (0.455 g) dropped from a height of 350 mm (measured velocity just before the impact was 2.24± 0.01 m/s) and their corresponding Fourier spectra (right column), under various static precompression forces: (a), (b) 10 N; (c), (d) 30 N; (e), (f) 50 N; (g), (h) 74 N; (i), (j) 106N and (k), (l) 193 N. All the forces are recorded by three sensors embedded in the fifth (leading signal), ninth (middle signal), and thirteenth (last signal) steel cylinders.

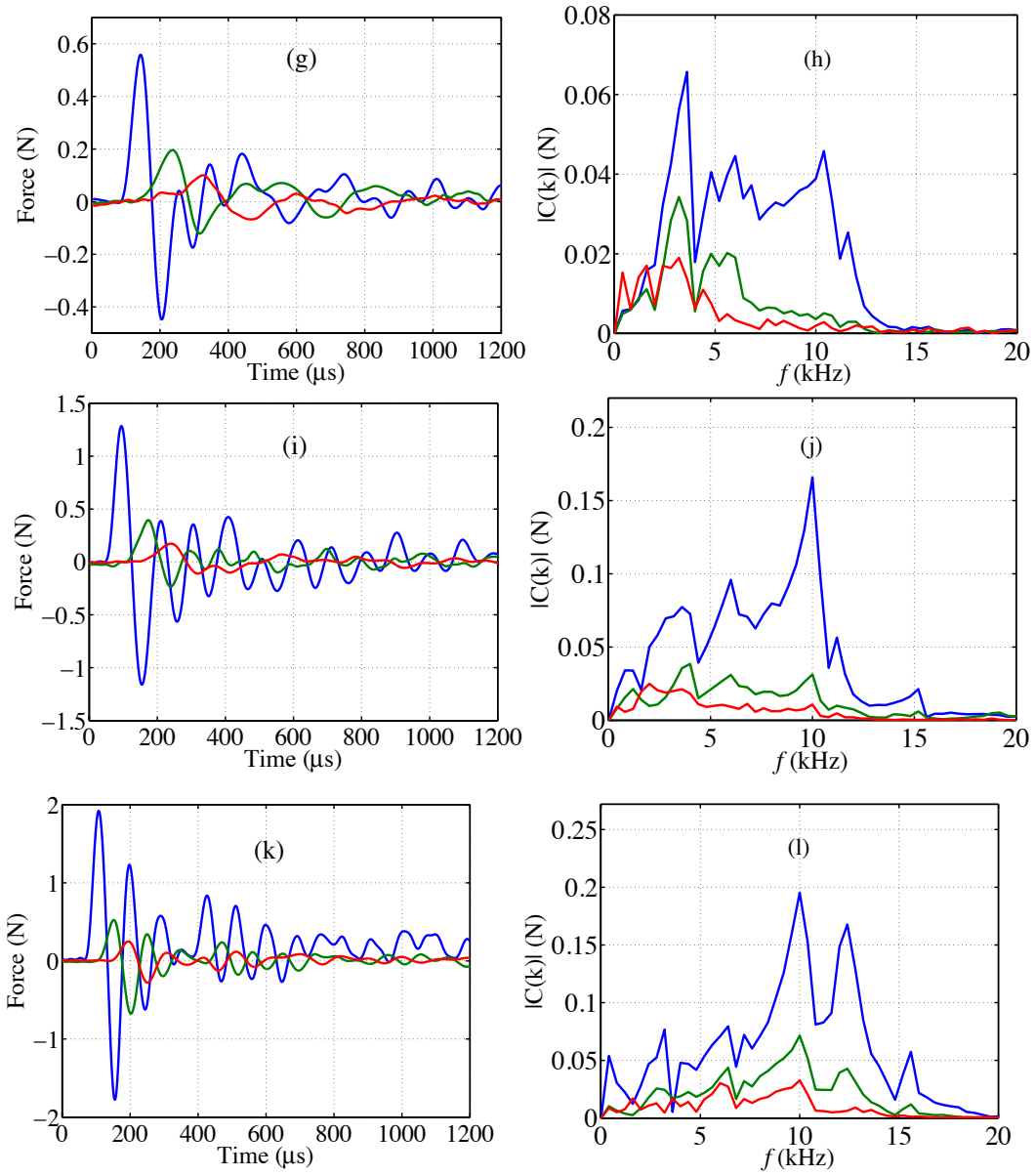

Figure 3.2: Stress pulses (left column) generated in a chain of stainless steel cylinders and Nitrile O-rings by a steel striker (0.455 g) dropped from a height of 350 mm (measured velocity just before the impact was 2.24± 0.01 m/s) and their corresponding Fourier spectra (right column), under various static precompression forces, continued.

Table 3.1: Speeds ($V+$) and widths [$L_{exp,+}/(a-x_0)$] of positive pulses for different precompression forces detected in experiments.

F_0 (N)	10	30	50	74	106	193
$V+$ (m/s)	128±12	165±9	209±8	268±8	310±8	482±15
$L_{exp,+}/(a-x_0)$	4.6	4.5	3.9	3.8	3.7	4.8

Table 3.2: Speeds ($V-$) and widths [$L_{exp,-}/(a-x_0)$] of negative pulses for different precompression forces detected in experiments.

F_0 (N)	10	30	50	74	106	193
$V-$ (m/s)	96±9	126±7	156±8	225±7	288±10	457±15
$L_{exp,-}/(a-x_0)$	4.3	3.7	3.1	2.4	3.0	3.4

From Table 3.1, we can see that the speed of positive pulses dramatically increases with precompression. The accuracy of the speed measurement was within 10% and within this limit the speeds of positive and negative pulses were close demonstrating a weak dispersion of the whole signal. Still a speed of negative pulse is lower than the speed of positive pulse. This may be due to more dispersive behavior of weakly nonlinear negative pulses in comparison with the positive pulses, e.g., the system supports weakly nonlinear compression solitary wave, but it does not support stationary rarefaction solitary wave. Thus we can expect more pronounced change of the shape of weakly nonlinear negative pulses in comparison with positive pulses. In this chapter, I will mainly focus on the positive phase of the stress pulses.

The durations of positive pulses significantly decreased with the increase of precompression (Table 3.1). Despite the increase of the speed with precompression, their space scale of positive pulse also decreases until the largest force 193 N was applied.

In experiments the stress pulse amplitude is less than 10% of the initial precompression force. Thus, the values of the pulse speed in experiments could be used to estimate the long wave sound speed in a continuum limit in a agreement with the theoretical approach with an appropriately selected dynamic elastic properties of O-rings [5]. Applying a moderate force (10 – 193 N), the sound speed of the system (associated with the speed of relatively small amplitude pulses in comparison with precompression forces) was increased up to 4 times (Table 3.1). This is very unusual in common solids.

Another general conclusion that can by drawn from experimental data is that the attenuation of signal positive amplitude shows a strong dependence on the precompression force, the larger the force the faster the amplitude attenuation (Fig. 3.2). The dependence of the attenuation of signal amplitude with the depth of a chain under different initial compression conditions is presented in Fig. 3.3. The vertical axis represents the ratios of the amplitudes of signal in gauges embedded in the 6th, 9th, 12th, 15th and 18th cylinders to the amplitudes in gauge embedded in the 3rd cylinder with different precompression forces (10 N, 59 N, 106 N and 193 N).

It is interesting to mention that negative pulse attenuates faster than positive, except the largest compression case. Meanwhile, the amplitude of the leading negative pulse is found to be smaller than the amplitude of corresponding positive pulse. This probably can be connected to the difference in contact stiffness between first cylinder and following O-ring (“soft” contact) and between first steel cylinder, striker and hollow steel rod (“rigid” contacts) used to apply a precompression static force

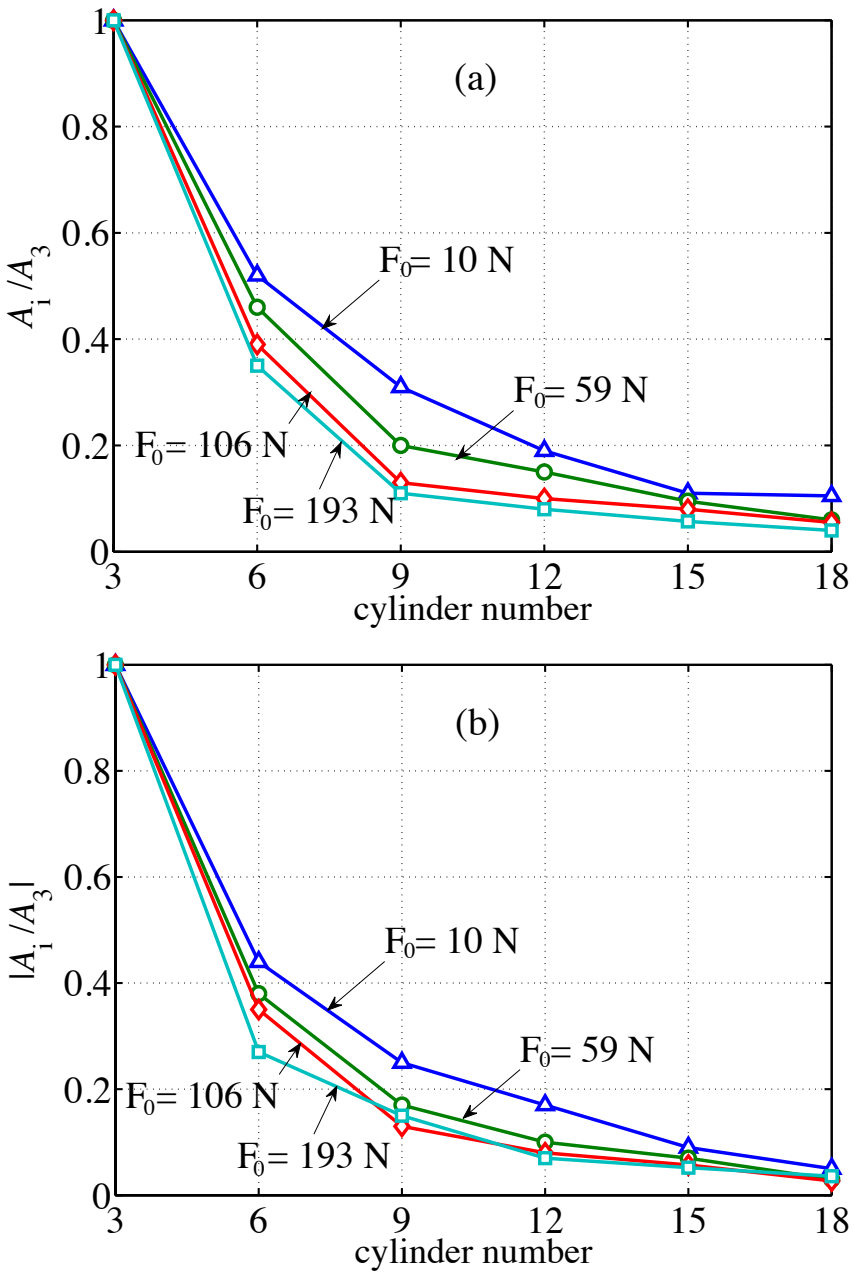

Figure 3.3:The attenuation of the (a) positive and (b) negative stress pulse amplitudes on the depth of a chain under different precompression forces in experiments. The vertical axis corresponds to the ratio of signal amplitude detected in the *i*-th cylinder, A_i (*i*=3, 6, 9, 12, 15, and 18) to signal amplitude detected in the 3rd cylinder under different precompression forces F_0: (Δ) 10 N, (O) 59 N, (◊) 106, and (□) 193 N. The chain is impacted by a 4.76 mm diameter steel sphere (with mass 0.455 g) dropped from the height of 350 mm, velocity before impact is equal to 2.24 ± 0.01m/s.

From the experimental results shown in Fig. 3.2, it is also noticed that increasing the system initial precompression above 50 N qualitatively change the shape of the pulse – an oscillating tail appears instead of smooth tail similar to the critically damped behavior of oscillator. This could be explained by the increase rigidity of the system with increasing initial static compression resulting in the increase of critical value of viscosity corresponding to the transition from oscillatory motion to critically damped motion of steel cylinders.

Further, besides the dispersion of the nonlinear system and the viscoelastic behavior of O-rings, the solid friction between the locally deformed O-ring and the surface of steel plates could also be a reason for the strong attenuation in signal amplitude with the increasing precompression force. To investigate the role of friction on the signal attenuation in this metamaterial we lubricated the Nitrile O-rings and surfaces of the cylinders with 5w30 motor oil to reduce the contact solid friction. The experimental results related to the chain with lubricated interfaces between O-rings and cylinders at the least and most precompressed case (F_0 = 10 N and 193 N) are presented in Fig. 3.4. The chain was impacted in similar way as the chain without lubrication.

The comparison between these two results (with/without lubricants) represented in Table 3.3 demonstrates that at both precompression forces the signal speeds are the same within corresponding accuracy of their measurements [compare Fig. 3.2(a) with Fig. 3.4(a), and Fig. 3.2(k) with Fig. 3.4(b)].

The shapes of corresponding signals at F_0=10N were similar, but at precompression 193 N the signal detected by the gauge in the fifth cylinder demonstrated a smaller attenuation of the oscillating pulse. The lubrication resulted in

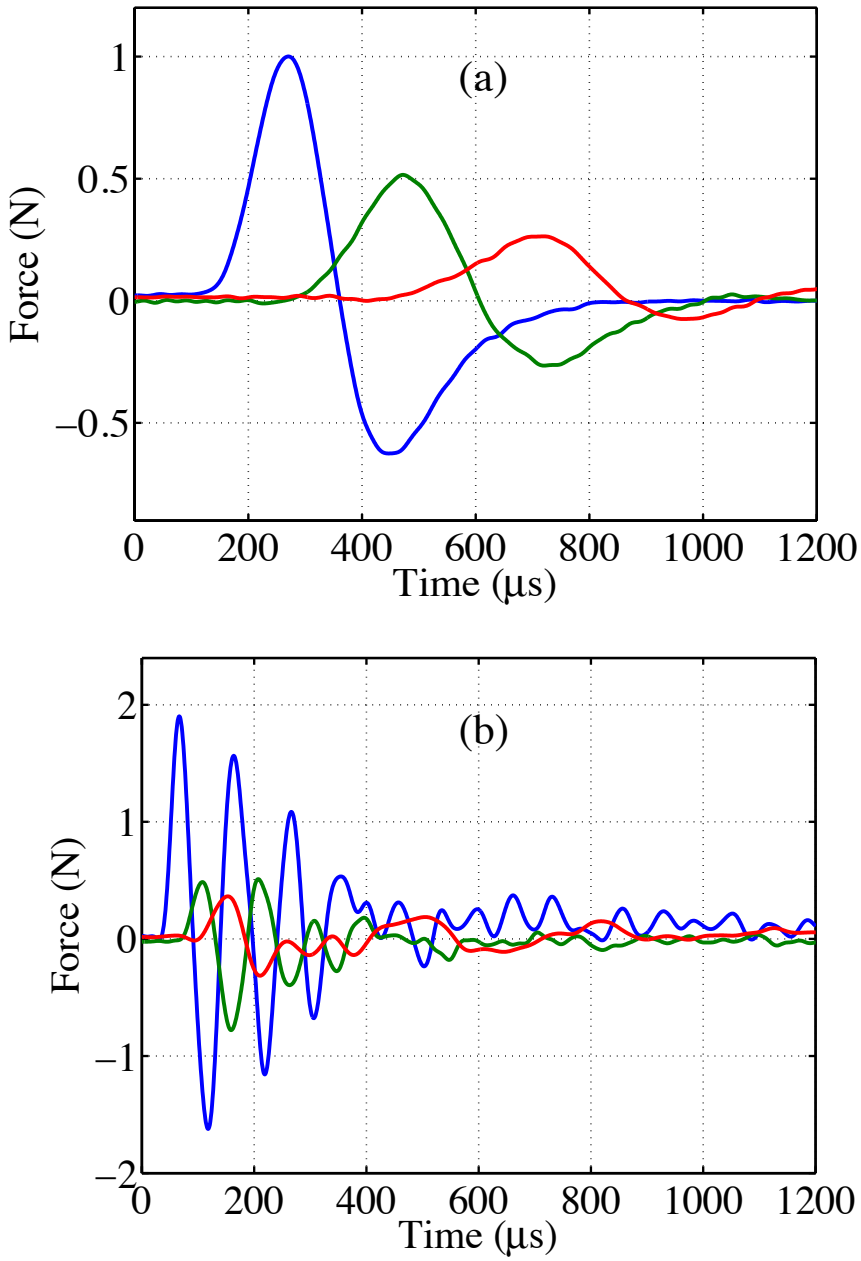

Figure 3.4: Attenuation of the stress pulse in the lubricated chain (5w30 motor oil). The chain is impacted by a 4.76 mm diameter steel sphere (mass 0.455 g) dropped from the height of 350 mm (velocity before impact is equal to 2.24 ± 0.01 m/s). The precompression force is: (a) 10 N and (b) 193 N.

Table 3.3: Speeds ($V+$), widths [$L_{exp,+}/(a-x_0)$] and the attenuation of positive pulses (A_9/A_5 and A_{13}/A_5) for different precompression forces with lubricants (5w30 motor oil) and without lubrication detected in experiments.

	F_0 (N)	$V+$ (m/s)	$L_{exp,+}/(a-x_0)$	A_9/A_5	A_{13}/A_5
Without lubrication	10	128	4.6	0.62	0.36
	193	482	4.8	0.27	0.14
With lubrication	10	128	4.4	0.51	0.27
	193	498	4.6	0.25	0.17

a slightly increased attenuation of the leading positive pulse in the initial stage of signal propagation for both precompression forces (data for A_9/A_5). A reduced attenuation of the leading pulse was observed on later stage of pulse propagation (data for A_{13}/A_5) only at precompression force 193 N (Table 3.3). Since the differences related to the experimental results with/without lubricants is insignificant, we may conclude that the dry contact friction between Nitrile O-rings and metal cylinders does not play a major role in the signal attenuation, and the viscoelastic deformation of O-rings is the major source of dissipation in the investigated metamaterial.

3.4 Numerical Calculation and Comparison with Experiments

The numerical simulation for a chain of steel cylinders and Nitrile O-rings shown in Fig. 3.1 as a 1D lattice with a double power-law interaction between neighboring rigid cylinders with/without considering viscous dissipation is carried out by using MATLAB.

The gravitational force was applied to all particles of the chain in the numerical calculations, and the first particle in our numerical model represents the precompressing

mass, including the hollow steel rod and the additional weight attached to it as shown in Fig. 3.1. It was assumed that there was a Hertzian type interaction force between the precompression mass and the top cylinder (third particle of our model) in the chain. The second particle represents the steel striker, given an initial speed as 2.24 m/s measured in experiments by using a high-speed camera as mentioned in section 3.3.

Two numerical models were considered: one is based on the linear elastic interaction between particles (referred as Model I), where no dissipation was included in all contact interactions. But the coefficient K, when selected to match experimental results on the wave speed, may represent effective rigidity influenced by the viscoelastic behavior. This approach was used in Ref. [5] to find the effective stiffness of the system by determining the characteristic propagation speed of small amplitude pulses associated with the sound speed, which is not significantly affected by the dissipation.

The other approach uses a double power-law interaction force between particles including a viscous dissipation term (referred as Model II). Unlike Model I, this approach introduces an elastic and viscous components of the force. This separation allows a calculation of attenuation depending on the applied precompression, which was not possible in the frame of Model I.

3.4.1 Equation of motion in numerical modeling

The first order differential equations of motion of N cylinders inside a periodic chain and the boundary conditions are presented below (similar to the method used in Ref. [5]):

$$\dot{x}_i(\bar{x}) = \begin{cases} x_{N+i}, & i = 1, \dots, N-1; \\ \varphi_i(\bar{x}) - \psi_i(\bar{x}) + g, & i = N+1, \dots, 2N-1; \end{cases} \tag{3.9}$$

and $\bar{x} = (x_1, \dots, x_{N,} x_{N+1}, \dots, x_{2N})$; (3.10)

where $g = 9.81$ m/s^2 is the gravitational acceleration.

For the non-dissipative Model I:

$$\varphi_i(\bar{x}) = \begin{cases} 0, & i = N+1, N+2; \\ \frac{C}{m}\delta_{i-2-N,i-N}^{\frac{3}{2}} H(\delta_{i-2-N,i-N}) + \frac{D}{m}\delta_{i-1-N,i-N}^{\frac{3}{2}} H(\delta_{i-1-N,i-N}), & i = N+3; \\ [A_0(x_{0,i-1-N})^{\frac{3}{2}} + B_0(x_{0,i-1-N})^6 + \frac{K_{i-1-N}}{m}(\delta_{i-1-N,i-N} - x_{0,i-1-N})] & \\ H(\delta_{i-1-N,i-N}), & i = N+4, \dots, 2N-1; \end{cases} \tag{3.11a}$$

$$\psi_i(\bar{x}) = \begin{cases} \frac{C}{M}\delta_{i-N,i+2-N}^{\frac{3}{2}} H(\delta_{i-N,i+2-N}), & i = N+1; \\ \frac{D}{m_{imp}}\delta_{i-N,i+1-N}^{\frac{3}{2}} H(\delta_{i-N,i+1-N}), & i = N+2; \\ [A_0(x_{0,i-N})^{\frac{3}{2}} + B_0(x_{0,i-N})^6 + \frac{K_{i-N}}{m}(\delta_{i-N,i+1-N} - x_{0,i-N})] H(\delta_{i-N,i+1-N}), & \\ & i = N+3, \dots, 2N-1; \end{cases} \tag{3.11b}$$

For the dissipative Model II:

$$\varphi_i(\bar{x}) = \begin{cases} 0, & i = N+1, N+2; \\ \frac{C}{m}(\delta_{i-2-N,i-N}^{\frac{3}{2}} + \frac{3}{2}\delta_{i-2-N,i-N}^{\frac{1}{2}}\mu_C\delta_{i-2,i}) H(\delta_{i-2-N,i-N}) & \\ + \frac{D}{m}(\delta_{i-1-N,i-N}^{\frac{3}{2}} + \frac{3}{2}\delta_{i-1-N,i-N}^{\frac{1}{2}}\mu_{D\delta_{i-1,i}}) H(\delta_{i-1-N,i-N}), & i = N+3; \\ [A_0(x_{0,i-1-N})^{\frac{3}{2}} + B_0(x_{0,i-1-N})^6 + \frac{K_{i-1-N}}{m}(\delta_{i-1-N,i-N} - x_{0,i-1-N}) & \\ + \frac{K_{i-1-N}}{m}\alpha\delta_{i-1,i}] H(\delta_{i-1-N,i-N}), & i = N+4, \dots, 2N-1; \end{cases} \tag{3.12a}$$

$$\psi_i(\bar{x}) = \begin{cases} \frac{C}{M}(\delta_{i-N,i+2-N}^{\frac{3}{2}} + \frac{3}{2}\delta_{i-N,i+2-N}^{\frac{1}{2}}\mu_C\delta_{i,i+2})H\left(\delta_{i-N,i+2-N}\right), & i = N+1; \\ \frac{D}{m_{imp}}(\delta_{i-N,i+1-N}^{\frac{3}{2}} + \frac{3}{2}\delta_{i-N,i+1-N}^{\frac{1}{2}}\mu_D\delta_{i,i+1})H\left(\delta_{i-N,i+1-N}\right), & i = N+2; \\ [A_0\left(x_{0,i-N}\right)^{\frac{3}{2}} + B_0\left(x_{0,i-N}\right)^6 + \frac{K_{i-N}}{m}\left(\delta_{i-N,i+1-N} - x_{0,i-N}\right) \\ + \frac{K_{i-N}}{m}\alpha\left(\delta_{i,i+1}\right)]H\left(\delta_{i-N,i+1-N}\right), & i = N+3,\ldots,2N-1; \end{cases}$$

(3.12b)

where $\delta_{1,3} = x_1 - x_3$, and $\delta_{i-1-N,i-N} = x_{i-1-N} - x_{i-N}$, for i=N+3,…,2N. (3.13)

And $K_{i-1-N} = 1.5(1.25\pi D_m\, E_d d^{-\frac{1}{2}})x_{0,i-1-N}^{\frac{1}{2}} + 6(50\pi D_m E_d d^{-5})x_{0,i-1-N}^5, i = N+4,\ldots,2N.$ (3.14)

The boundary conditions are defined as:

$\dot{x}_i(\bar{x}) = 0,\ i = N, 2N.$ (3.15)

And the initial conditions corresponding to the gravitationally loaded chain are:

$x_N(t=0) = 0;\ \ x_{N-i}(t=0) = x_{N-i+1}(t=0) + x_{0,N-i},\quad i = 1,\ldots,N-3;$

$x_2(t=0) = x_3(t=0);\quad x_1(t=0) = x_3(t=0) + x_{0,1};$

$x_{N+1}(t=0) = 0;\ \ x_{N+2}(t=0) = 2.24\ m/s;\ \ x_{N+i}(t=0) = 0,\quad 3 \le i \le N.$ (3.16)

The variable x_i (i=1,…,N) is the displacement of the i-th particle from its equilibrium position in a undeformed chain assumed due to the gravitational force, static loading and dynamically perturbation, while for i=N+1, ..., 2N they are the velocity of the (i-N)-th particle. The value of $x_{0,1}$ is the intial displacement of the precompression mass refer to the top cylinder under gravitational force, $x_{0,2}$ =0. Variables $x_{0,i}$ (i = 3,…, N-1) correspond to the initial change of heights of the O-ring between the i-th and (i+1)-th cylinders due to the gravitational force.

The Heaviside function $H(\delta)$ is used to account for the seperation between the neighboring elements in the chain. The prefactors $C=\frac{2E_{\text{steel}}}{3(1-\nu^2)}R_{\text{rod}}^{1/2}$ and $D=\frac{2E_{\text{steel}}}{3(1-\nu^2)}R_{\text{striker}}^{1/2}$ represent the nonlinear Hertzian type interactions between the precompressing mass (particle 1) and the top steel cylinder (particle 3) and between the striker (particle 2) and the top cylinder, where ν and E_{steel} are the Poison ratio and elastic modulus. R_{rod} and R_{striker} are the radius of the hollow steel rod and steel striker. The precompressing mass and striker have mass M and m_{imp}, respectively. Parameters μ_C and μ_D are the viscosity coefficient between the precompression mass and the top cylinder, and between the striker and top cylinder, which were used only in numerical calculations with Model II.

3.4.2 Non-dissipative model I

The results of modification of pulse shapes while they propagate in the system at different precompression forces in the non-dissipative numerical calculations in the frame of Model I are shown in Fig. 3.5 using effective elastic modulus E_{eff} = 105 MPa. This value provided a good description of the pulse speeds and correctly describes its behavior as well as increased frequency of pulses with precompression similar to the experimental data [5].

The speeds and widths of the positive and negative pulses calculated in the frame of Model I are presented in Tables 3.4 and 3.5.

From the comparison between the data from numerical calculations (Table 3.4) and from experiments (Table 3.1), it can be seen that the selected modulus 105 MPa fits experimental data better at low precompression than at larger precompression. The

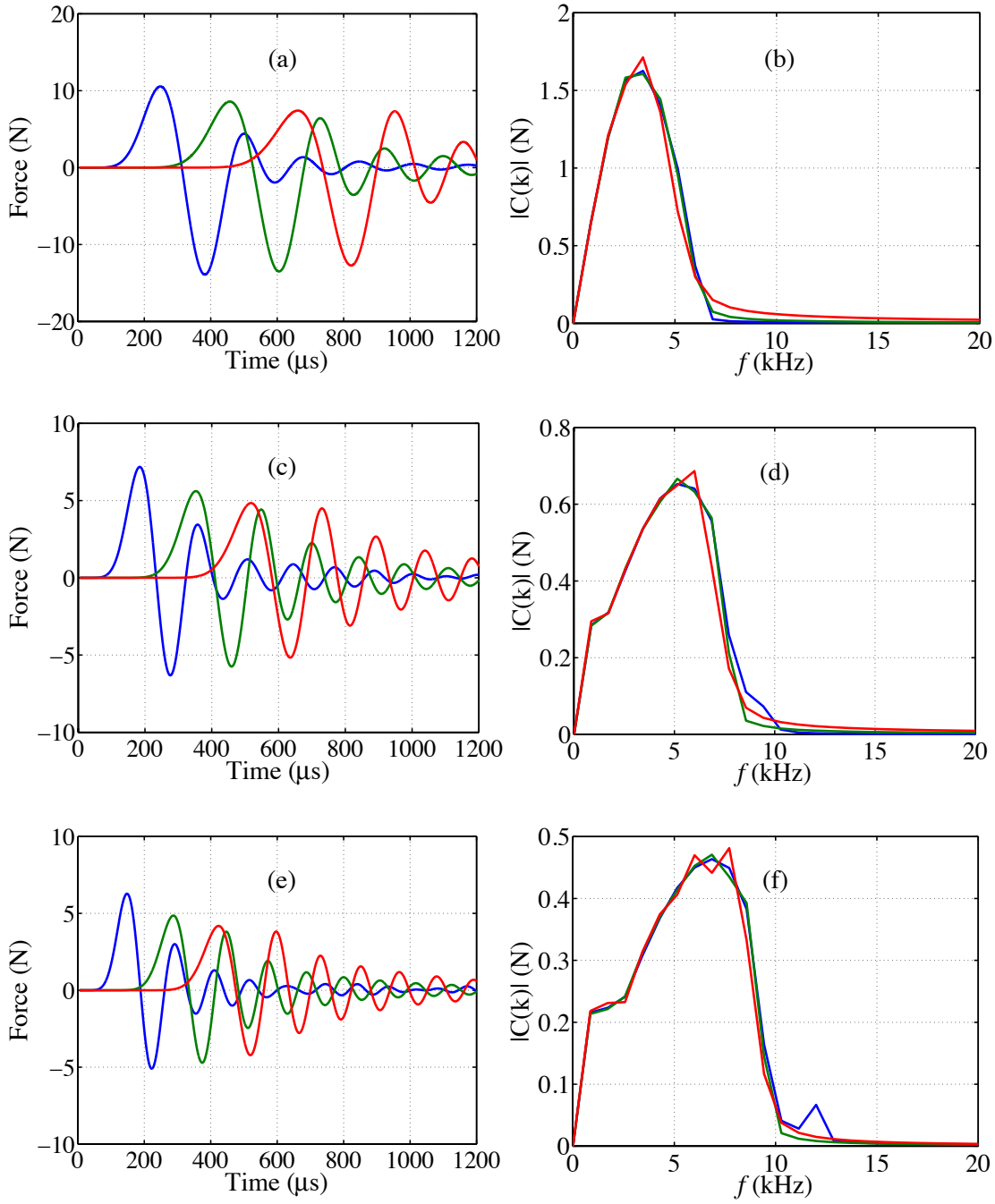

Figure 3.5: Stress pulses obtained in numerical calculations using Model I (without dissipation term between all elements in the system, and using effective elastic modulus E_{eff} = 105 MPa) and their corresponding Fourier spectra in a double power-law system under various preload conditions: (a),(b) F_0= 10 N; (c),(d) 30 N; (e),(f) 50 N; (g),(h) 74 N; (i),(j) 106 N; and (k),(l) 193 N. Curves represent the average dynamic force in the fifth (leading curve), ninth (middle curve), and thirteenth (bottom curve) steel partial.

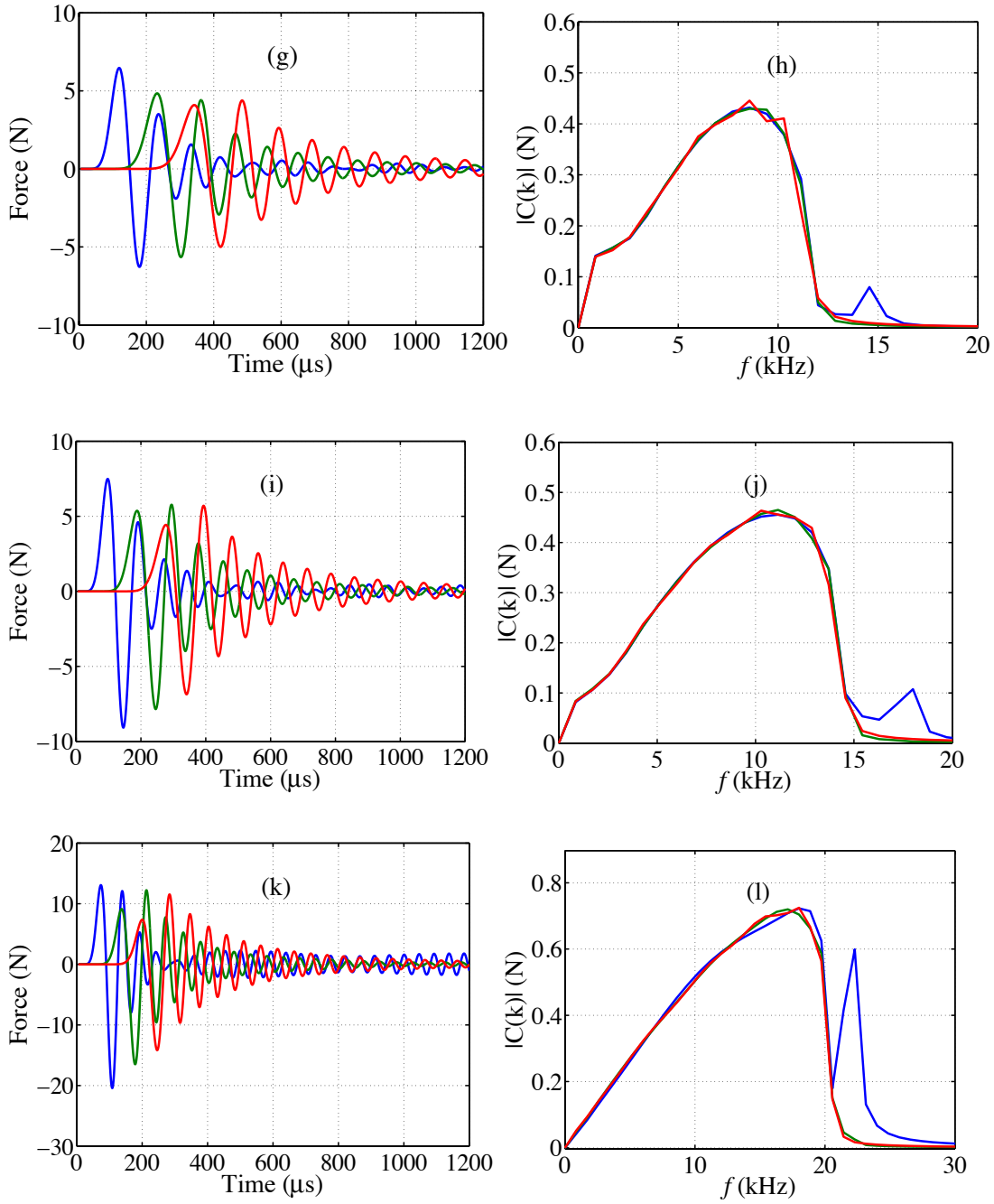

Figure 3.5: Stress pulses obtained in numerical calculations using Model I (without dissipation term between all elements in the system, and using effective elastic modulus E_{eff} = 105 MPa) and their corresponding Fourier spectra in a double power-law system under various preload conditions, continued.

significant decrease of the pulse width with the increasing precompression demonstrated in numerical calculations [e.g., compare Figs. 3.5(a) and 3.5(k)], is due to the nonlinear behavior of this metamaterial reflecting the similar tendency observed in experiments [e.g., compare Figs. 3.2(a) and 3.2(k)].

Table 3.4: Results of the numerical calculation using Model I for speeds ($V+$) and their normalized width [$L_{num,+}/(a-x_0)$] of positive pulses under different static precompression forces.

F_0 (N)	10	30	50	74	106	193
$V+$ (m/s)	127	154	182	222	272	386
$L_{num,+}/(a-x_0)$	4.1	3.9	3.8	3.5	3.5	3.5

Table 3.5: Results of the numerical calculation using Model I for speeds ($V-$) and their normalized widths [$L_{num,-}/(a-x_0)$] of negative pulses under different static precompression forces.

F_0 (N)	10	30	50	74	106	193
$V-$ (m/s)	119	140	166	204	248	342
$L_{num,-}/(a-x_0)$	2.6	2.0	2.0	2.0	2.1	2.2

Due to the dispersion caused by periodic structure of the system, it is observed that a slow decrease of the positive signal amplitude and ramping of their fronts even in the absence of dissipation (Figs. 3.5). In experiments the negative pulses attenuated faster than positive (except at the largest precompression). This behavior is opposite to the tendency in pulse amplitude change in numerical calculations with Model I where their change is solely due to the dispersion. The dependence of attenuation of positive signal amplitude on the depth for Model I is presented in Fig. 3.6 (compare with the

experimental results in Fig. 3.3). From Fig. 3.6, it is found that the rate of attenuation with depth decreases faster at larger precompression forces, this tendency is similar to that observed in experiments.

But the amplitudes of signal in this numerical calculation (Model I) were always larger than the experimental data due to the non-dissipative approach used in the calculations (compare corresponding Figs. 3.2 and 3.5). The significant attenuation observed in experiments (Figs. 3.2 and 3.3) did not match with the attenuation in numerical calculations using Model I (Figs. 3.5 and 3.6). This indicated that the dispersion effects cannot be mostly responsible for the observed attenuation in experiments. Thus the strong attenuation introduced by dynamically deformed Nitrile O-rings cannot be explained in the frame of Model I.

The increase of precompression also results in a shift of frequencies in the FFT spectra toward significantly higher frequencies (under the same impacting condition). For example, at precompression 10 N all frequencies are below 10 kHz [Fig. 3.5(b)] and at precompression 193 N there is a peak at frequency spectrum at 22 kHz, and the propagating pulse has frequency below 20 kHz [Fig. 3.5(l)]. This shift in frequency spectra is similar to that observed in experiments [compare Fig. 3.2(b) and 3.2(l)], though the shape of spectrum is different and in numerical calculations we did not observe the decrease of frequency components in propagating signal, except of frequency peak at larger precompression [Fig. 3.5(l)]. The latter is related to the dispersion effect.

From the presented analysis of the non-dissipative Model I, it can be concluded that it qualitatively describes some features observed in experiments outlined above.

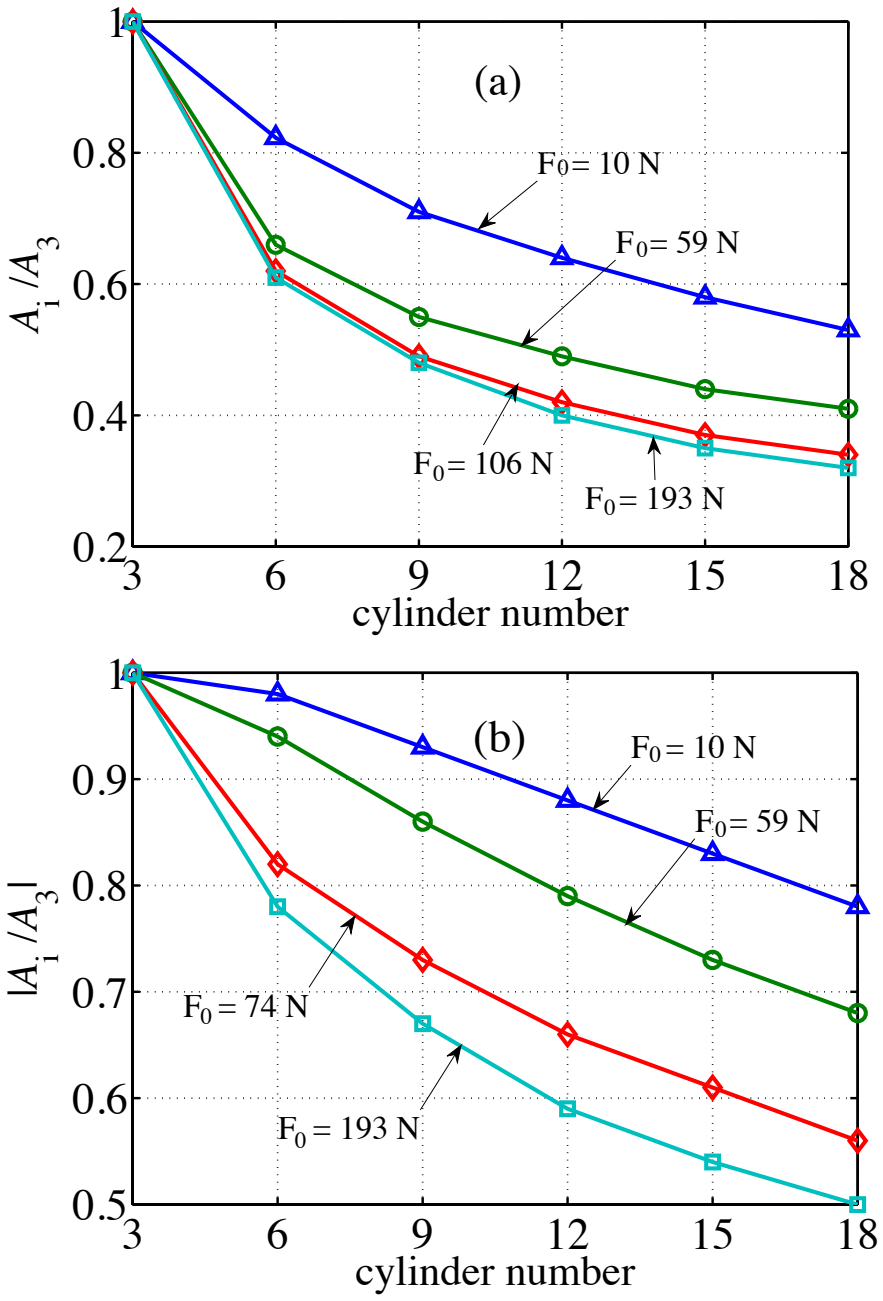

Figure 3.6: Results of the numerical calculations of the attenuation of (a) positive and (b) negative signals with the depth in Model I under different precompression condition (compare with experimental data in Fig. 3.5). A_i is the amplitude of the signal in the *i*-th (*i*=3, 6, 9, 12, 15, and 18) cylinder under different precompression forces: (Δ) 10 N, (O) 59 N, (◊) 106, and (□) 193 N.

But it is clear that this model significantly overestimates the amplitude of the signals, underestimates their attenuation and speed (at higher precompression forces) and it does not explain details of a frequency spectrum especially at the larger precompression. On the other side, a nonlinear dependence of amplitude attenuation on the precompression is observed that in experiments. Thus it is necessary to consider introduction of the nonlinear viscosity into the modeling, which is accomplished in the frame of Model II presented below.

3.4.3 Dissipative model II

In the numerical calculations for the strongly nonlinear viscoelastic model (Model II) we attempted to find out the appropriate combination of two fitting parameters E_d and μ to get a closer agreement with the experimental data related to the rate of leading pulse attenuation, its speed and frequency spectrum. It should be mentioned that the ability to model amplitude and duration of the leading compression pulse is the most important goal for design of protection devices. To simulate experimental conditions at the impacted side of the chain, I introduced slightly different values of μ_C and μ_D, corresponding to various precompression forces, to match the recoil velocity of the striker in numerical calculations with the experimental data. This ensured that a linear momentum introduced into the system in numerical calculations at the impacted end was similar to the experiment.

We explore a combination of constant elastic modulus E_d = 87 MPa with various viscosity coefficient α range from 5 μs to 45 μs, and a combination of a constant viscosity coefficient α = 30 μs with varying elastic modules E_d range from 70 MPa to

105 MPa. The couple E_d=87 MPa and α = 30 μs provided the most satisfactory fit to the experimental data related to the pulse amplitude, speed, width, and rate of attenuation of the signal amplitude. The results of numerical calculations are presented in Fig. 3.7.

The reason why E_d for viscous dissipative Model II is smaller than the effective modulus E_{eff} for purely elastic Model I is that the viscosity term contributes to increase the system effective rigidity and the increases of pulse speed of this metamaterial additionally to the linear elastic term determined by the coefficient K_1 [Eq. (3.6)].

The speeds and widths of the positive and negative pulses calculated in the frame of Model II are presented in Tables 3.6 and 3.7. Compared with experimental results (Tables 3.1 and 3.2), the calculated speed of positive and negative pulses using Model II are in a good agreement at all the precompression forces. The effective negative pulse speed in numerical calculation (Model II) is always lower than the positive pulse speed (Tables 3.6 and 3.7), which is consistent with the observation in experiments. The signal widths calculated in Model II also reproduce the same tendency as in experiments – decreasing with the precompression until the larger static load was applied (> 74 N).

The dependence of attenuation of positive and negative signal amplitude on the depth at different preload conditions for Model II is presented in Fig. 3.8 (compare with the experimental results in Fig. 3.3). Since Model II takes into account a dissipative property and thus more pronounced attenuation of signals amplitude (compare Figs. 3.5 and 3.7) was achieved.

In a separate calculation we found that a classical dashpot model (viscous force does not depend on precompression and linearly dependent on strain rate) cannot

explain the tendency observed in experiments: the faster attenuation of signal amplitude at higher precompression. Such behavior can be explained by the dependence of effective viscosity on precompression as in Model II. More details of the classical linear dashpot model are presented in Appendix A section 2.

It has been seen that numerical calculations using Model II correctly explain a tendency to higher attenuation at higher precompression force being consistent with the experimental results. It should be mentioned that Model I also shows a faster attenuation for larger precompression even without dissipation due to more active dispersion mechanism [Fig. 3.6(a)], although the rate of attenuation was lower than experimental data.

From the comparison of the numerical results obtained using two models and experimental results, it is concluded that the numerical calculations with strongly nonlinear dissipative term (Model II) were able to predict the pulse speed dependence on precompression and attenuation of the leading positive pulse amplitude depending on the precompression. The dissipation term is essential to simulate the strong attenuation. The mechanism of this dissipation most probably is caused by viscoelastic behavior of the rubber O-ring and not by the effects of friction. The dispersion effects only, as shown in Fig. 3.5, did not significantly change the amplitude and shape of the stress. On the contrary to what is observed in experiments, the attenuation of negative pulse is slightly lower than the attenuation of positive part in both numerical models. This may indicate that the dissipation on the loading path is higher than dissipation on the unloading path and on subsequent cycles.

The increase of precompression also results in a shift of frequency in FFT

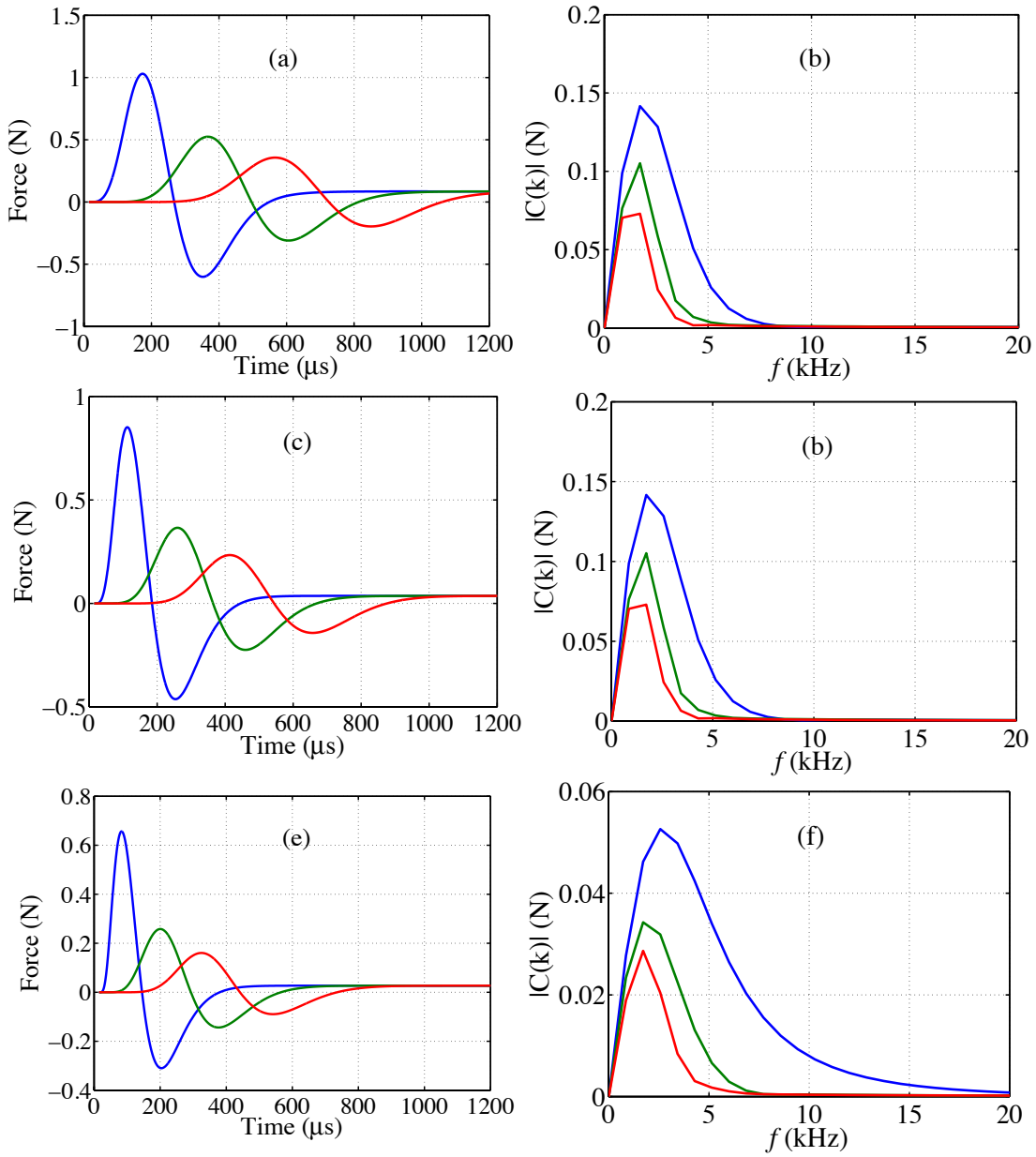

Figure 3.7: Stress pulses obtained in numerical calculations using Mode II (with dissipation term $\alpha = 30$ μs, and using dynamic elastic modulus $E_d = 87$ MPa) and their corresponding Fourier spectra in a double power-law system under various preload conditions: (a),(b) $F_0 = 10$ N; (c),(d) 30 N; (e),(f) 50 N; (g),(h) 74 N; (i),(j) 106 N and (k),(l) 193 N. Curves represent the average dynamic force in the fifth (leading curve), ninth (middle curve), and thirteenth (bottom curve) steel partial.

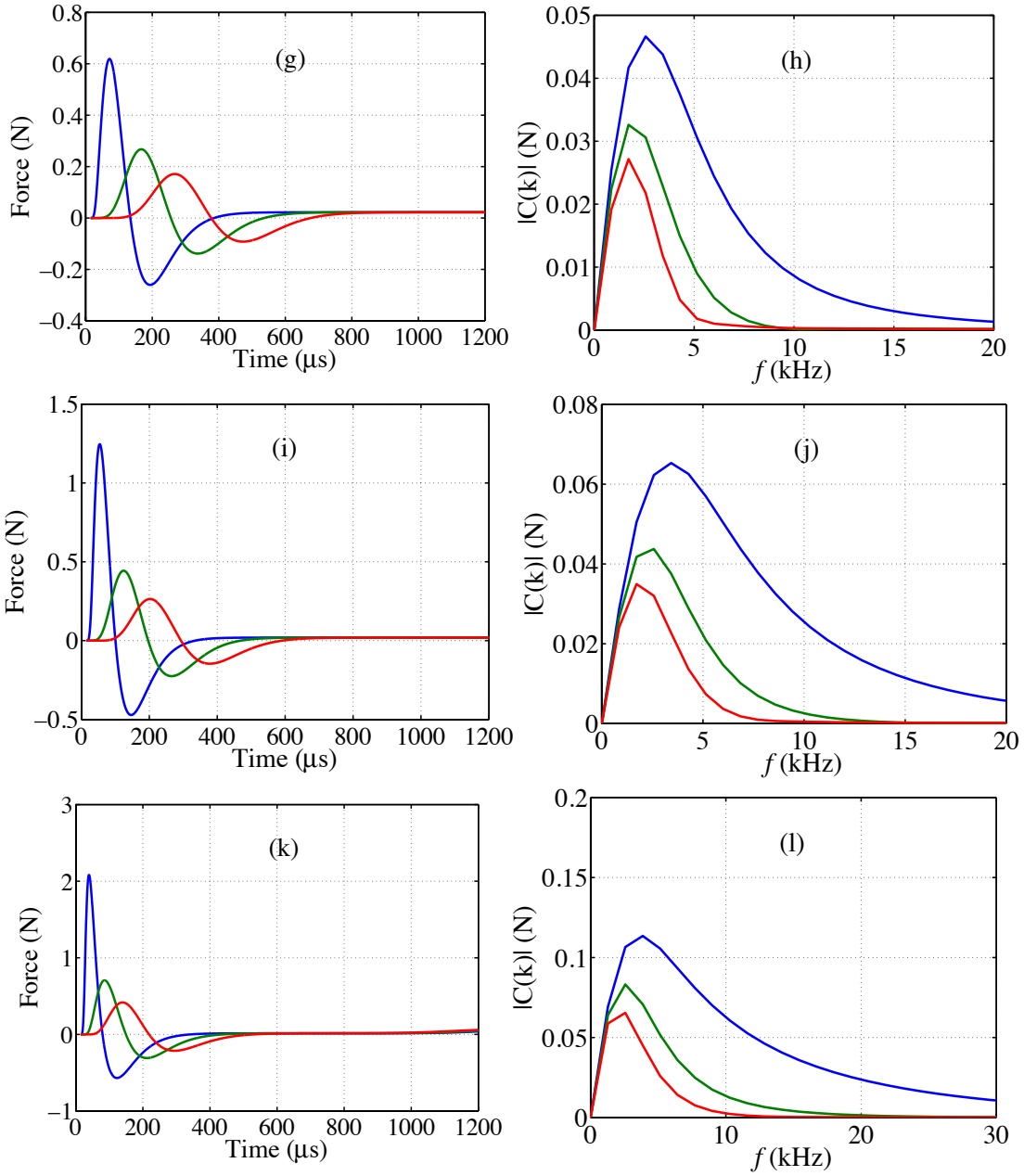

Figure 3.7: Stress pulses obtained in numerical calculations using Mode II (with dissipation term $\alpha = 30$ μs, and using dynamic elastic modulus $E_d = 87$ MPa) and their corresponding Fourier spectra in a double power-law system under various preload conditions, continued.

Table 3.6: Results of the numerical calculation using Model II (E_d = 87 MPa, α = 30 μs) for speeds ($V+$) and normalized width [$L_{num,+}/(a-x_0)$] of positive pulses under different static precompression forces.

F_0 (N)	10	30	50	74	106	193
$V+$ (m/s)	136	170	214	260	320	480
$L_{num,+}/(a-x_0)$	4.6	4.2	4.0	4.5	4.6	5.0

Table 3.7: Results of the numerical calculation using Model II (E_d = 87 MPa, α = 30 μs) for speeds ($V-$) and normalized widths [$L_{num,-}/(a-x_0)$] of negative pulses under different static precompression forces.

F_0 (N)	10	30	50	74	106	193
$V-$ (m/s)	109	132	157	179	218	292
$L_{num,-}/(a-x_0)$	4.4	5.1	5.1	7.0	7.5	9.9

spectra to significantly higher frequencies under the same impact condition as in experiments and in Model I. This shift in frequency spectra is accompanied by the decrease of frequency components amplitude in propagating signal, similar to that observed in experiments. The maximum in frequency spectra in Model II was shifted to lower frequency with signal propagation, unlike it in Model I where it stayed at the same frequency. This tendency picked up by Model II is similar to the observed in experiments though the shape of spectra in experiments and in Model II are different.

However, the numerical results based on Model II have a distinct discrepancy with the experimental data – the dissipation term, which correctly explains the attenuation of leading pulse amplitude completely eliminates the oscillating tail of the pulse at higher precompression forces. This difference is demonstrated by the oscillating character of the signals in experiments after first negative pulse at larger precompression

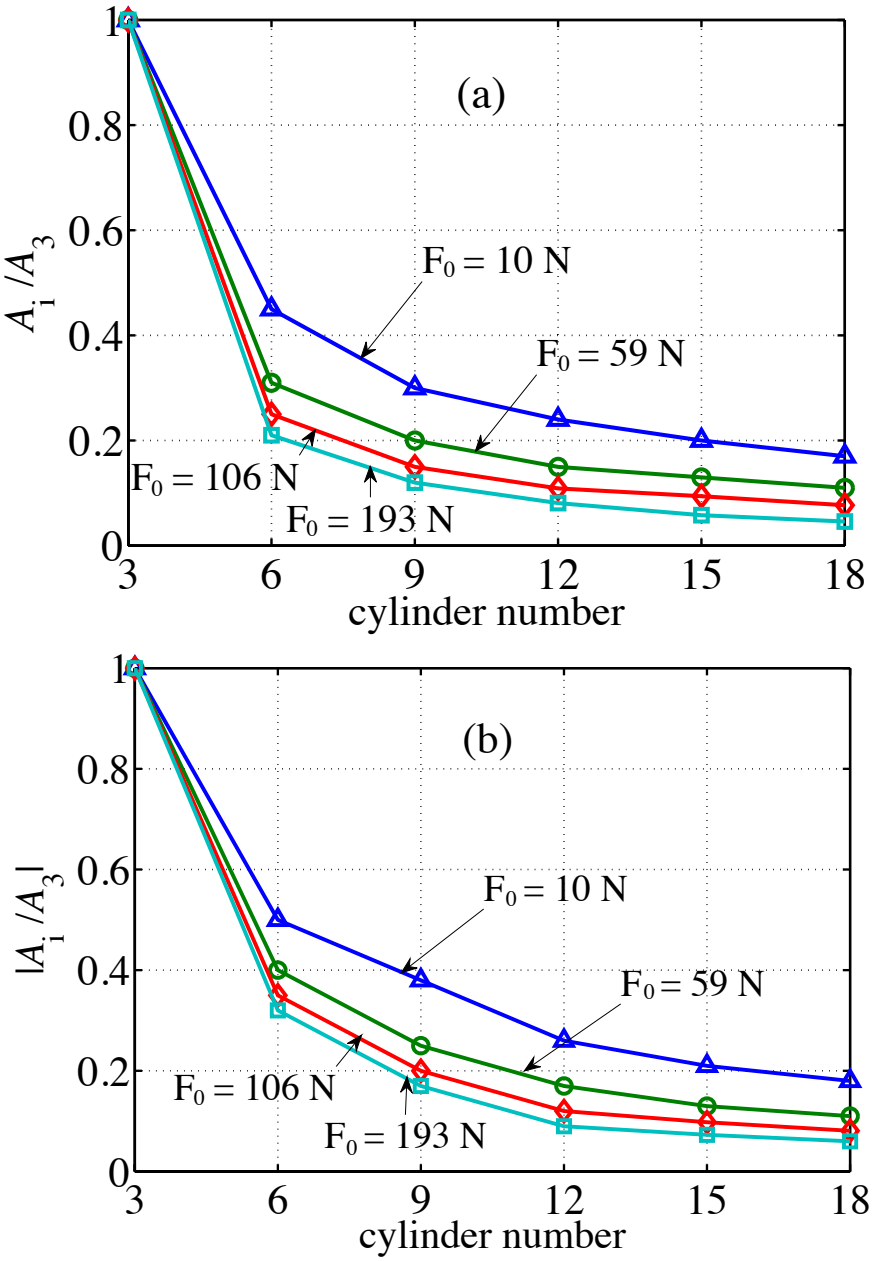

Figure 3.8: The attenuation of positive (a) and negative (b) signals with the depth in Model II under different precompression in numerical calculations. A_i is the amplitude of the signal in the i-th (i=3, 6, 9, 12, 15, and 18) cylinder under different precompression forces: (Δ) 10 N, (O) 59 N, (◊) 106, and (□) 193 N.

forces starting at 50 N [Figs. 3.2(e), 3.2(g), 3.2(i) and 3.2(k)]. It is also very clear from comparison of frequency spectra at larger precompression forces in experiments and in Model II [compare Figs. 3.2(h), 3.2(j) and 3.2(l) with Figs. 3.7(h), 3.7(j) and 3.7(l)].

Thus, Model II predicts an "over damped" behavior of the pulse at higher precompression. It should be emphasized that Eq. (3.4) related to the Model II is based on a quasi-static approach. It requires that the characteristic time of dynamic deformation is much longer than the relaxation time for the dissipative viscoelastic processes in the O-ring [14,15]. In our experiments with largest precompression the rise time of the signal [about 42 μs, Fig. 3.2(k)] is comparable to the relaxation time of O-ring (μ = 30 μs) which provided the most satisfactory fit to the experimental data related to the pulse amplitude, speed, width, and rate of attenuation of the leading signal amplitude. Thus, at largest precompression a quasi-static approach may significantly overestimate dissipative properties resulting in "over damped" behavior in numerical calculations when using Model II.

The oscillating pulse observed in experiments at higher precompression could be qualitatively explained by the increased rigidity of strongly nonlinear O-rings with precompression, which results in an increase of the critical value of damping coefficient describing the transition from under damped to over damped behavior. But the increase of elastic modulus in Model II with precompression (sufficient to explain increase of the signal speed) is not enough to insure the under damped behavior of this metamaterial. This may suggest that Nitrile O-rings have a more complicated viscoelastic behavior than assumed in quasi-static Model II. The probable qualitative explanation may be a path dependent behavior of the O-ring under the cyclic loading (decrease of dissipative

properties of O-ring on the unloading path after the first compression cycle), which is not captured by our quasi-static models.

3.5 Conclusions

The strongly nonlinear dispersive and dissipative properties of the metamaterial composed of the toroidal O-rings and steel cylinders were experimentally and numerically explored based on the measurements of signal speed of the compression pulse, the shape of the pulse and the attenuation of its amplitude. This metamaterial is suitable for impact mitigation because strongly nonlinear elements made from rubber O-rings completely recover even after high-energy impact [11,12]. Thus its dissipative properties can be used for multiple impacts, unlike metamaterials composed from metal spherical particles, where the plastic deformation of contacts is not recoverable.

The signal speed in this metamaterial increases with the precompression force faster than in the chain of elastic spherical particles making it more tunable. The sound speed of this system (and acoustic impedance) could be tuned by a relative small static compression force to the extent which is unattainable at common solids.

The presented experimental approach allowed measurements of the dynamic stiffness of O-rings at very small level of dynamic deformation imposed on the initial static precompression. This is possible because directly measured long wave signal speed in metamaterials is dependent on the derivative of the global stress versus dynamic strain. A similar approach can be used for the evaluation of dynamic modulus of other small-scale elements.

A dramatic increase of dynamic modulus of Nitrile O-rings was observed and

successfully modeled using the strongly nonlinear double power law model. Our results demonstrated that the design of O-rings, which are very important elements with widespread use in machinery, should take into account their dramatic increase of rigidity under dynamic conditions even at low impact velocities.

It was demonstrated that short stress pulse with length around four cell size of the system could be dramatically attenuated and ramped within a very short distance (comparable to the pulse width) due to strongly dissipative behavior of O-rings. This property is very attractive for the design of protective barriers mitigating impact loading. A nonlinear, viscous dissipative quasi-static model explained the nonlinear dependence of amplitude attenuation on the static precompression observed in experiments but at largest precompression a quasi-static approach may significantly overestimate dissipative properties resulting in "over damped" behavior in numerical calculations.

Part of the Chapter 3 has been published in the *Journal of Applied Physics*, **117**, art. 11430, pp. 1-12 by Yichao Xu and Vitali F. Nesterenko. The dissertation author was the primary investigator and author of this paper.

References

[1] E. B. Herbold and V. F. Nesterenko, Appl. Phys. Lett. **90**, 261902 (2007).

[2] E. B. Herbold and V. F. Nesterenko, AIP Conf. Proc. **955**, 231–234 (2007).

[3] I. L. D. Pinto, A. Rosas, A. H. Romero and K. Lindenberg, Phys. Rev. E **82**, 031308 (2010).

[4] A. Spadoni, C. Daraio, W. Hurst and M. Brown, Appl. Phys. Lett. **98**, 161901 (2011).

[5] Y. Xu and V. F. Nesterenko, Philos. Trans. R. Soc. A **372**, 20130186 (2014).

[6] P. B. Lindley, J. Strain Anal. Eng. Des. **1**, 190 (1966).

[7] P. W. Allen, P. W. Lindley and A. R. Payne, *Use of Rubber in Engineering* (Maclaren and Sons, London, 1966), pp. 1–23.

[8] P. K. Freakley and A. R. Payne, *Theory and Practice of Engineering with Rubber* (Applied Science Publishers Ltd., London, 1978), pp.146–165.

[9] S. J. Jerrams, M. Kaya and K. F. Soon, Mater. Des. **19**, 157 (1998).

[10] H. Hertz, J. Reine Angew. Math. **92**, 156 (1881).

[11] C. Lee and V. F. Nesterenko, J. Appl. Phys. **114**, 083509 (2013).

[12] C. Lee and V. F. Nesterenko, J. Appl. Phys. **116**, 083512 (2014).

[13] G. Kuwabara and K. Kono, Jpn. J. Appl. Phys., Part 1 **26**, 1230 (1987).

[14] N. V. Brilliantov, F. Spahn, J. Hertzsch and T. Poschel, Phys. Rev. E **53**, 5382 (1996).

[15] N. V. Brilliantov, A. V. Pimeniva and D. S. Goldobin, Europhys. Lett. **109**, 14005 (2015).

[16] W. Morgado and I. Oppenheim, Phys. Rev. E **55**, 1940 (1997).

[17] C. Daraio, V. F. Nesterenko, E. B. Herbold and S. Jin, Phys. Rev. E **72**, 016603 (2005).

[18] C. Daraio, V. F. Nesterenko, E. B. Herbold and S. Jin, J. Phys. IV France **134**, 473 (2006).

[19] C. Daraio and V. F. Nesterenko, Phys. Rev. E **73**, 026612 (2006).

CHAPTER 4

STRONGLY NONLINEAR WAVES IN STRONGLY DISSIPATIVE SONIC VACUUM

The discrete metamaterial assembled from alternating steel cylinders and Nitrile O-rings, where the strongly nonlinear interacting forces between adjacent particles obey a double power-law, can be described as sonic vacuum when the system is under zero precompression. Impact on this metamaterial will result in unique wave dynamics. This chapter presents the results of numerical and experimental research on the nature of pulses generated by impact in strongly dissipative metamaterial in the state of sonic vacuum.

4.1 Introduction

A one-dimensional discrete metamaterial composed of alternating steel cylinders and polymer toroidal rings represents a new class of metamaterials with strong nonlinearity [1-8]. Recent research shows that this metamaterial has a better potential for shock/impact mitigation combining dispersive properties of periodic discrete system and dissipation from viscoelastic Nitrile O-ring. It can also be used in applications requiring dramatic tuning of acoustic impedances.

Unlike in the well-studied metamaterials composed of rigid elastic steel spheres with the Hertz type of contact interaction [9], the introduction of "soft" element – polymer O-ring, obeying a double power-law $F \propto (\delta^{3/2}+\delta^{6})$ [10-12], results in a higher

sensitivity of pulse speed to the static precompression. Thus this metamaterial has a stronger nonlinearity and greater tunability than the Herzian-type system, where relatively small external forces can significantly tune its behavior. For example, the sound wave speed in this metamaterial increases with the precompression force faster than in the chain of elastic spherical particles making it more tunable [6]. The long-wavelength approximation [13-15] and binary collision approximation [3] were used to predict the pulse propagation behavior in this metamaterial, providing analytic results in both precompression and no precompression cases.

It has been shown that strongly nonlinear solitary and shock waves were supported by the one-dimensional metamaterial composed of steel plates and Teflon O-rings [1]. In both experiments and numerical calculations (without consideration of the dissipation), there is a tendency for an initial pulse to split into a train of solitary waves in this metamaterial. The shape of the solitary wave propagating through this system is observed to be amplitude dependent and highly tunable. Though the dissipation of Teflon O-rings caused some dissipation in experiments, the numerical calculations ignoring the dissipation reasonably estimated the major properties of the oscillatory shock waves and the tendency of the splitting of pulse into trains of solitary waves.

Researchers showed that, in elastically rigid metamaterials composed of metal spheres, the adjustment of geometric and material properties results in a unique phenomenon – tunable band gaps, where signals decay exponentially within certain frequencies. This characteristic was experimentally verified in the metamaterials composed of alternating steel cylinders and linear elastic O-rings made of polytetrafluoroethylene (PTFE) [3]. Besides, this metamaterial permits load-bearing

capabilities, its acoustic response can be controlled and tailored by the external static precompression.

More recently, the metamaterial composed of steel cylinders and Nitrile rubber O-rings was proposed and investigated [4-8]. Nitrile O-rings are much softer than Teflon O-rings and have a better potential for the high-energy absorption and smaller speed of signal propagation. Compared with the traditional metamaterials composed of elastic spherical particles, this system with toroidal Nitrile O-rings is more tunable and exhibits more dissipative behavior. However, the dynamic behavior of Nitrile O-rings is not thoroughly studied, only few papers were published where the complex dynamic behavior of Nitrile O-rings under impact was investigated [4-8]. It was found that during a single impact test the dynamic stiffness of uncompressed Nitrile O-rings increased about three times in comparison with the value from quasi-static compression loading [5]. The numerical modeling used to analyze and explain the dynamic behavior of the uncompressed O-rings under impact also confirmed the influence of strain-rates on the dynamic response.

It should be mentioned that previous investigation of the metamaterial composed of steel cylinders and polymer toroidal rings neglect the dissipation of polymer, though there were some discrepancies in the experiments and numerical estimation. In the metamaterial composed of steel cylinders and Nitrile rubber O-rings, the dissipation due to the dynamic deformation of viscoelastic Nitrile rubber O-rings plays a significant role in the propagation of stress pulses [6,7]. It was found that the attenuation of signal positive amplitude due to the viscos dissipation of Nitrile O-ring shows a strong dependence on the compression force, the larger the static precompression the faster the

attenuation of pulse amplitude [7]. The comparison of experimental data with numerical calculations using different models (non-dissipative, linear dashpot and nonlinear dissipative model following Brilliantov *et al*. approach [16,17]) also demonstrated the importance of the nonlinear viscous dissipation to describe the major properties of propagating pulses [6,7].

This chapter studies the effects of dissipation on the wave profile of the metamaterial composed of alternating steel cylinders and Nitrile O-rings without precompression. In case of zero precompression this system is characterized as "sonic vacuum". The following aspects of the behavior of stress pulses excited by the striker impact in sonic vacuum will be focused on: (a) the stress pulse speed dependence on its amplitude; (b) the relevance of dissipation and dispersion for the transformation of wave profile; (c) the unusual transfer of linear momentum and energy from the striker to the "soft" metamaterial. The experimental observation and different numerical models have been used to investigate the dynamic behavior of this strongly nonlinear metamaterial with no precompression.

4.2 Theoretical Analysis

Consider a one-dimensional metamaterial composed of N steel cylinders alternated by Nitrile O-rings with no precompression (Fig. 4.1). The small Nitrile O-rings are considered as massless nonlinear springs based on the large ratio of mass of steel cylinder to the mass of Nitrile O-ring.

The quasi-static force between the contact particles is described by a double power-law [10-12]. A non-dissipative equation of cylinders motion in this strongly nonlinear

system is presented below:

$$\ddot{x}_i = A[(x_{i-1} - x_i)^{\frac{3}{2}} - (x_i - x_{i+1})^{\frac{3}{2}}] + B[(x_{i-1} - x_i)^6 - (x_i - x_{i+1})^6], \quad (4.1)$$

where x_i denotes the displacement of the i-th cylinder from its equilibrium positions in the system without precompression, and $A = 1.25\pi D_{\mathrm{m}}\, E_{\mathrm{imp}}/md^{1/2}$, $B = 50\pi D_{\mathrm{m}}\, E_{\mathrm{imp}}/md^5$, d and D_{m} are the initial cross section and mean diameter of the O-rings. The equivalent elastic modulus of Nitrile rubber O-ring in the propagating wave generated by impact (E_{imp}) on the uncompressed system is different from its static value E_0 due to a possible frequency dependence of the dynamically deformed O-ring. It also can be different than the elastic modulus E_{eff} introduced in chapters 2 and 3 and related to the elastic behavior of O-ring in the vicinity of statically precompressed state.

At relative small strains investigated in this chapter (less than 0.3), the system still obeys Hertzian type interaction law, i.e., the dependence of force on the height of deformed O-ring obeys Hertzian behavior [first term on the right in Eq. (4.1) with exponent 3/2]. Without considering the dissipation of O-rings, this metamaterial in sonic vacuum state supports the Nesterenko solitary wave. Its speed Vs in long wave approximation is determined by the amplitude of the dynamic force (F_{m}) [15]:

$$V_{\mathrm{s}} = \frac{2}{\sqrt{5}} a A^{1/3} m^{-1/6} F_{\mathrm{m}}^{1/6}, \quad (4.2)$$

where a (=h+d, and h is the height of steel cylinder) is the distance between the centers of neighboring cylinders.

To include the dissipation, the viscous term should be added to Eq. (4.1) [7]. The presence of dissipation allows propagation of another, shock-like stress wave with speed different than the speed of the solitary wave. The speed of the stationary shock

like stress wave with force F_{sh} in the equilibrium state has the following expression (independent on the type of dissipation):

$$V_{sh} = aA^{1/3}m^{-1/6}F_{sh}^{1/6}. \quad (4.3)$$

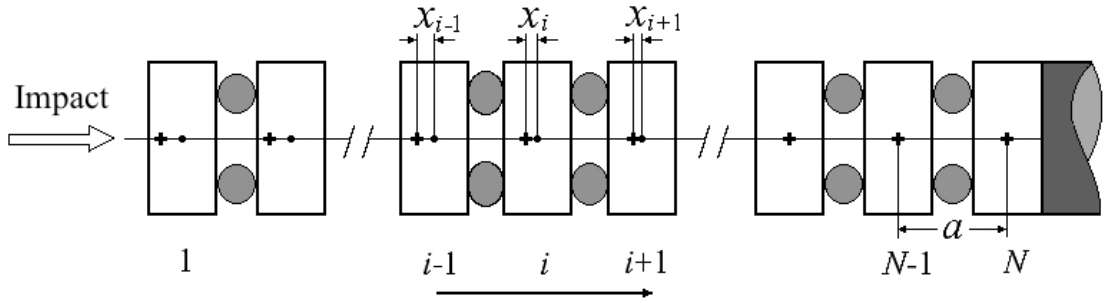

Figure 4.1: A schematic representation of wave propagation in one-dimensional metamaterial composed of N steel cylinders alternated by Nitrile O-rings without initial compression force. The value of a is the distance between centers of neighboring steel cylinders in the uncompressed chain in front of propagating wave and x_i is the displacement of the i-th steel cylinder from its position in the uncompressed chain caused by wave propagation. The crosses show the initial positions of cylinder centers in the uncompressed chain. The solid dots correspond to the position of the cylinder centers in the wave. At the bottom the arrow shows the direction of impulse propagation, the left part of the chain is unloaded but first and second cylinders are still in contact (depending on the impact conditions they can be separated) and the right part is not loaded yet.

The above Eqs. (4.2) and (4.3) describe speeds of different type of waves in a non-compressed metamaterial ("sonic vacuum"). It is interesting that in case of $F_m = F_{sh}$, V_s is smaller than V_{sh}, so the material behavior in solitary wave is "softer" than in a shock wave with the same amplitude. Equations (4.2) and (4.3) are based on the assumption that the elastic properties of the O-ring and the Hertzian nonlinearity are the same during the whole cycles of O-rings dynamic deformation including loading and unloading.

If this metamaterial is statically precompressed then its static deformation is determined by the elastic modulus E_0, which can be significantly different from its values characterized for dynamic deformation E_d and E_{imp}. Moreover, the last two elastic moduli even at the same level of overall global strains can be different due to the difference in the corresponding loading paths [5]: elastic modulus E_d is related to small dynamic strains about statically precompressed state and E_{imp} is describing the elastic behavior of an initially uncompressed O-ring.

To describe the small dynamic deformation of O-rings at the vicinity of initially precompressed state, a linear elastic dynamic response, depending on the initial precompression, was introduced in Ref. [6]:

$$F_{el} = A_0 m {x_0}^{3/2} + B_0 m {x_0}^6 + K x_d, \tag{4.4a}$$

$$K = 1.5(1.25\pi D_m E_{eff} d^{-1/2}) x_0^{1/2} + 6(50\pi D_m E_{eff} d^{-5}) x_0^5, \tag{4.4b}$$

where x_0 is the initial change of height of O-ring due to the static precompression force, and x_d is the dynamic deformation of O-ring during the wave propagation in the precompressed system.

These equations result in the following equation for the sound speed in the precompressed chain [6]:

$${c_0}^2 = K a_1^2/m = a_1^2\left[1.5 A_{eff} (x_0)^{1/2} + 6 B_{eff} (x_0)^5\right], \tag{4.5}$$

where $A_{eff} = 1.25\pi D_m E_{eff}/m d^{1/2}$, $B_{eff} = 50\pi D_m E_{eff}/m d^5$. And a_1 (=h+d-x_0) is the cell size in the precompressed system. The values of sound speed at different precompression were much larger than the values predicted using the static elastic modulus of O-rings E_0, because E_{eff} is much larger than E_0 [6].

It is interesting to compare the speeds of shock wave [Eq. (4.3)] and Nesterenko

solitary waves [Eq. (4.2)] in the uncompressed metamaterial with the sound speed (or speed of stress wave with relatively small amplitude) in the compressed chain at the similar overall forces (including static precompression). This helps to compare the effective elastic properties of O-rings characteristic for different loading paths. Due to the domination of the Hertzian type behavior at relatively small deformation of O-rings the second term in Eq. (4.5) is about 0.09% and 7.15% of the first term at static forces F_0 equal 10 N and 30 N correspondingly. If O-rings obey the Hertzian behavior and the amplitude of force in the wave is much smaller than the static precompression force, then the sound speed (or the speed of stress wave with relatively small amplitude) measured in Ref. [6] is equal to:

$$c_0 = \sqrt{\frac{3}{2}} a_1 \left(\frac{A_d^{1/2}}{A_0^{1/6}}\right) m^{-1/6} F_0^{1/6}. \tag{4.6}$$

The coefficient $A_0 = 1.25\pi D_{\mathrm{m}} E_0 / m d^{1/2}$ relates the change of height of the O-ring (x_0) to the static force F_0 using static elastic modulus E_0 of Nitrile O-ring (according to Ref. [6], E_0 = 7.6 MPa). It should be mentioned that the sound speed c_0 in Eq. (4.6) is not the sound speed in the steel cylinder or speed in the material of O-rings. It is a long wave sound speed in metamaterial where steel cylinders are considered as rigid bodies and O-rings obey the Hertzian behavior.

The speed of the sound at statically precompressed system [Eq. (4.6)] can be larger than the speed of shock like stress wave in the uncompressed system [Eq. (4.3)] with dynamic force amplitude equals the static precompression force in the former system. The difference can be caused by the possible significant difference between E_{imp} and E_{d} due to different loading paths (the difference between a and a_1 in the Hertzian

system is small). But even if elastic moduli are the same there is still a significant difference between c_0 and V_{sh}. If amplitude of shock in uncompressed system is equal to the static precompression force in compressed system (F_{sh}=F_0=30 N), the ratio of corresponding speeds of waves propagation in these systems is equal to c_0/V_{sh} =1.9 (assume E_{imp}=E_d=105 MPa).

In the numerical calculations we investigated the role of two different mechanisms (geometrical dispersion and dissipation) on the pulse shape and amplitude in sonic vacuum. In the non-dissipative chain represented by Eq. (4.1), waves with relatively short wavelengths may be transformed only due to the dispersion mechanism. In a dissipative chain with a linear dashpot a dissipative term depends on the relative velocity between neighboring particles with an effective viscosity coefficient μ. This coefficient is a fitting parameter found by comparison with experimental results. The corresponding equation of cylinder motion in this initially non-compressed system is:

$$\ddot{x}_i = A\left[(x_{i-1}-x_i)^{\frac{3}{2}} - (x_i - x_{i+1})^{\frac{3}{2}}\right] + B[(x_{i-1}-x_i)^6 - (x_i - x_{i+1})^6] + \frac{\mu}{m}(\dot{x}_{i-1} - 2\dot{x}_i + \dot{x}_{i+1}). \quad (4.7)$$

In this paper we explore if this approach can be applied for the dynamic behavior of the dynamic deformation in a large amplitude stress waves propagating in sonic vacuum.

4.3 Experimental Procedure, Results and Discussion

4.3.1 Experimental setup

The experimental setup is shown in Fig. 4.2. It has a frame holding the hollow

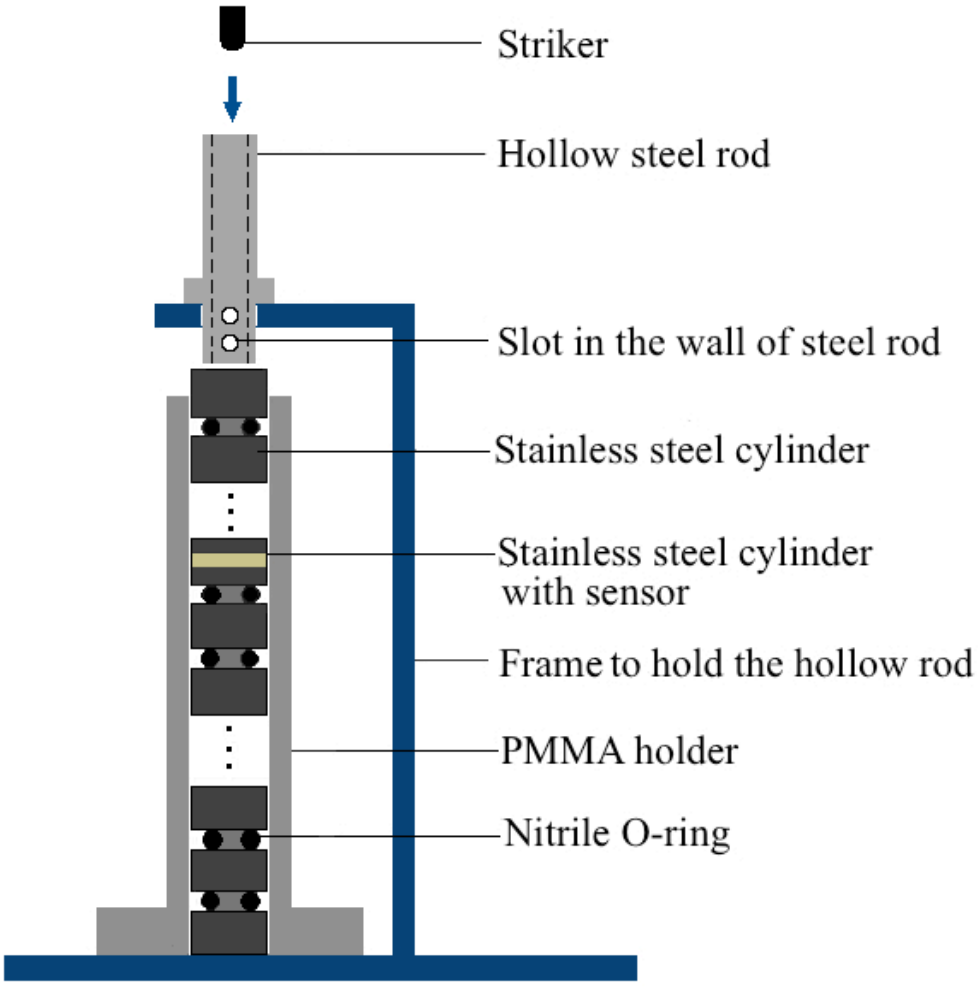

Figure 4.2: Experimental setup showing one-dimensional metamaterial composed of alternating stainless steel cylinders and Nitrile O-rings. The hollow steel rod was used to guide the striker. It has two slots near the end to measure the impact velocity of the striker by using the high-speed camera. Three piezo sensors are placed in the ninth, thirteenth and seventeenth cylinders.

steel rod (aligned with the chain) to guide the striker with two slots at the end. These slots were used to measure the impact velocity of the striker just before its impact with the top end of the chain using high-speed camera (Phantom V12). The vertical PMMA tube is used as a holder to assemble the one-dimensional metamaterials consisting from 33 stainless steel cylinders (height h = 5mm, diameter 10 mm, and mass 3.065 g) and 32 Nitrile O-rings (with a cross-section diameter d = 1.78 mm, mean diameter D_m = 6.22 mm, and mass 0.0625 g). The system was only under gravitational precompression, which played a negligible role in stress wave propagation at investigated amplitudes. Three piezo gauges were placed inside the ninth, thirteenth and seventeenth steel cylinders to measure the dynamic forces.

The stress pulses were generated by the impact of four different strikers (2.38 mm radius steel tip) with varying masses (Striker 1-0.455 g, Striker 2-3.236 g, Striker 3-9.308 g and Striker 4-30.718 g) on the top steel cylinder of the chain. The initial velocities of the strikes were measured (using images from high-speed camera) to be 2.24 m/s, 2.43 m/s, 2.53 m/s and 2.59 m/s for Striker 1, Striker 2, Striker 3 and Striker 4, respectively. Images from high-speed camera were also used to capture the details of the interaction between striker and top steel cylinder (displacements and separation of the striker from the top cylinder).

The forces inside cylinders in transmitted stress waves were measured using three calibrated piezo gauges (RC of the electrical circuit ~ 5.24 ms) connected to an oscilloscope (Tektronix TDS2014).

4.3.2 Properties of attenuating stress waves and comparison of experimental data and theoretical predictions

The experimentally detected stress wave profiles (Fig. 4.3) were generated by strikers with different masses and similar velocities (with the intention to generate the incoming pulses of different durations and amplitudes).

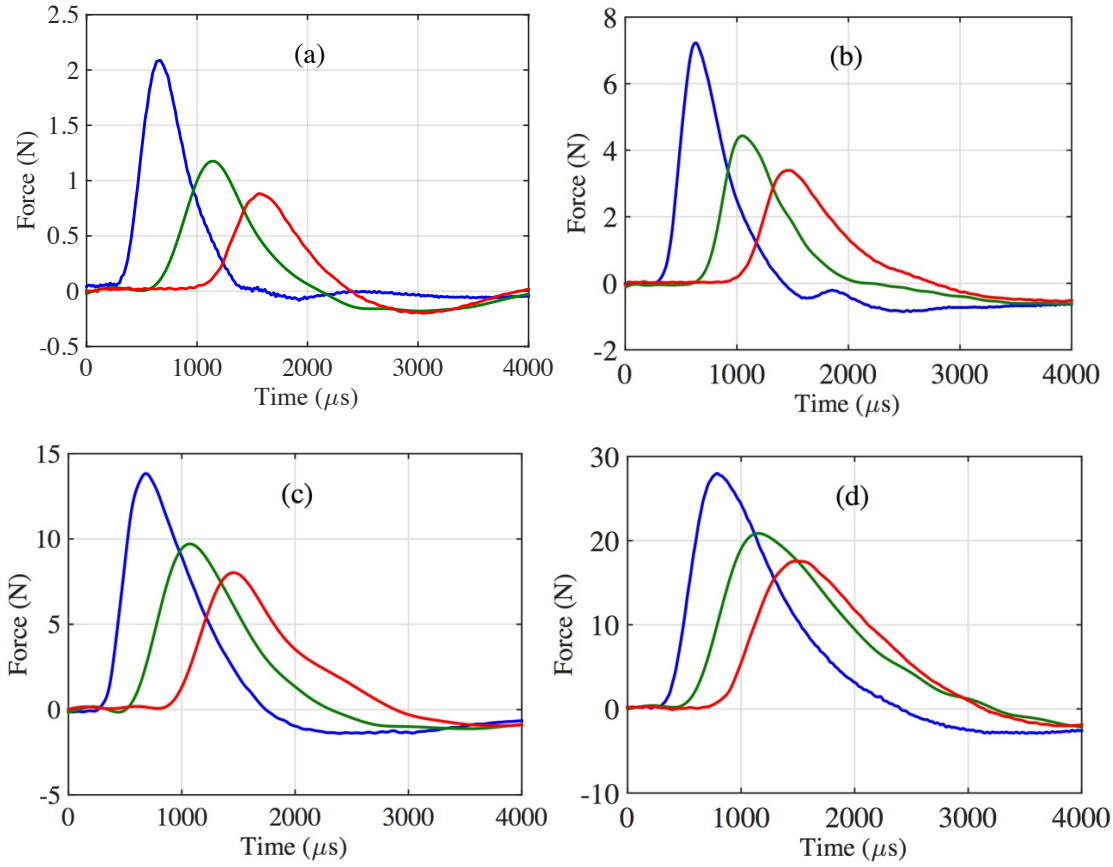

Figure 4.3: Attenuation of waves with different amplitudes in uncompressed chain composed of alternating stainless steel cylinders and Nitrile O-rings. The system was impacted by four different strikers: (a) 0.455 g Striker with a 2.38 mm radius having a velocity of 2.24 m/s; (b) 3.236 g Striker with a 2.38 mm radius steel tip having a velocity of 2.43 m/s; (c) 9.308 g Striker with a 2.38 mm radius steel tip having a velocity of 2.53 m/s; (d) 30.718 g Striker with a 2.38 mm radius steel tip having a velocity of 2.59 m/s. Three piezo gauges were embedded in the ninth (leading signal), thirteenth (middle signal), and seventeenth (last signal) steel cylinders to record dynamic forces.

The properties of the detected stress waves are presented in the Table 4.1 below. In this table parameters V_{exp}(m/s) 9-13 or V_{exp} (m/s) 13-17 correspond to the signal speed

measured by propagation time and distance between 9 and 13 cylinders with embedded gauges. Parameters A_n, T_n, L_n, $T_{FWHA,n}$, $L_{FWHA,n}$, $T_{f,n}$, and $L_{f,n}$ are corresponding to the signal amplitudes, total positive phase of pulse duration, the space span of the positive pulse, the full time width at half of the maximum amplitude, full space width at half amplitude, the duration of the front and corresponding front width based on measurements by gauges embedded into *n*-th cylinder. The full time or space width at half maximum amplitude is introduced to minimize the role of the negative signal at the end part of the pulse which is not of mechanical origin though it is often present in other research using similar type of sensors [18].

It is interesting that the increase of the striker mass by 67 times (compare the mass of Strike 1 and Striker 4) resulted in the increase of pulse duration only two times. The duration of positive phase of pulses demonstrates a tendency to increase with their propagation more noticeable for lower amplitude incoming pulses generated by small mass strikers.

The range of dynamic amplitudes of compression pulses (2-27 N) in sonic vacuum, presented in Fig. 4.3, is significantly larger than the dynamic amplitudes of pulses in strongly precompressed system (0.28–0.68 N, signal in the 9th cylinder [7]) corresponding to the static precompression forces 10-193 N. In the former case pulses had durations in the interval 1000 μs to 2000 μs and ramp times 400-500 μs unlike in the latter case where the compression pulses had much smaller durations 340-80 μs and the corresponding ramp times 220–50 μs [7]. Thus the deformation paths of O-rings investigated in this paper are very different than the small amplitude waves in the same metamaterial but strongly precompressed [6,7].

Table 4.1: Experimental data for speed (V_{exp}), amplitude (A_n), duration (T_n) of the positive phase of the pulse, full time width at half maximum amplitude T_{FWHA}, normalized full space width at half maximum amplitude ($L_{FWHA,n}/a$), and normalized width of positive phase of pulse (L_n/a) of the compression stress waves detected in the ninth, thirteenth, and seventeenth cylinder of the metamaterial excited by different strikers.

Striker mass (g)	**0.455g**	**3.236g**	**9.308g**	**30.718g**
V_{exp}**(m/s)**	55±3	66±4	70±5	75±5
T_9 **(μs)**	1152	1132	1452	2080
L_9/a	9.3	11.0	15.0	23.0
$T_{FWHA,9}$ **(μs)**	452	424	648	816
$L_{FWHA,9}/a$	3.7	4.1	6.7	9.0
$T_{f,9}$ **(μs)**	392	368	412	501
$L_{f,9}/a$	3.2	3.6	4.3	5.5
T_{13} **(μs)**	1472	1416	1764	2696
L_{13}/a	11.9	13.8	18.2	29.8
$T_{FWHA,13}$ **(μs)**	628	564	788	1136
$L_{FWHA,13}/a$	5.1	5.5	8.1	12.6
$T_{f,13}$ **(μs)**	552	424	548	688
$L_{f,13}/a$	4.5	4.1	5.7	7.6
T_{17} **(μs)**	1458	1800	1828	2456
L_{17}/a	11.8	17.5	18.9	27.2
$T_{FWHA,17}$ **(μs)**	642	676	786	1180
$L_{FWHA,17}/a$	5.2	6.6	8.1	13.1
$T_{f,17}$ **(μs)**	616	556	626	812
$L_{f,17}/a$	5.0	5.4	6.5	9.0
A_{13}/A_9	0.56	0.60	0.69	0.73
A_{17}/A_9	0.41	0.46	0.56	0.63

It is interesting that the sonic vacuum (uncompressed system) is less dissipative than the statically precompressed chain based on the rate of amplitude attenuation. This is evident from the comparison of pulse amplitudes decay at the comparable overall forces (dynamic amplitude of the wave investigated in this paper versus static precompression plus dynamic force in the latter). For example, in Fig. 4.3(c), the dynamic amplitude of leading wave in the uncompressed chain is 13.84 N, which can

be compared with the overall force 10.7 N (sum of static precompression force 10 N and amplitude of wave about 0.7 N) in chapter 3. In the sonic vacuum the leading pulse is attenuated by 30% after the propagation of waves through four cell sizes (from the ninth cylinder to thirteenth cylinder). While in the precompressed system, it is reduced by 44% travelling through the same distance (four cells, from the ninth cylinder to the thirteenth cylinder). Similar behavior is observed when the experimental results presented in Fig. 4.3(d) are compared with the wave amplitude propagating in the precompressed chain by static force 30 N. The amplitude of leading pulse in the ninth cylinder (27.98 N) in former cases attenuated by 27% in four cell size comparing to the attenuation rate 55% in the precompressed system (the stress wave propagated from the ninth to the thirteenth cylinder).

Despite the increased amplitude of leading pulse in experiments in sonic vacuum the attenuation rate of the stress wave amplitude decreased from 44% [Fig. 4.3(a)] to 27% [Fig. 4.3(d)]. This behavior is in drastic contrast with the increase attenuation of pulse with the increase of static precompression force [7] demonstrating a qualitatively different behavior of O-rings in different loading paths.

Behavior of O-rings starts to deviate from the Hertzian law (with exponent 3/2 for the force dependence on displacement) at force above 50 N [6]. In experiments presented in this paper the stress wave amplitudes are in the interval 2-28 N (Fig. 4.3). Thus the interaction law caused by the compression of O-rings can be considered as Hertzian type if they follow the static behavior.

The characteristic size of single Nesterenko solitary wave in a non-dissipative Hertzian chain, which supposed to be generated by the striker with mass less or equal

the mass of the cell in the system (e.g., striker mass 0.455 g and 3.236 g), is supposed to be equal to 5 particles (or cells) and the solitary wave front is composed from 2.5 particles (or cells) [15]. The obtained normalized width of the stress wave front in experiments ($L_{f,9}/a$, Table 4.1) is close to 3.2-3.6 cell sizes, which is larger than the expected for the solitary wave front in a Hertzian chain. The length of the positive phase of the stress wave is about two times larger than the expected solitary wavelength corresponding to the chain with Hertzian type force between masses. Thus the detected compression pulse is not a Nesterenko solitary wave expected in the chain with a Hertzian interaction law between masses under the short duration of impact. This deviation from the behavior of non-dissipative chain with masses interacting by the Hertz law is probably due to the dissipation, thus this propagating pulse is more like shock like stress waves.

It may be also explained if the dynamic behavior of O-rings is less nonlinear than the Hertzian interaction and characterized by the dependence of the force on displacement with exponent less than 3/2. The solitary wave has increased length (L_n) for smaller values of exponents n [15], as clear from the following equation:

$$L_n = \frac{\pi a}{n-1}\sqrt{\frac{n(n+1)}{6}}. \tag{4.8}$$

When the exponent $n<3/2$, the value of the solitary wave length L_n is larger than the solitary wave length $\sqrt{\frac{5}{2}}\pi a \approx 5a$ corresponding to exponent 3/2. The values of solitary wave lengths equal $9.3a$ and $11a$ correspond to exponent values equal 1.23 and 1.19.

The Nesterenko solitary wave in a sonic vacuum [at any values of exponent n,

see Eq. (4.8)] has a length which is independent on its amplitude [15]. But in our experiments we observed the increase of the length of the pulses with the amplitude increase [compare Figs. 4.3(a) and 4.3(b) and the corresponding data in Table 4.1 related to the striker masses 0.455 g and 3.236g, which supposed to generate a single solitary waves]. Thus properties of these stress pulses do not correspond to the Nesterenko solitary wave expected from a power law type deformation of O-rings even at lower values of exponent n. Thus the observed behavior in general cannot be explained by the decreased nonlinearity of dynamically deformed O-rings.

The impact of striker with mass significantly larger than the mass of cell in the non-dissipative strongly nonlinear Hertzian chain generates a train of multiple Nesterenko solitary waves at relatively short distances from the entrance (10-20 cells [15]). But this behavior is not observed in the experiments with striker masses 9.308 g and 30.718 g. This demonstrates that the dissipation dominates the response of strongly nonlinear discrete system suppressing the role of dispersion.

The type of nonlinear interaction law between masses in strongly nonlinear system determines not only the size of the solitary wave being independent on the amplitude, but also the dependence of solitary wave and shock wave speeds on their amplitudes.

The dependence of the small amplitude stress pulse speed on the static precompression force is following the expected from Hertzian interaction [15], but we may expect a different behavior of uncompressed O-rings under the different path of dynamic deformation.

The shock wave speed for power law interaction $V_{sh,n}$ from Ref. [15] can be

transformed to the following equation representing the speed dependence on the maximum force F_m:

$$V_{sh,n} = aA_n^{1/2n} m^{-(n-1)/2n} F_m^{(n-1)/2n}. \quad (4.9)$$

The coefficient A_n is similar to the coefficient A in Eq. (4.1) only for the case when exponent 3/2 is replaced with exponent n.

The strongly nonlinear stress pulses in experiments exhibited an increase of the propagation speed with the increase of their amplitude – from 55±3 m/s [averaged on the distance between 9th and 13th cylinders, where pulse amplitude was in the interval 2.03-1.15 N, Fig. 4.3(a) generated by the lightest striker with mass 0.455 g] to 75±5 m/s [averaged on the same distance at pulse amplitude in the interval 26.97-19.56 N, Fig. 4.3(d) generated by the impact of heaviest striker with mass 30.718 g]. We can estimate the value of exponent n in Eq. (4.9), which will provide the observed weak dependence of the speed of the pulses with their amplitude F_m, assuming that the deformation of O-ring results in a power law interaction between cylinders. The corresponding values of exponent n is 1.323±0.1633, based on the ratio of average amplitudes F_m of the stress waves [using Eq. (4.9)] in the 9th and 13th cylinders generated by Strikers 1 (1.59 N) and 4 (23.27 N) and pulse speeds (55±3 m/s and 75±5 m/s, correspondingly).

The estimated value of the exponent in the dependence of the wave speed on its pulse amplitude is consistent with the theoretical expectation of the dependence of strongly nonlinear shock wave speeds on its maximum amplitude in a Hertzian-type system with the elastic modulus not depending on the amplitude of pulse [15]. The comparison between the measured nonlinear stress pulse speed and the theoretical shock wave speeds [corresponding to Eq. (4.3)] are presented in Table 4.2 for different values

of elastic modulus.

Table 4.2: Comparison of the experimental measurements of pulse speed (V_{exp}) measured between the 9th and 13th cylinders and the calculated theoretical value of shock wave speeds [V_{sh}, using Eq. (4.3)] in an elastic Hertzian chain with various elastic modulus E_{imp}.

Striker number/mass (g)	**Amplitude $(A_9+A_{13})/2$ (N)**	**V_{exp} (m/s)**	**E_{imp}=7.6 MPa**	**E_{imp}=87 MPa**	**E_{imp}=105 MPa**
			V_{sh}	V_{sh}	V_{sh}
1/0.455	1.59	55±3	21.7	48.9	52.0
2/3.236	5.41	66±4	26.6	59.9	63.8
3/9.308	11.68	70±5	30.2	68.1	72.5
4/30.718	23.27	75±5	33.9	76.4	81.4

Data in the Table 4.2 demonstrate that we have very large difference in the predicted speeds of the strongly nonlinear pulses in sonic vacuum and experimental data if we use the static elastic modulus for O-ring (7.6 MPa). We can see that the pulse speed in the sonic vacuum can be satisfactory described by the elastically nonlinear interaction caused by deformation of O-rings with effective elastic modulus 105 MPa. The situation is similar to what was observed in the estimation of long-wave sound speed in the similar, but precompressed system [6]. In statically compressed chain we have initial strain ξ_0, which we reached through the static deformation with elastic modulus 7.6 MPa. If we have a small dynamic deformation added to this value we must use much stiffer response, still based on the elastic Hertzian law, with larger effective elastic modulus 105 MPa [6]. But this approach is not able to explain the attenuation of the pulse amplitude.

Dynamic modulus E_d=87 MPa in combination with viscous dissipation (providing additional input into the "rigidity") used in Brilliantov approach [7] provided

a reasonable estimation for the value of sound speed and the amplitude attenuation in the precompressed chain.

In uncompressed chain we drive system in single pulse from zero strain to the similar maximum strain $\xi_m=\xi_0$. If we include viscous dissipation producing additional contribution to the stiffness we need smaller effective elastic modulus 87 MPa (Brilliantov *et al.* approach [7]) to explain the dependence of the pulse speed on the precompression and its attenuation.

It is interesting to compare the speed of these shock like stress pulses in sonic vacuum with the long-wave sound speed in the same metamaterial being strongly precompressed assuming nonlinear elastic behavior with the same modulus. We can see that the sound speed in statically precompressed chain at precompression force 30 N is equal to 165±9 m/s and the speed of the stress wave in the uncompressed chain with similar amplitude of dynamic force is equal to 75±5 m/s. Their ratio is equal to 2.22±0.27 which is close to the expected ratio of 1.89 [based on the comparison of Eqs.(4.3) and (4.6) applicable for the nonlinear elastic chain with constant elastic modulus of O-rings].

4.4 Numerical Calculations

Numerical calculations modeling experimental set up shown in Fig. 4.2 were conducted using MATLAB.

In the first numerical approach we consider the non-dissipative interactions between elements in the chain and between the striker and the top cylinder (referred as Model I). The steel cylinders were treated as rigid bodies connected by the nonlinear

spring according to a double power-law [Eq. (4.1)]. The striker in numerical calculations was given initial velocity (2.24 m/s, 2.43 m/s, 2.53 m/s and 2.59 m/s for Strikers 1, 2, 3 and 4, respectively). A strongly nonlinear elastic Hertzian type interaction was assumed between the striker and the top steel cylinder similar to Ref. [7]. The gravitational force was not included in the numerical simulation, since in separate numerical calculations we demonstrated that the gravitational forces acting on the particles did not affect the speed, amplitude and shape of the signals in the investigated range of numbers of particles and time of experiments.

The second approach is a linear dashpot dissipative Kelvin-Vogt model (referred as Model II). A dissipation term with linear dependence on the particle relative velocity was introduced to the whole system, while a dissipative term was added or excluded between the striker and the top cylinder of the chain.

4.4.1 Numerical modeling results using non-dissipative model

Figure 4.4 and Table 4.3 show the numerical results corresponding to Model I with the elastic modulus of O-ring E_{imp} being equal to 105 MPa.

It is clear that a single Nesterenko solitary wave was generated when the mass of striker was smaller than the mass of steel cylinder in the system [Figs. 4.4(a) and 4.4(b)], which is also expected for this system [15]. The spatial width of the ramp of these waves for all strikers' mass shown is equal to 2.3a (Fig. 4.4). This size is consistent with the expected size of half of Nesterenko solitary wave in a Hertzian chain [15]. But in experiments the spatial size of ramp was equal to 3.2a for small amplitude pulse [Fig. 4.3(a)] and 5.5a for largest amplitude [Fig. 4.3(d)].

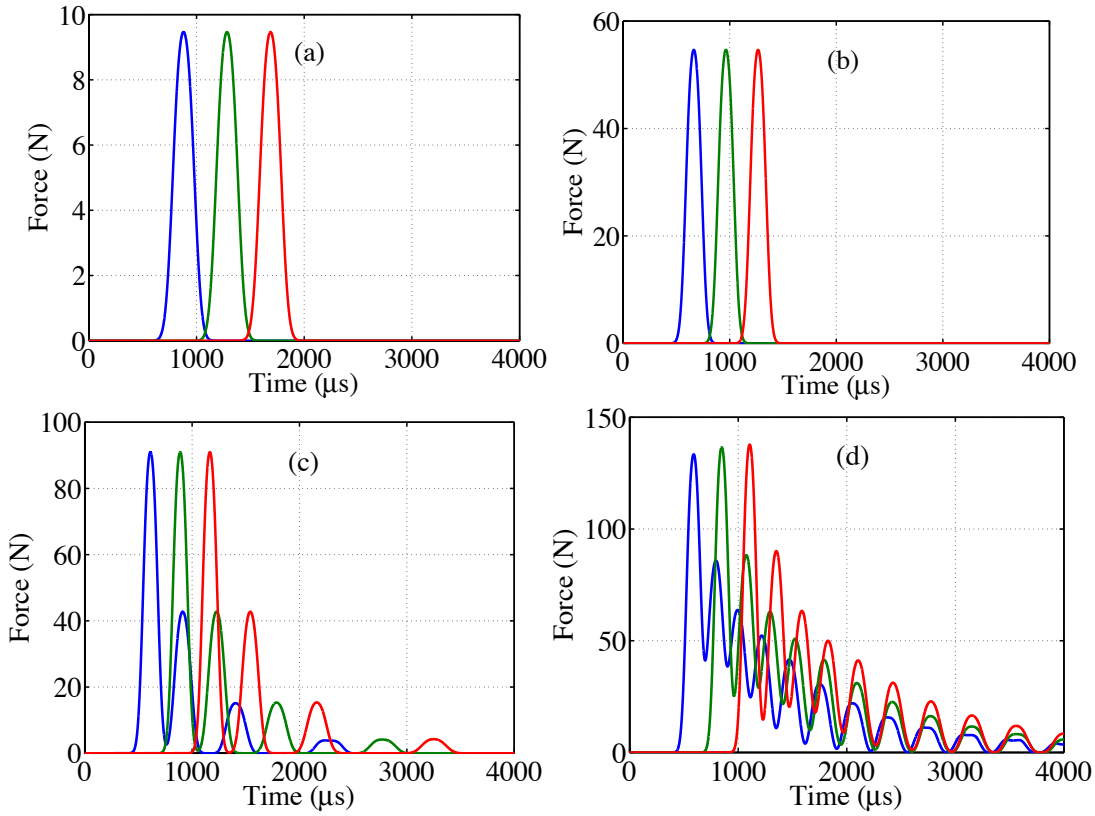

Figure 4.4: Stress profiles in the propagating waves in numerical simulation using non-dissipative model I (E_{imp} = 105 MPa) in the ninth (leading signal), thirteenth (middle signal), and seventeenth (last signal) cylinders. The system was impacted by four different strikers: (a) Striker 1 (0.455 g, with velocity 2.24 m/s); (b) Striker 2 (3.236 g, with velocity 2.43 m/s); (c) Striker 1 (9.308 g, with velocity 2.53 m/s); (d) Striker 1 (30.718 g, with velocity of 2.59 m/s).

Impact by the striker with larger mass resulted in the stress pulse disintegrated into trains of Nesterenko solitary waves (Striker 3 and 4) in the numerical calculations [Figs. 4.4(c) and 4.4(d)]. The change of wave profile in Fig. 4.4, illustrates that the number of Nesterenko solitary waves in the train is determined by the ratio of the striker mass to the mass of the cylinder in the system. But in experiments there was no splitting of pules intro trains of solitary waves. Instead an asymmetrical bell shape pulse is detected in the apparent disagreement with the results of non-dissipative model

calculations (Fig. 4.4).

Table 4. 3: Comparison of numerical results (using non-dissipative model at E_{imp} = 105 MPa) and experimental data on speed, normalized width, and amplitude of transmitted pulses when the system was impacted by four different strikers: Striker 1 – 4.

	Model I (E_{imp} = 105 MPa)				Experimental data			
Striker mass (g)	0.455	3.236	9.308	30.718	0.455	3.236	9.308	30.718
V (m/s)	67	90	98	105	55±3	66±4	70±5	75±5
$L_{f,9}/a$	2.3	2.3	2.3	2.3	3.2	3.6	4.3	5.5
A_9 (N)	9.5	54.7	90.9	133.5	2.03± 0.04	6.75± 0.15	13.85 ±0.05	26.97 ±0.49

The amplitudes of waves in non-dissipative numerical calculations were much higher than in the experiments.

Moreover, the amplitude of the stress waves in the numerical modeling did not attenuate during propagation within four cell size, which is in contradiction to the attenuation observation observed in experiments (Fig. 4.3).

The wave speed in numerical calculations was significantly larger than the value in experiments (Table 4.3). It should be mentioned that using E_{imp} =105 MPa results in a good prediction of the shock wave speed in an elastic Hertzian chain if the amplitudes from the experiments were used in Eq. (4.3).

In the attempt to reduce amplitudes of the signals and their speed we also used lower elastic modulus E_{imp}=87 MPa in numerical calculation. The corresponding stress profiles in propagating waves are shown in Fig. 4.5 and the numerical values are presented in Table 4.4.

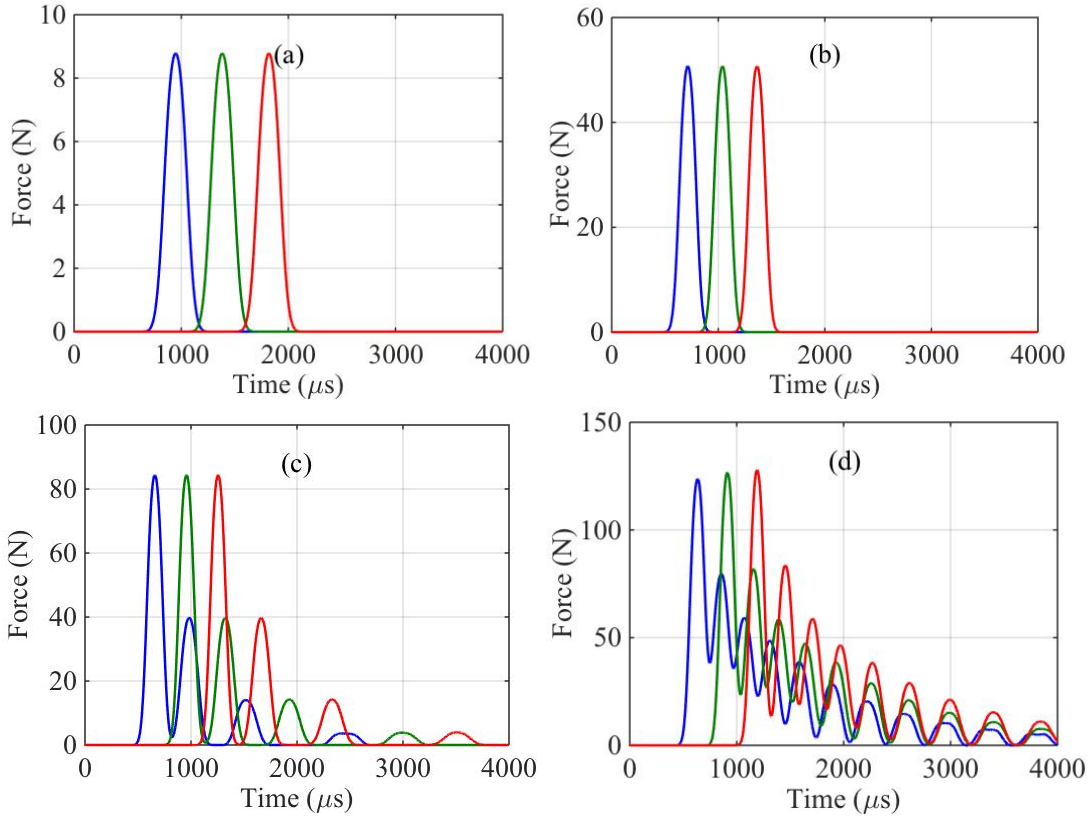

Figure 4.5: Stress profiles in the propagating waves in numerical simulation using non-dissipative Model I (E_{imp} = 87 MPa) in the ninth (leading signal), thirteenth (middle signal), and seventeenth (last signal) cylinders. The system was impacted by four different strikers: (a) Striker 1 (0.455 g, with velocity 2.24 m/s); (b) Striker 2 (3.236 g, with velocity 2.43 m/s); (c) Striker 1 (9.308 g, with velocity 2.53 m/s); (d) Striker 1 (30.718 g, with velocity of 2.59 m/s).

Table 4.4: Comparison of numerical results (using non-dissipative model at E_{imp} = 87 MPa) and experimental data on the speed, normalized width, and amplitude of transmitted pulses when the system was impacted by four different strikers: Striker 1—4.

	Model I (E_{imp} = 87 MPa)				Experimental data			
Striker mass (g)	0.455	3.236	9.308	30.718	0.455	3.236	9.308	30.718
V (m/s)	62	85	91	98	55±3	66±4	70±5	75±5
$\boldsymbol{L_{f,9}/a}$	2.4	2.4	2.4	2.4	3.2	3.6	4.3	5.5
$\boldsymbol{A_9}$ **(N)**	8.8	50.7	84.3	123.7	2.03	6.75	13.85	26.97

We can see that reduction of elastic modulus indeed resulted in the reduction of the pulse speeds and amplitudes. But still significant differences with experimental data are evident, specifically with the spatial size of the ramp of waves, dramatically different shapes of pulses and their amplitudes, absence of attenuation in numerical calculations versus decay in experiments.

It is clear that it is necessary to introduce a dissipation to address the outlined differences between numerical simulations and experiments.

4.4.2 Numerical modeling results using linear dissipative model

From the comparison of numerical results and experimental data above, it is clear that we must introduce the dissipation mechanism in numerical calculations. It should be mentioned that the nonlinear behavior in the investigated metamaterial is due to the dynamic deformation of rubber O-rings which is a complex process due to the rubber itself and due to the contact interaction between O-ring and steel plates with large gradients of strain and stresses in the rubber. It is not reasonable to expect exact match of numerical results and experiments.

It is interesting that it is in a dramatic contrast to the behavior of discrete systems composed from steel spherical particles or spherical particles and cylinders where role of dissipation was rather weak [18-21].

The numerical results of stress wave profiles for a linear dashpot model (μ = 22 Ns/m) for the cylinder interaction in the chain caused by dynamic compression of O-rings are presented in Fig. 4.6 (no dissipation term was added between the striker and the top cylinder).

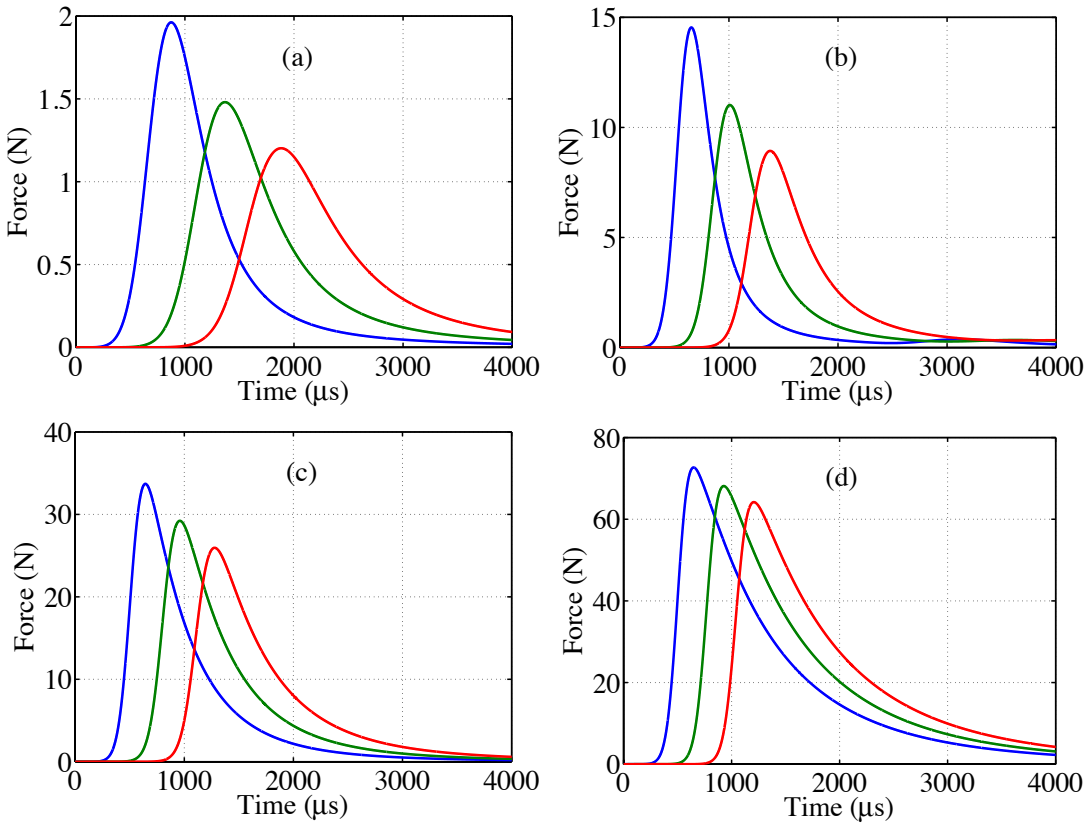

Figure 4.6: Profiles of the stress waves versus time obtained in numerical simulation using dissipative Model II (E_{imp} = 105 MPa, μ = 22 Ns/m and μ_s =0) in the ninth (leading signal), thirteenth (middle signal), and seventeenth (last signal) cylinders. The system was impacted by four different strikers: (a) Striker 1 (0.455 g, with velocity 2.24 m/s); (b) Striker 2 (3.236 g, with velocity 2.43 m/s); (c) Striker 1 (9.308 g, with velocity 2.53 m/s); (d) Striker 1 (30.718 g, with velocity of 2.59 m/s).

It is evident that the viscous dissipation resulted in the asymmetric stress wave profiles similar to what observed in experiments (compare Fig. 4.3 and 4.6). This dissipation mechanism eliminated the splitting of incoming stress pulses into trains of Nesterenko solitary waves and reduced the amplitudes of stress pulses. In a separate calculation, it is proved that the selected value of effective coefficient of viscosity (μ) will not affect the recoil velocity of striker if no viscous dissipation was introduced for contact between the striker and the op cylinder. The recoil motion of the striker can be

changed by adding a viscous term (with viscosity coefficient μ_s) for the corresponding contact between the striker and the top cylinder.

Comparison of the results of numerical calculations for dissipative chain with experimental data is presented in Table 4.5.

Table 4.5: Comparison of numerical results (using dissipative model at E_{imp} = 105 MPa, μ=22 Ns/m and μ_s=0 Ns/m) and experimental data for speed, normalized width of ramp (0.1-0.9), full width at half maximum L_{FWHA} and amplitudes of transmitted pulses for the system impacted by four different strikers: Striker 1—4.

	Linear dashpot Model				Experimental data			
M_{imp} (g)	0.455	3.236	9.308	30.718	0.455	3.236	9.308	30.718
V (m/s)	55	76	86	97	55±3	67±	70±	75±5
$L_{f,9}/a$	4.9	4.2	4.6	5.0	3.2	3.6	4.3	5.5
$L_{FWHA,9}/a$	5.1	4.3	6.5	10.6	3.7	4.1	6.7	9.0
A_9 (N)	1.96	14.54	33.71	72.68	2.03	6.75	13.85	26.97
A_{13}/A_9	0.75	0.76	0.87	0.94	0.56	0.60	0.69	0.73
A_{17}/A_9	0.61	0.61	0.77	0.88	0.41	0.46	0.56	0.63

From Fig. 4.6 and Table 4.5 we can see that the profiles of stress waves and their spatial sizes in numerical calculations are closer to the experimental data. But still the amplitudes and speeds of pulses generated by Strikers 2-4 are higher than in experiments. Additionally, the attenuation of signal amplitude in numerical calculations is lower than in experiments. Ramp times in numerical calculations are less dependent on the pulse amplitude than in experiments.

In the attempt to achieve a better fit to experimental results, the numerical calculations with linear dashpot model using different elastic modulus (E_{imp} = 87 MPa, μ=22Ns/m and μ_s=0) was conducted. No dissipation term introduced between the striker and the top cylinder because the steel/steel contact is less dissipative than

rubber/steel contacts. The results are presented in Fig.4.7 and Table 4.6.

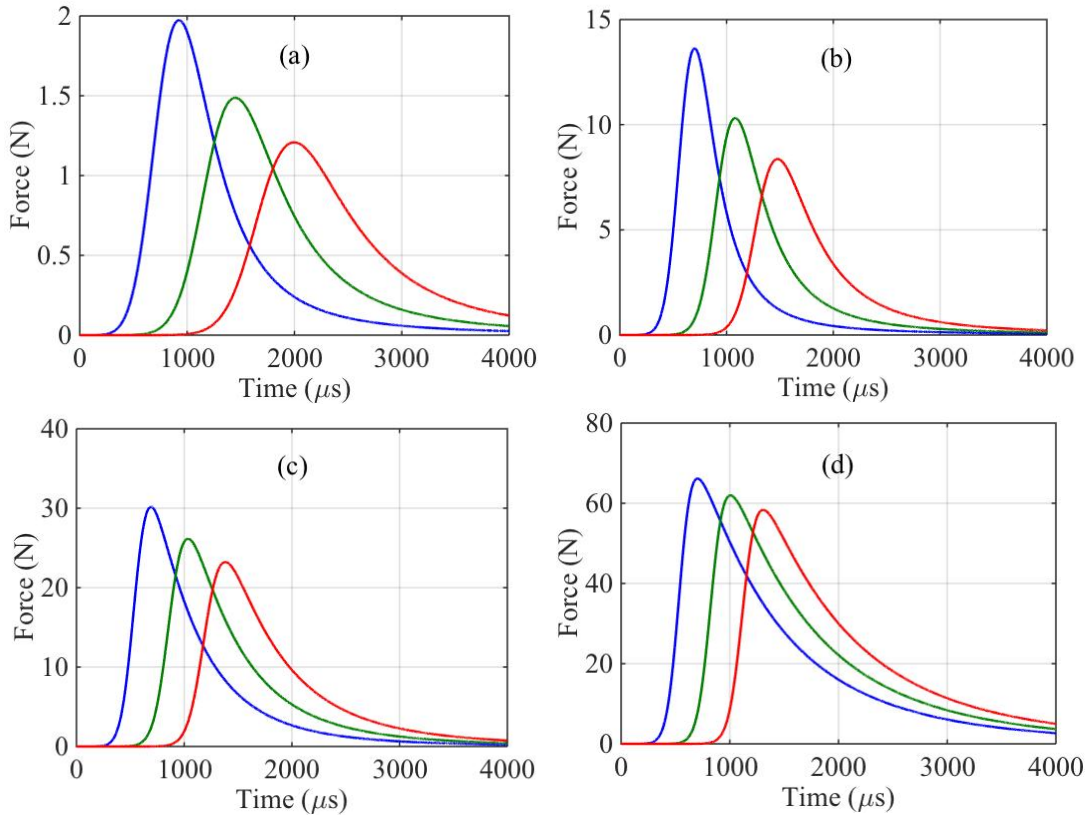

Figure 4.7: Profiles of the stress waves versus time obtained in numerical simulation using dissipative model II (E_{imp} = 87 MPa, μ = 22 Ns/m, and μ_s=0 Ns/m) in the ninth (leading signal), thirteenth (middle signal), and seventeenth (last signal) cylinders. The system was impacted by four different strikers: (a) Striker 1 (0.455 g, with velocity 2.24 m/s); (b) Striker 2 (3.236 g, with velocity 2.43 m/s); (c) Striker 1 (9.308 g, with velocity 2.53 m/s); (d) Striker 1 (30.718 g, with velocity of 2.59 m/s).

From Fig. 4.7 and Table 4.6 we can see that profiles of stress waves and their spatial sizes in numerical calculations are in better agreement with the experimental data than in the previous dissipative case presented in Fig.10 and Table V. But the amplitudes and the speeds of pulses are higher than in experiments and the attenuation in numerical

Table 4. 6: Comparison of numerical results (using dissipative model at E_{imp} = 87 MPa, μ=22 Ns/m and μ_s=0) and experimental data for speed, normalized width of ramp, full width at half maximum L_{FWHA} and amplitudes of transmitted pulses for the system impacted by four different strikers: Striker 1—4.

	Linear dashpot Model				Experimental data			
M_{imp} (g)	0.455	3.236	9.308	30.718	0.455	3.236	9.308	30.718
V (m/s)	52	71	79	90	55	67	70	75
$L_{f,9}/a$	4.9	4.2	4.5	5.6	3.2	3.6	4.3	5.5
$L_{FWHA,9}/a$	5.3	4.5	6.9	11.0	3.7	4.1	6.7	9.0
A_9 (N)	1.97	13.63	30.16	66.16	2.03	6.75	13.85	26.97
A_{13}/A_9	0.76	0.75	0.87	0.94	0.56	0.60	0.69	0.73
A_{17}/A_9	0.61	0.61	0.77	0.88	0.41	0.46	0.56	0.63

calculations is lower than in experiments. Ramp times in numerical calculations are closer to what observed in experiments.

The viscous dissipation at the striker top cylinder contact can also influence the generated pulses in the addition to increased viscous dissipation due to the dynamic deformation of O-rings. The role of these dissipative mechanism is investigated in numerical calculations and the corresponding results are presented in Fig. 4.7 and Table 4.6. In these calculations the following parameters in dashpot model were used correspondingly for O-rings and contact between striker and top cylinder: E_{imp} = 87 MPa, μ=125 Ns/m and μs=9.5 Ns/m).

From Fig. 4.8 and Table 4.7 we can see that the profiles of stress waves and their spatial sizes in numerical calculations are in satisfactory agreement with the experimental data as well as the speeds of pulses. But there are differences in amplitudes and rate of attenuation. The ramp times and values for $L_{FWHA,9}/a$ are also higher than the experimental values.

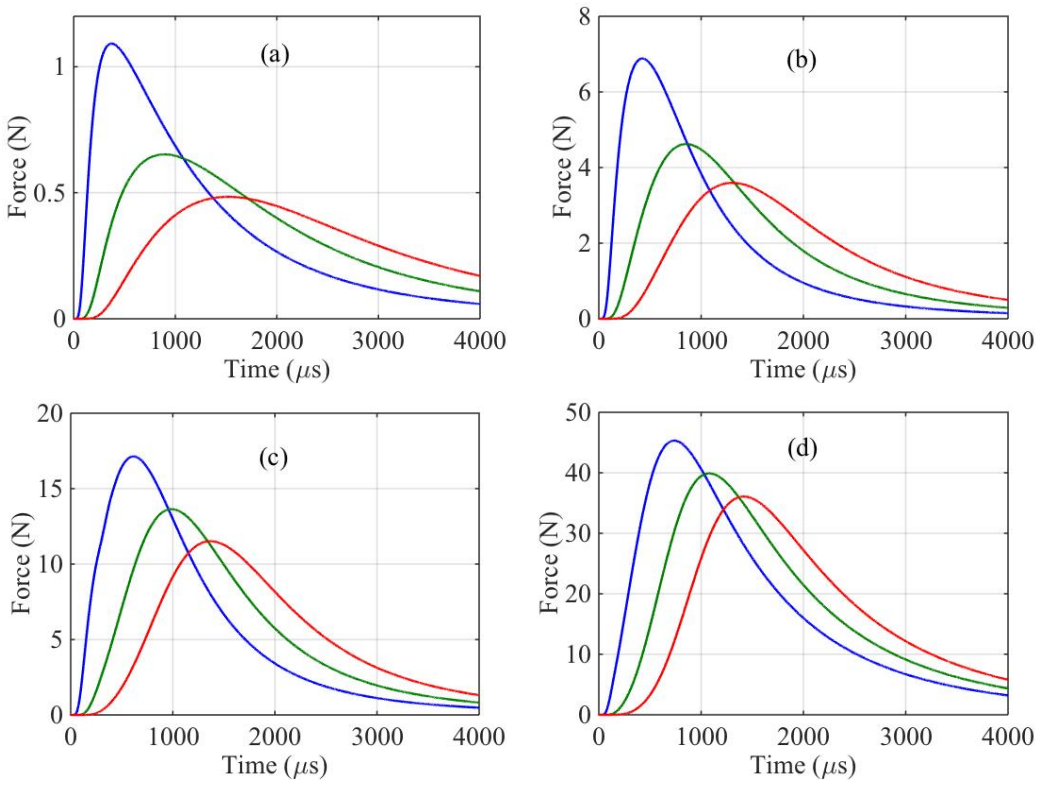

Figure 4.8: Profiles of the stress waves versus time obtained in numerical simulation using dissipative Model II (E_{imp} = 87 MPa, μ = 125 Ns/m, and μ_s =9.5 Ns/m) in the ninth (leading signal), thirteenth (middle signal), and seventeenth (last signal) cylinders. The system was impacted by four different strikers: (a) Striker 1 (0.455 g, with velocity 2.24 m/s); (b) Striker 2 (3.236 g, with velocity 2.43 m/s); (c) Striker 1 (9.308 g, with velocity 2.53 m/s); (d) Striker 1 (30.718 g, with velocity of 2.59 m/s).

Table 4.7: Comparison of numerical results (E_{imp} = 87 MPa, μ = 125 Ns/m, and μ_s =9.5 Ns/m) and experimental data for speed, normalized width of ramp, full width at half maximum L_{FWHA} and amplitudes of transmitted pulses for the system impacted by four different strikers: Striker 1—4.

	Linear dashpot Model				Experimental data			
M_{imp} (g)	0.455	3.236	9.308	30.718	0.455	3.236	9.308	30.718
V (m/s)	52	63	73	79	55	67	70	75
$L_{f,9}/a$	2.5	3.6	5.9	7.9	3.2	3.6	4.3	5.5
$L_{FWHA,9}/a$	9.1	8.4	11.8	15.4	3.7	4.1	6.7	9.0
A_9 (N)	1.09	6.89	17.13	45.32	2.03	6.75	13.85	26.97
A_{13}/A_9	0.60	0.67	0.80	0.88	0.56	0.60	0.69	0.73
A_{17}/A_9	0.44	0.52	0.67	0.80	0.41	0.46	0.56	0.63

Thus we can conclude that linear dashpot model provided only partial agreement with the experimental results which is most probably due to the more complex, path dependent dissipative behavior of O-rings. The complexity of their behavior even in a single loading cycle is illustrated by results of [4,5].

4.5 Conclusions

Strongly nonlinear behavior of dissipative discrete metamaterial composed of steel cylinders and Nitrile O-rings was investigated in experiments and numerical calculations. The speed of the strongly nonlinear stress wave in uncompressed chain can be described by the equation for the speed of shock like stress wave with relatively high elastic modulus (105 MPa) in comparison with its static value (7.6 MPa) similar to the behavior of the sound wave in precompressed chain [6]. Thus O-rings are much stiffer under these conditions of dynamic deformation, their dramatically different behavior must be taken into account in the design of heavy machinery under similar impact conditions.

The speed of the stress wave with given amplitude in initially uncompressed chain was lower than the sound speed in the compressed chain with precompression force similar to the amplitude of the stress wave in uncompressed chain. This is in agreement with the expected theoretical behavior of stress wave speeds in uncompressed and strongly compressed chain. Moreover, the weakly nonlinear amplitude dependence of the speed of these stress waves is in agreement with the expectation for the shock wave in the Hertzian chain.

The viscous dissipation related to the dynamic deformation of O-rings dramatically changes the nature of propagating stress waves from the trains of Nesterenko solitary waves (characteristic for non-dissipative discrete chains) to the asymmetrical bell shape waves.

The introduction of viscoelastic interaction between cylinders in numerical calculations completely eliminates train of Nesterenko solitary waves replacing them with a triangular profile stress wave. The linear viscous Kelvin-Voigt model was able to explain only part of experimental observations. It is probably due to more complex, path dependent behavior of O-rings which can be subject for the future research.

Chapter 4 contains material currently being prepared for publication with the tentative title “Waves generated by impacts on dissipative sonic vacuum” by Yichao Xu and Vitali F. Nesterenko. The dissertation author was the primary investigator and author of this paper.

References

[1] E. B. Herbold and V. F. Nesterenko, Appl. Phys. Lett. **90**, 261902 (2007).

[2] I. L. D. Pinto, A. Rosas, A. H. Romero and K. Lindenberg, Phys. Rev. E **82**, 031308 (2010).

[3] A. Spadoni, C. Daraio, W. Hurst and M. Brown, Appl. Phys. Lett. **98**, 161901 (2011).

[4] C. Lee and V. F. Nesterenko, J. Appl. Phys. **114**, 083509 (2013).

[5] C. Lee and V. F. Nesterenko, J. Appl. Phys. **116**, 083512 (2014).

[6] Y. Xu and V. F. Nesterenko, Phil. Trans. A **372**, 20130186 (2014).

[7] Y. Xu and V. F. Nesterenko, J. Appl. Phys. **117**, 114303 (2015).

[8] Y. Xu and V. F. Nesterenko, in Proceeding of the 19th Biennial APS Conference on Shock Compression of Condensed Matter, Tampa, 2015, edited by Ricky Chan, Tim Germann and Thomas Sewell.

[9] C. Coste and B. Gilles, Eur. Phys. J. B **7**, 155 (1999)

[10] P. W. Allen, P. W. Lindley and A. R. Payne, *Use of Rubber in Engineering* (Maclaren and Sons, London, 1966), pp. 1–23.

[11] P. K. Freakley and A. R. Payne, *Theory and Practice of Engineering with Rubber* (Applied Science Publishers Ltd., London, 1978), pp.146–165.

[12] S. J. Jerrams, M. Kaya and K. F. Soon, Mater. Des. **19**, 157 (1998).

[13] V. F. Nesterenko, Prikl. Mekh. Tekh. Fiz. **24**, 136 (1983) [J. Appl. Mech. Tech. Phys. **24**, 733 (1984)].

[14] N. Lazaridi, and V.F. Nesterenko, Prikl. Mekh. Tekh. Fiz. **26**, 115 (1985) [J. Appl. Mech. Tech. Phys. **26**, 405 (1985)].

[15] V. F. Nesterenko, *Dynamics of heterogeneous materials* (Springer, NY, 2001), Chap. 1, pp. 1-53.

[16] N. V. Brilliantov, F. Spahn, J. Hertzsch and T. Poschel, Phys. Rev. E **53**, 5382 (1996).

[17] N.V. Brilliantov, A.V. Pimeniva, and D.S. Goldobin, EPL **109**, 14005 (2015).

[18] C. Coste, E. Falcon, and S. Fauve, Phys. Rev. E **56**, 6104 (1997).

[19] C. Coste and B. Gilles, Eur. Phys. J. B **7**, 155 (1999).

[20] S. Job, F. Melo, A. Sokolow, and S. Sen, Phys. Rev. Lett. **94**, 178002 (2005).

[21] S. Sen, J. Hong, J. Bang, E. Avalos, and R. Doney, Phys. Rep. **462**, 21(2008).

CHAPTER 5

TRANSFER OF ENERGY AND MOMENTUM FROM STRIKER TO THE STRONGLY NONLINEAR DISSIPATIVE METAMAERIAL

The pulses in the metamaterial without precompression (chapter 4) were excited by the striker impact on the top cylinder with relatively rigid contact interaction in comparison with the contact interaction between steel cylinders separated by O-rings. We will see that this results in a few distinctive time scales determining striker interaction with metamaterial and interaction between steel cylinders separated by soft O-rings. To understand how the striker interacts with this metamaterial, the high-speed camera is used to record the collision between the striker and the metamaterial. The optical images of moment of collision were presented in this chapter for different strikers. In experiments, a single or multiple impacts between the striker and the top steel cylinder transferring the linear momentum and energy from the striker to the metamaterial were observed.

The unusual transfer of linear momentum and kinetic energy from striker to the investigated "soft" metamaterial in state of sonic vacuum was observed in both experiments and numerical simulation.

5.1 Striker Behavior in Experiments

Four different strikers with various masses were used to impact the one-dimensional chain composed of alternating steel cylinders and Nitrile rubber O-rings

without precompression force. It will be seen that there are multiple impacts between the striker and the top steel cylinder transferring the linear momentum and energy from striker to the metamaterial in case of relatively large striker mass. This rattling behavior of the striker happened during dozens microseconds. A high-speed camera (Phantom V12) was used to capture this phenomenon. The optical images of striker collisions with the top cylinder are presented in Figs. 5.1-5.4.

In experiments with striker mass being smaller than the mass of cylinders (3.065 g) in the chain (striker is a steel sphere with mass 0.455 g, impact velocity 2.24 m/s) the single impact event was observed and the striker rebounds moving away from the chain with a velocity 1.39 m/s (Fig. 5.1). This impact corresponds to the force profiles shown in the Fig. 4.3(a).

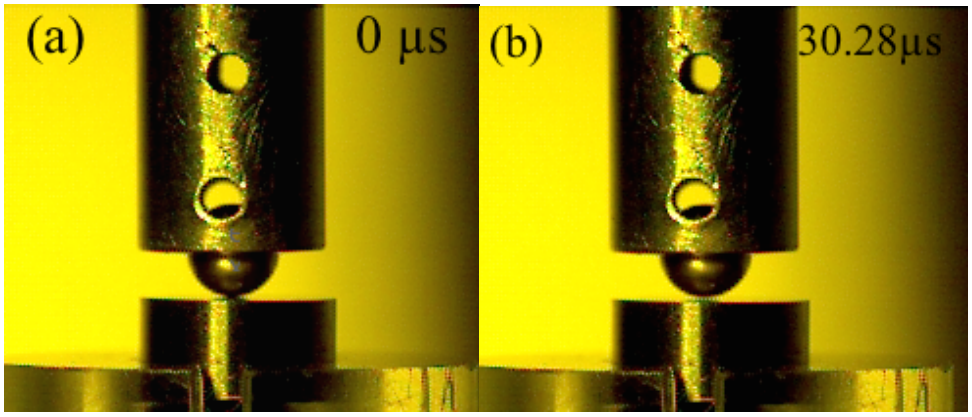

Figure 5.1: High-speed images of the interaction between the lightest Striker 1 (0.455 g) and the top steel cylinder: (a) the first impact moment; (b) recoil motion of striker at t=30.28μs.

The clear separation of striker from the top cylinder can be seen in a second frame after the moment of contact between striker and the top cylinder around 30.28 μs

[Fig. 5.1(b)]. Thus the duration of the impact was less than 30.28 μs. The top cylinder did not rebound in the optical images until arrival of the reflected wave from the bottom of the chain being in contact with granite plate. The generated pulse has approximately symmetric shape because unloading phase is controlled by the reverse motion of the top cylinder which did not produce significant disturbance after the colliding with the striker on the recoil motion.

The high speed images of the impact by heavier Striker 2 (M_{imp} = 3.236 g, velocity of impact 2.43 m/s), corresponding to the force history presented in Fig. 4.3(b), are shown in Fig. 5.2.

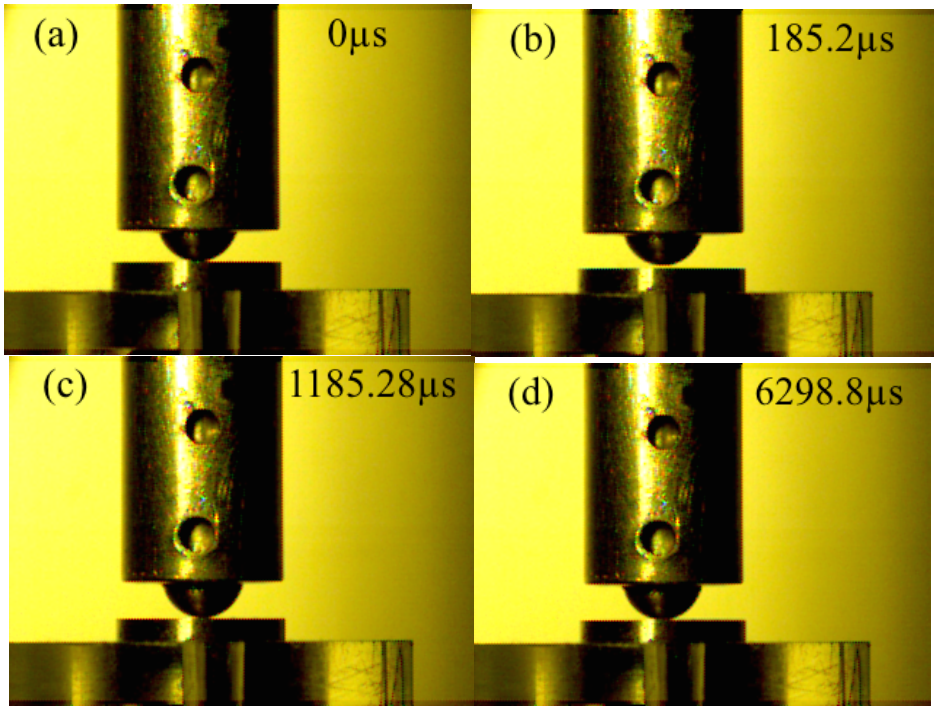

Figure 5.2: High-speed images of multiple impacts and separations of Striker 2 (3.236 g) and the top steel cylinder: (a) the first impact; (b) opening of maximum gap due to separation of striker from the top cylinder after the first impact; (c) the second impact; (d) the striker and top cylinder move back together without separation.

The increase of striker mass results in a qualitatively new dynamic of its interaction with the metamaterial. The image of the first impact event is shown in Fig. 5.2(a). In the third high speed image (not shown in Fig. 5.2) taken after 37.04 μs after the first image the striker practically stopped moving, while the top cylinder was moving forward. This behavior is expected for the collision of bodies with similar masses. Based on the high speed images the duration of impact is less than 37.04 μs.

Due to the difference in velocities the top cylinder separated from the striker [Fig. 5.2(b)]. The former starts to compress the O-ring in front of it losing its velocity, pushing the second cylinder forward and later recoiling. Due to the much less rigid contact of O-ring with the steel cylinder than the contact between the striker and the top steel cylinder, the process of O-ring deformation resulting in recoil motion of the top cylinder takes much longer time than the impact duration between the striker and the top cylinder. The former process determines the ramp time in the force history of generated wave in metamaterial, which is significantly larger than the duration of impact (about 20 times).

The second impact happened at t = 185.28 μs [Fig. 5.2(b)] mostly due to the recoil motion of the top cylinder and remaining positive velocity of the striker after the first impact, both are weakly affected by gravitation. Though this secondary impact is qualitatively new feature in comparison with the striker interaction with the top cylinder in the previous case, this second impact does not produce significant input into the propagating pulse due to the relatively low impact velocities in comparison with the first impact. After the second impact, the striker and the top cylinder practically stopped being at rest until 6298.8 μs when the reflected wave from the bottom arrived pushing

them upward.

Like in the previous case, corresponding to Figs. 4.3(a), the generated pulse has approximately symmetric shape [Figs. 4.3(b)] because unloading phase is controlled by the reverse motion of the top cylinder.

The impact by the Striker 3 (M_{imp} = 9.308 g, velocity of impact 2.53 m/s) with mass about 3 times larger than the mass of cylinder demonstrates increased role of multiple impacts between striker and top cylinder. The few optical images of the collision between Striker 3 and the top cylinder corresponding to the force history presented in Fig. 4.3(c) are shown in Fig. 5.3. We could distinguish a few impacts between Striker 3 and the top cylinder in the optical images.

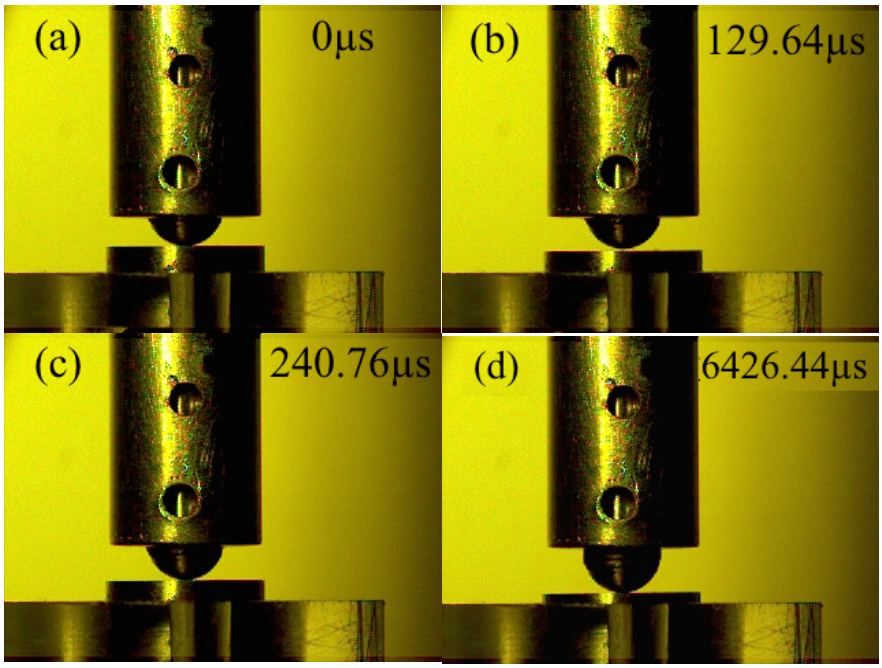

Figure 5.3: High-speed images of interaction between Striker 3 (9.308 g) and the top cylinder: (a) The first impact; (b) opening of maximum gap due to separation of striker from the top cylinder after the first impact; (c) second impact; (d) striker and top cylinder move back together without separation due to arrival of reflected wave from the bottom.

At 129.64 μs [Fig. 5.3(b)] we can observe a first maximum separation of striker from the first cylinder due to the larger velocity of the latter. The gap is also recognized by the larger displacement of the top cylinder (relative to the top of the PMMA holder) in comparison with the displacement of the striker relative to the end of the hollow steel rod. The second impact happened at 240.76 μs [Fig. 5.3(c)] mostly due to the remaining forward velocity of the striker being larger than velocity of the top cylinder (visible in Fig. 5.3 by different length of the visible part of striker moving from the hollow steel rod). At 370.4 μs (not shown in Fig. 5.3) the second separation between the striker and the top cylinder is distinguishable, the top cylinder and striker are still moving forward, but slowing down. Third impact can be detected in optical images at t = 500.04 μs. At 6426.44 μs we can see the maximum displacements of the striker and top cylinder [Fig. 5.3(d)] the striker and the top cylinder moved in reverse direction due to the arriving reflected waves. Apparently striker would not recoil without arrival of the reflected wave from the bottom. This is very unusual behavior allowing preventing of the striker recoil which was stopped by this metamaterial.

In the last two cases we see more clearly emergence of the third time scale (about ~3900μs) related to the multiple impacts of the striker with the top cylinder reducing striker's velocity to zero. The first and fastest time scale is related to the interaction of steel striker and the top steel cylinder with rigid contact (the duration of striker impact is less than 38 μs). The second, longer time scale is related to the interaction between cylinders due to the deformation of soft rubber O-ring (~222 μs). The difference between the second and third time scales results in the distortion of the shape of the propagating stress profile which becomes more asymmetric with the increase of striker

mass [compare Figs. 4.3(a), 4.3(b) and 4.3(c)]. The second and third times scales determining the interaction of the striker with the top cylinder are reflected in the ramp and unloading times of the propagating stress profiles (Fig. 4.3). The multiple impacts of the Striker 3 and the top cylinder results in a slow unloading path in the stress pulse [Fig. 4.3(c)].

The heaviest Striker 4 had a mass 30.718 g. Stages of its collision (initial impact velocity 2.59 m/s) with the metamaterial are presented in the high speed images in Fig. 5.4. The duration of the first impact for the heaviest striker in experiments was found to be less than 55.56 μs (separation of the striker and top cylinder is detectable in the third frame, time step between frames is 18.52 μs).

Considering that the first impact happened at $t = 0$ [Fig. 5.4(a)], the maximum gap between the striker and the first cylinder was detected at the frame corresponding to 92.6 μs from the frame where the first contact between the striker and the top cylinder was detected [Fig. 5.4(b)]. The second impact happened at $t = 166.68$ μs due to the higher remaining velocity of striker comparing to the top cylinder interacting with the second cylinder (the process is seen in the Fig.5.4 by different length of the visible part of striker from the hollow steel rod). No rebound motion of top cylinder was visible yet, it kept moving forward but slowing down. At t = 259.28 μs, the second largest gap was detected between the tip of striker and the top cylinder, both moved forward slowing down.

The striker and the top cylinder came to rest at t=6185.68 μs, displacement of the striker starting from the first contact with top cylinder is 3.48 mm. This displacement is caused by the dynamic deformation of multiple O-rings and can be used as one of the

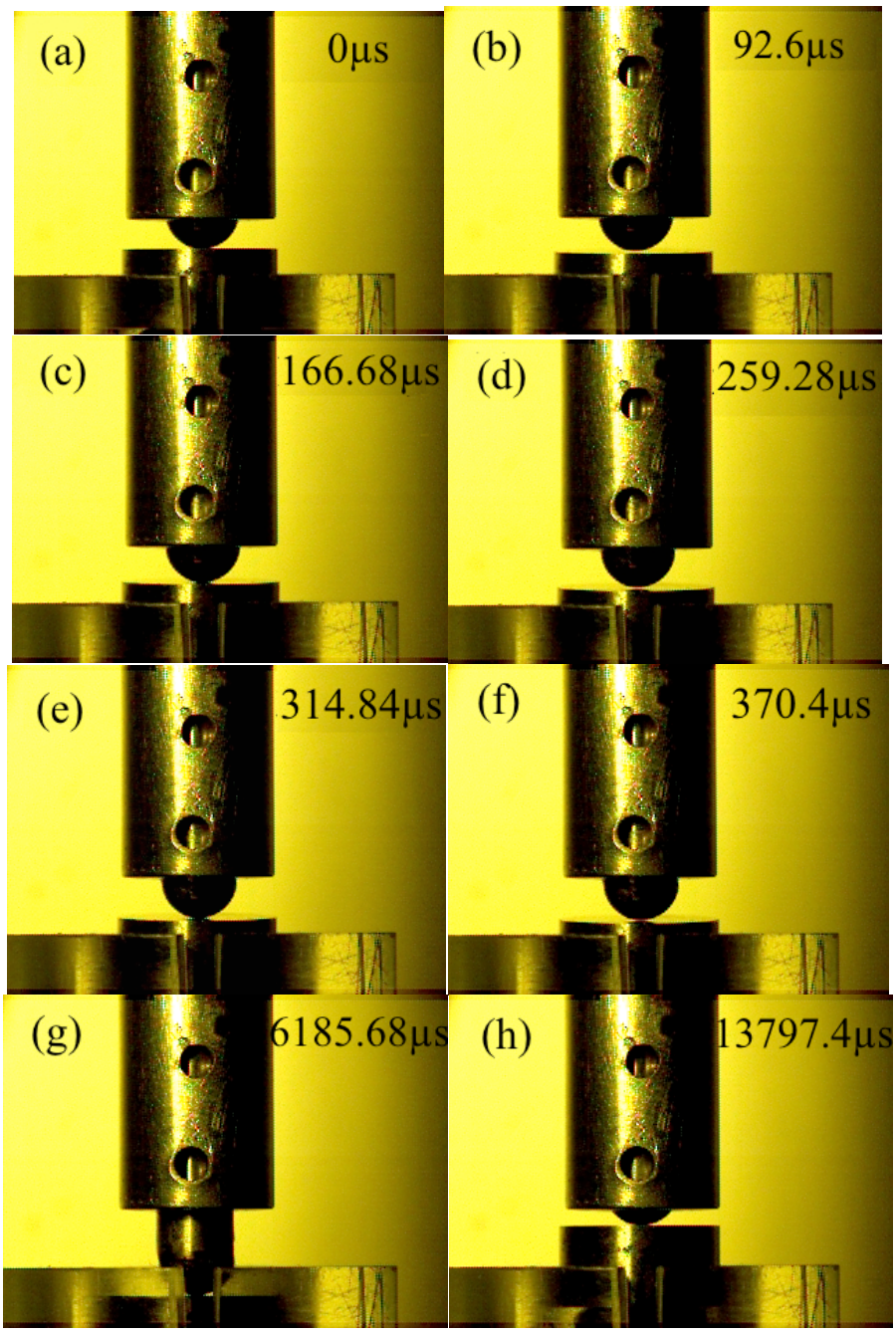

Figure 5.4: High-speed images of multiple impacts and separations between Striker 4 (mass 30.718 g, impact velocity 2.59 m/s) and the top cylinder: (a) The first impact; (b) first opening of maximum gap due to separation of striker from the top cylinder; (c) the second impact; (d) second maximum gap due to separation of striker from the top cylinder; (e) the third impact; (f) third maximum gap due to separation of striker from the top cylinder; (g) the striker and top cylinder came to rest at t=6185.68 μs; (h) striker and top cylinder move back together without separation.

parameters to compare with the results of numerical simulations.

It is clear that the time of interaction between the striker and the top cylinder is much smaller than the time scale related to the interaction between the top cylinder and the O-ring in front of it when it was moving forward. The latter time scale determined the ramp time of the leading signal. This is probably a reason why the sequence of pulses in Fig. 4.3(d) did not exist despite the multiple impacts.

It is clear that the increased mass of the striker results in larger number of its multiple impacts with the top cylinder. Due to larger difference in their relative velocities more clear separation of the striker from the top cylinder after each impact is observed. The heaviest Striker 3 did not recoil and kept moving forward, but slowed down by multiple impact between the striker and the top cylinder. The striker and top cylinder completely stopped at t = 6185. 85 μs. They started to move back together only after the arrival of reflected stress wave from the granite plate supporting the chain at the bottom. This unusual impact behavior is reflected in the stress wave profile in Fig. 4.3(d), where the unloading path of the stress wave was slower compared with the previous case (impacted by lighter strikers) resulting in a more asymmetrical shape of the signal.

In high speed optical images (some of them are presented in Fig. 5.4) nine impacts after the first interaction of striker and the top cylinder were detected. But this did not result in trains of solitary waves propagating in the metamaterial [Fig. 4.3(d)].

5.2 Striker Behavior in Numerical Calculation

Experimental data based on the high speed imaging provided very unusual

picture of interaction between strikers and the top cylinders (Figs. 5.1-5.4). Especially interesting are the multiple collisions of the striker (rattling) with the system determined by three time scales in case when striker mass is larger than the mass of cylinders. This behavior was modeled by the non-dissipative and linear dissipative models, the results and the data related to the feature the impact process are presented in Figs. 5.5, 5.6 and Table 5.1, correspondingly. The longer chains were selected in calculations to avoid the effects of the reflected wave on the the striker behavior.

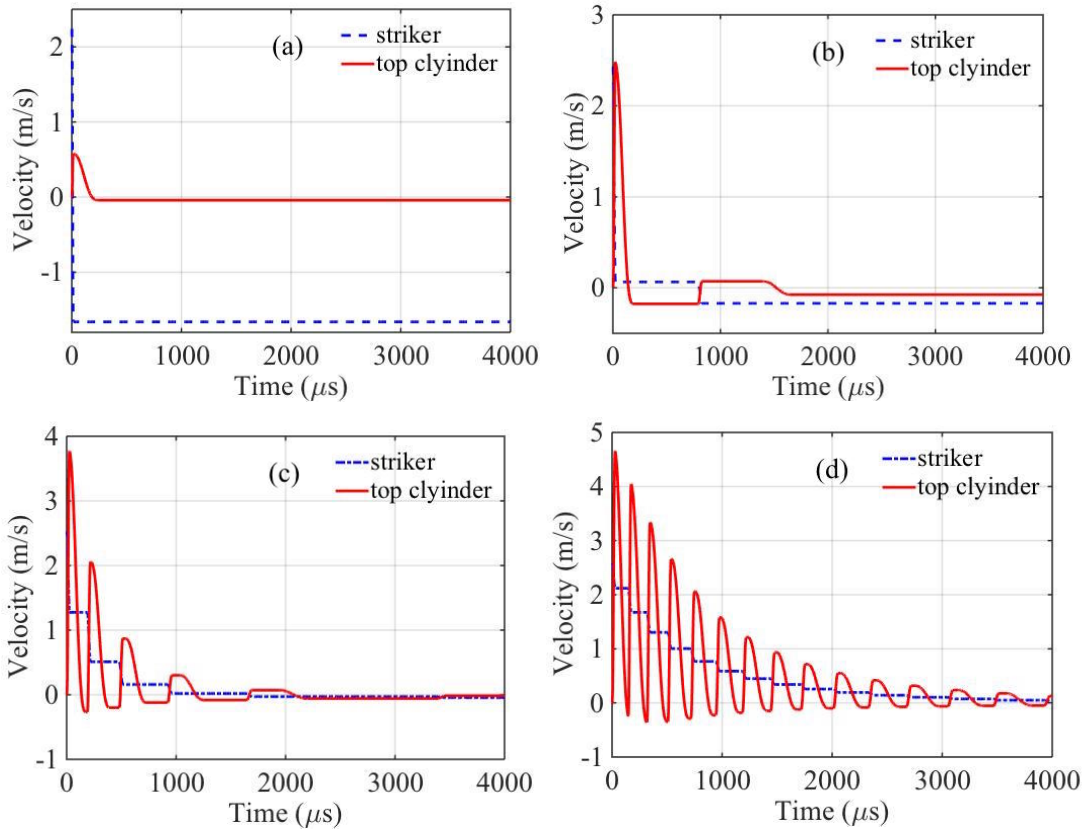

Figure 5.5: Rattling behavior of the top cylinder in the chain under impact in numerical calculation (non-dissipative model, E_d = 105 MPa) by multiple strikers: (a) 0.455 g steel sphere striker with a 2.38 mm radius having a velocity of 2.24 m/s, (b) 3.236 g striker with a 2.38 mm radius steel tip having a velocity of 2.43 m/s, (c) 9.308 g striker with a 2.38 mm radius steel tip having a velocity of 2.53 m/s; (d) 30.718 g striker with a 2.38 mm radius steel tip having a velocity of 2.59 m/s.

Table 5.1: Comparison of numerical calculation results of Model I (non-dissipative model, E_{imp}=105MPa) and II (linear dissipation model, E_{imp} = 87 MPa and μ= 22 Ns/m): the duration of first impact (T_{imp}), the velocity of striker ($V_{striker}$) and the top cylinder ($V_{cylinde}$) after the first impact, the interaction time of striker and the O-ring in front it when the former moving forward after the first impact (T_{oring}), and the time second impact happened ($T_{imp,2}$).

	Non-dissipative Model				Linear dissipation model			
M_{imp} (g)	0.455	3.236	9.308	30.718	0.455	3.236	9.308	30.718
T_{imp}	13.8	22.8	26.4	28.2	13.2	22.2	27.0	29.4
$V_{striker}$	-1.62	0.065	1.275	2.119	-1.672	0	1.235	2.10
$V_{cylindel}$	0.58	2.48	3.77	4.656	0.55	2.351	3.583	4.44
T_{oring}	226	164	148	118	~480	~1370	~206	~131
$T_{imp,2}$	N/A	792.6	187	147	N/A	N/A	234	159.6

From Fig. 5.5 we can see that the behavior of the striker is dramatically changes with the increase of its mass. If the striker mass is less than the cylinder mass, it recoils after the single collision with the top cylinder [Fig. 5.5(a)]. Increase of its mass results in multiple collisions generating a third time scale determined mostly by the striker movement in the gaps between the strike and the top cylinder. For example, for Striker 3 the maximum first 4 consecutive separations between the striker and the top cylinder corresponds to the moments when the striker's velocity becomes equal to the velocity of the top cylinder, at about 97, 316, 650 and 1170 μs.

The difference between the first deformation cycle of the O-rings and subsequent deformation caused by the multiple collisions of striker is most probable reason for asymmetry shape of the stress pulses observed in experiments (Fig. 4.3).

It was discussed that the dissipative properties of the system are able to dramatically change the nature of propagating stress pulse. Thus it is important to investigate how dissipation mechanisms on the contacts between the striker and the top

cylinder and also due to the dynamic deformation of O-rings change the striker's dynamics. The corresponding results of numerical calculations are presented in Fig. 5.6.

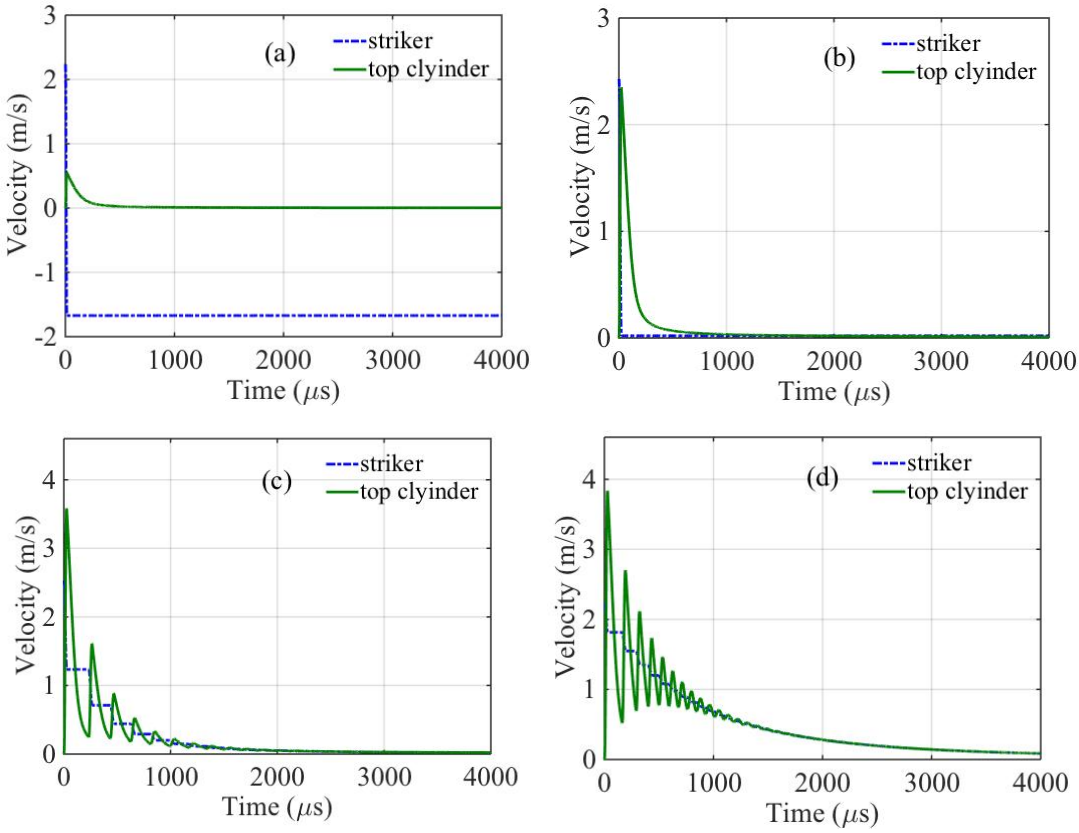

Figure 5.6: Rattling behavior of the top cylinder in the chain under impact in numerical calculation (linear dashpot model, E_d = 87 MPa, μ = 22 Ns/m and μ_s = 22 Ns/m) by multiple strikers: (a) 0.455 g steel sphere striker with a 2.38 mm radius having a velocity of 2.24 m/s, (b) 3.236 g striker with a 2.38 mm radius steel tip having a velocity of 2.43 m/s, (c) 9.308 g striker with a 2.38 mm radius steel tip having a velocity of 2.53 m/s; (d) 30.718 g striker with a 2.38 mm radius steel tip having a velocity of 2.59 m/s.

It is clear that dissipation changes rattling behavior of the striker but not eliminates it for larger striker masses. Thus we can conclude that the difference between first deformation cycle of the O-rings and subsequent deformation caused by multiple collisions of striker are most probable reasons for the asymmetry of the stress pulses

observed in experiments (Fig. 4.3).

5.3 Conclusions

The impact of the striker on this "soft" discrete metamaterial with a "rigid" interaction between the striker and the top steel cylinder demonstrate an unusual mechanism of the energy and linear momentum transfer into the metamaterial accompanied by a rattling of top cylinder between the striker and the rest of the chain. The heavier strikers' linear momentum was completely transferred to this strongly nonlinear "soft" metamaterial and its rebound was observed only after the arrival of the reflected weave from the wall supporting the chain at the bottom.

The large difference in rigidity between striker with steel rounded end part and cylinders in the chain (these multiple impacts were detected in experiments) results in multiple impacts on the top cylinder creating a single triangular propagating pulse in experiments. The numerical calculations using non-dissipative and linear dissipative models both demonstrated the multiple impacts behavior of the striker to the top cylinder when the striker mass is larger than the mass of cylinder in the chain. Thus multiple impacts observed in experiments did not result in the train of propagating train of solitary waves. I attributed this behavior to a viscoelastic behavior of O-rings.

Chapter 5 contains material currently being prepared for publication with the tentative title "Waves generated by impacts on dissipative sonic vacuum" by Yichao Xu and Vitali F. Nesterenko. Section 2 in Chapter 5, is been in press in the *AIP Conference Proceedings,* with the title "Strongly nonlinear stress waves in dissipative metamaterials"

authored by Yichao Xu and Vitali F. Nesterenko. The dissertation author was the primary investigator and author of this paper.

APPENDIX A

NUMERICAL INVESTIGATION OF THE STRONGLY NONLINEAR DISSIPATIVE SYSTEM WITH PRECOMPRESSION

A chain of 40 elements is used in numerical calculations to simulate the vertical chain composed of steel cylinders and Nitrile O-rings with a double power-law interaction between neighboring rigid cylinders as shown in Fig. A.1. The numerical calculation is carried out by using MATLAB. Several numerical models were considered to simulate the experimental results in an attempts to pick up the most distinguished features of the stress pulses observed in experiments.

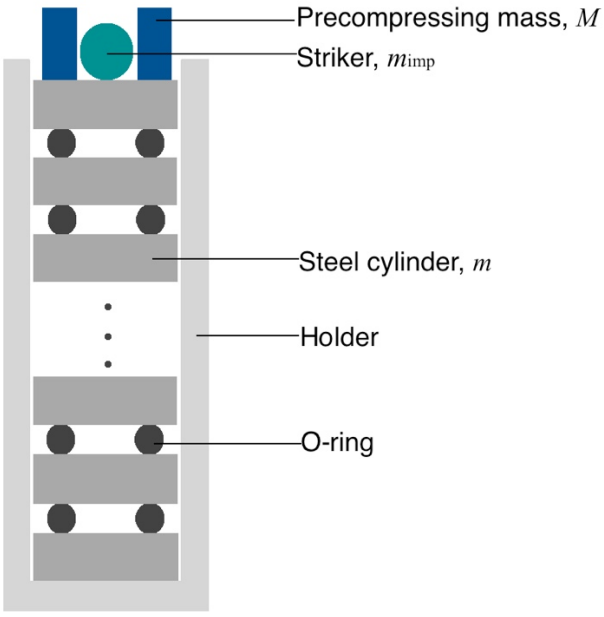

Figure A.1: System configuration used in numerical calculation for one-dimensional metamaterial with precompression.

Particle 1 in the numerical calculation represent the precompressing weight with mass M, providing the static precompression. Particle 2 in the numerical model defines the steel striker, and particle 3 is the top steel cylinder in the chain. It is assumed that the precompressing mass is in direct contact with the top cylinder (particle 3), and a Hertzian type contact interaction is assumed between them. Before the impact a steel striker (particle 2) is assumed at rest and next to the top cylinder, no static force applied to striker. Particle 1 and 2 have no interaction.

1. Non-dissipative Model

The first model is based on the linear elastic interaction (referred as Model-I), where no dissipation was included, but may include effective rigidity influenced by viscoelastic behavior.

The first order differential equations of motion of N cylinders inside a periodic chain in the frame of Model-I and the boundary conditions are presented in chapter 2 section 2.2.

The results of non-dissipative numerical calculations in the frame of the Model-I with different effective modulus E_{eff} (7.6 MPa and 105 MPa) are shown in Figs. A.2 and A.3. The corresponding data are presented in Tables A.1 and A.2.

From Table A.1, it is obvious that the pulse speed is significantly lower than the experimental data in the frame of Model I with E_{eff}=7.6MPa. It is clear that elastic modulus E_0=7.6MPa obtained from quasi-static process (chapter 2, section 2.1) can not be used to describe dynamic response of this system, the system behaves more rigid during the wave propagation. Thus it is necessary to introduce the effective elastic

modulus E_{eff} = 105 MPa, which provided the best fit of the pulse speed to the experimental data [refer to chapter 2 section 2.1]. Due to the dispersion caused by periodic structure of the system, a slow decrease of positive and negative signals amplitude and ramping of their fronts was observed.

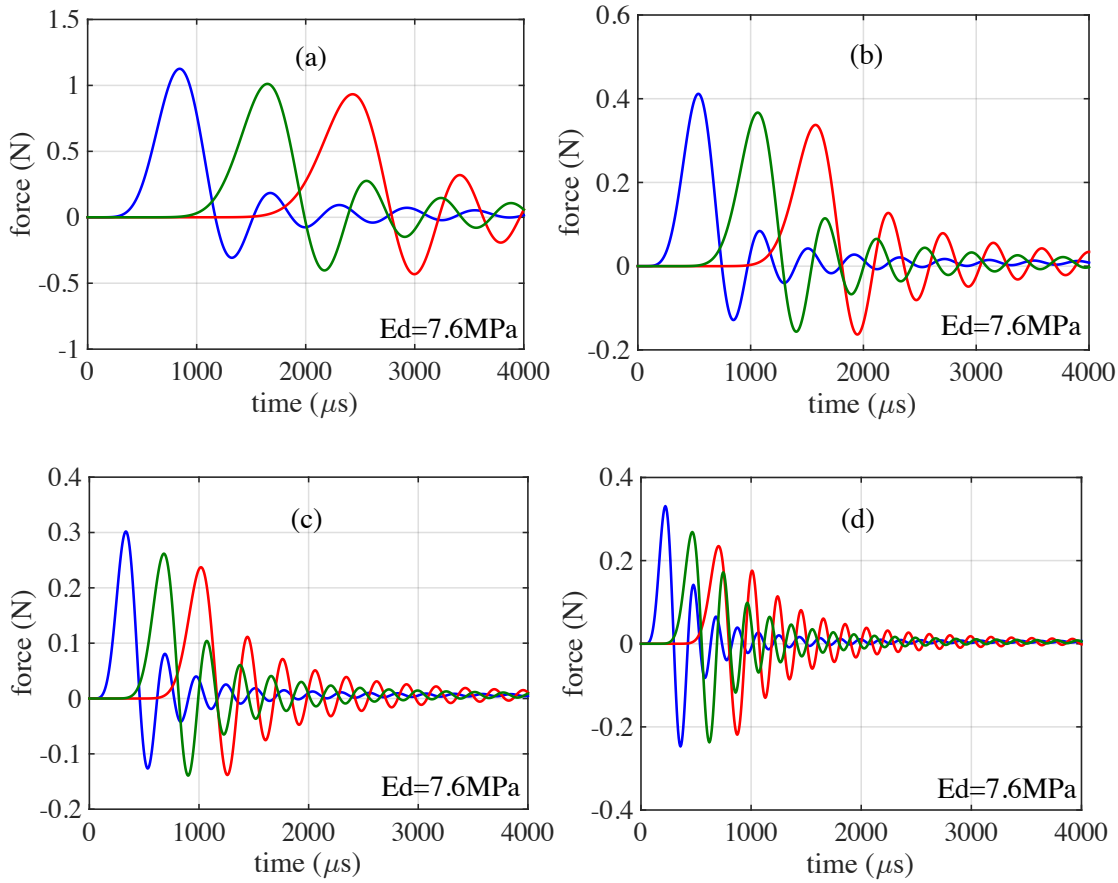

Figure A.2: Stress pulses obtained in numerical calculations using Mode-I (without dissipation term between all elements in the system, and using effective elastic modulus E_{eff} = 7.6 MPa) in a double power-law system under various preload conditions: (a) F_0= 10 N, (b) 50 N, (c) 106 N, (d) 193 N. Curves represent the average dynamic force in the fifth (leading curve), ninth (middle curve), and thirteenth (bottom curve) steel partial.

Compared Fig. A.3 with the experimental results, the amplitudes of signal in numerical calculation with E_{eff}=105MPa (Model-I) were always larger due to the non-

dissipative approach used in this calculations. And the significant attenuation observed in experiments and the lack of comparable attenuation in numerical calculations using Mode-I indicated the strong viscous dissipation introduced by the dynamically deformed Nitrile O-rings, which cannot be explained in the frame of Model-I.

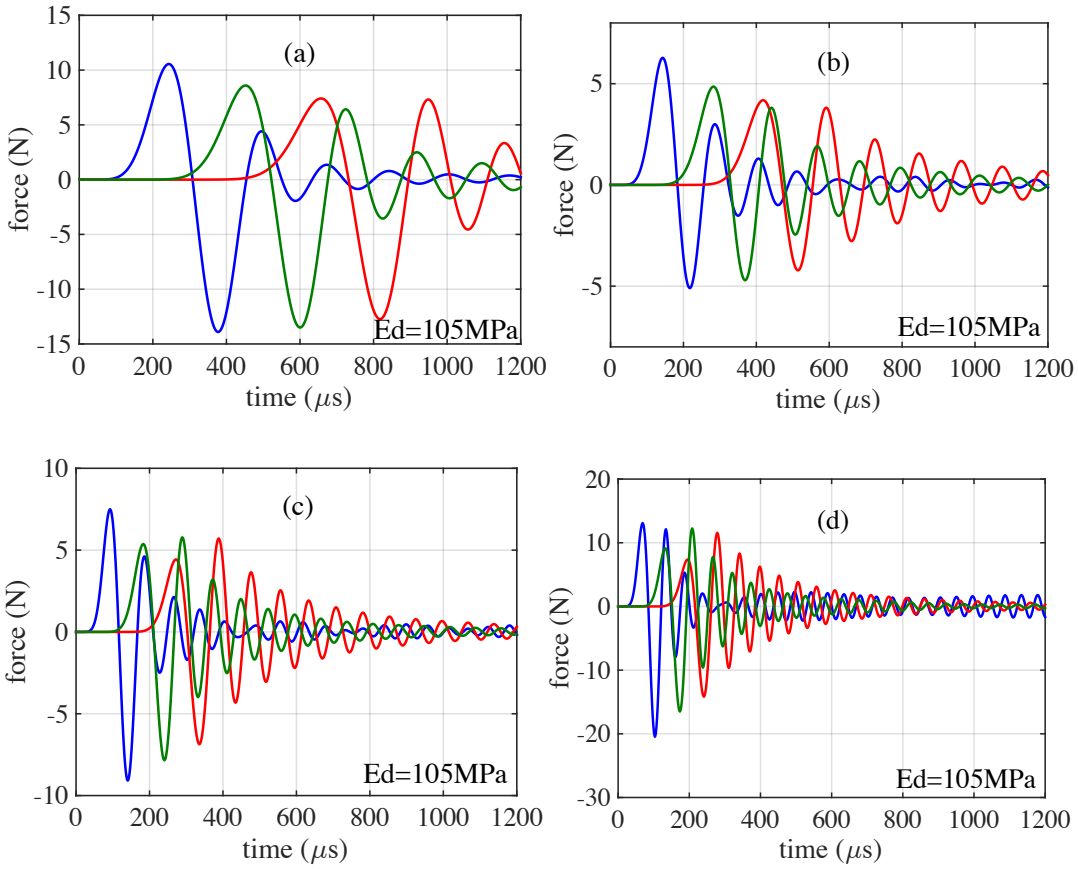

Figure A.3: Stress pulses obtained in numerical calculations using Mode-I (without dissipation term between all elements in the system, and using effective elastic modulus E_{eff} = 105 MPa) in a double power-law system under various preload conditions: (a) F_0= 10 N, (b) 50 N, (c) 106 N, (d) 193 N. Curves represent the average dynamic force in the fifth (leading curve), ninth (middle curve), and thirteenth (bottom curve) steel partial.

In numerical calculations without dissipation (Figs. A.2 and A.3) we observed that an effective speed of negative pulse is lower than speed of positive pulse. This

tendency was also observed in experiments and it can be explained by more dispersive behavior of weakly nonlinear negative pulses causing change of their shape and as result their effective velocity in comparison with positive pulses.

Table A.1: Non-dissipative numerical calculation results (Model-I, E_d=7.6MPa) for speeds ($V+$) and width [$L_{+,num}/(a-x_0)$] of positive pulses under different static precompression forces.

	Model-I (without dissipation, E_{eff} = 7.6 MPa)			
F_0 (N)	10	50	106	193
$V+$ (m/s)	33	49	70	91
$L_{num,+}/(a-x_0)$	4.5	4.4	4.1	3.7
A_9/A_5	0.90	0.90	0.87	0.82
A_{13}/A_5	0.83	0.83	0.80	0.70

Table A.2: Non-dissipative numerical calculation results (Model-I, E_d=105MPa) for speeds ($V+$) and width [$L_{+,num}/(a-x_0)$] of positive pulses under different static precompression forces.

	Model-I (without dissipation, E_{eff} = 105 MPa)			
F_0 (N)	10	50	106	193
$V+$ (m/s)	126	182	272	386
$L_{num,+}/(a-x_0)$	4.1	3.8	3.5	3.5
A_9/A_5	0.81	0.77	0.71	0.69
A_{13}/A_5	0.70	0.67	0.59	0.56

Based on the large difference between the numerical calculations and experimental data, we can conclude that the dissipation term must be added to the numerical model to correctly simulate this strongly nonlinear dissipative system.

2. Linear Dissipative Model

The comparison with experimental results make it clear that the non-dissipative model significantly overestimates the amplitude of the signals, underestimate their attenuation, their speed. It also results in the oscillatory profiles of the pulses unlike in the experiments at lower precompression. The natural approach to provide the better description of experimental results would be the introduction of classical dissipation using a liner dashpot model between elements in the system (between the striker, precompression mass and the top cylinder as well as between cylinders in the metamaterial).

The simplest way to include dissipation is an introduction of a linear viscous model (referred as Model-II), where the dissipation term linearly depends on the strain rate. Follow the configuration of the Kelvin-Voigt model. Then the system of linearized equations (valid for small dynamic strains in comparison with a strains caused by a static precompression) using a double power law potential plus a linear viscous dissipation term becomes:

$$\ddot{x}_i = \frac{K_1}{m}(x_{d,i-1} - 2x_{d,i-1} + x_{d,i+1}) + \frac{\mu}{m}(\dot{x}_{i-1} - 2\dot{x}_{i-1} + \dot{x}_{i+1}), \qquad \text{(A.1)}$$

where $$K_1 = 1.5(1.25\pi D_{\mathrm{m}}\, E_d d^{-1/2})x_0^{1/2} + 6(50\pi D_{\mathrm{m}} E_d d^{-5})x_0^5. \qquad \text{(A.2)}$$

The quantity of μ is the viscosity coefficient used in a dashpot model. It has no explicit dependence on the precompression and its value is selected to fit experimental data (though it can have different values for different precompression). It is related to the damping properties of O-rings in the condition of contact deformation with high strain rate and gradient of strains in the contact area. In this Model-I attempt to separate

the elastic and viscous contributions to the forces acting between metal cylinders due to the dynamic deformation of O-rings. The elastic modulus E_d is introduced to account for a possible difference in the elastic properties of O-rings in addition to their viscous behavior under the dynamic deformation.

The first order differential equations of motion of N cylinders inside a periodic chain and the boundary conditions are presented below:

$$\dot{x}_i(\bar{x}) = \begin{cases} x_{N+i}, & i = 1, \dots, N-1; \\ \varphi_i(\bar{x}) - \psi_i(\bar{x}) + g, & i = N+1, \dots, 2N-1; \end{cases}$$

and $\bar{x} = (x_1, \dots, x_N, x_{N+1}, \dots, x_{2N})$; (A.3)

$$\varphi_i(\bar{x}) = \begin{cases} 0, & i = N+1, N+2; \\ \frac{C}{m}(\delta_{i-2-N,i-N}^{\frac{3}{2}} + \mu_C \delta_{i-2,i}) H(\delta_{i-2-N,i-N}) + \frac{D}{m}(\delta_{i-1-N,i-N}^{\frac{3}{2}} + \mu_D \delta_{i-1,i}) H(\delta_{i-1-N,i-N}), & i = N+3; \\ [A_0(x_{0,i-1-N})^{\frac{3}{2}} + B_0(x_{0,i-1-N})^6 + \frac{K_{i-1-N}}{m}(\delta_{i-1-N,i-N} - x_{0,i-1-N}) & \\ \quad + \frac{\mu}{m}\delta_{i-1,i}] H(\delta_{i-1-N,i-N}), & i = N+4, \dots, 2N-1; \end{cases}$$

(A.4a)

$$\psi_i(\bar{x}) = \begin{cases} \frac{C}{M}(\delta_{i-N,i+2-N}^{\frac{3}{2}} + \mu_C \delta_{i,i+2}) H(\delta_{i-N,i+2-N}), & i = N+1; \\ \frac{D}{m_{imp}}(\delta_{i-N,i+1-N}^{\frac{3}{2}} + \mu_D \delta_{i,i+1}) H(\delta_{i-N,i+1-N}), & i = N+2; \\ [A_0(x_{0,i-N})^{\frac{3}{2}} + B_0(x_{0,i-N})^6 + \frac{K_{i-N}}{m}(\delta_{i-N,i+1-N} - x_{0,i-N}) + \frac{\mu}{m}(\delta_{i,i+1})] H(\delta_{i-N,i+1-N}), & \\ \qquad i = N+3, \dots, 2N-1. & \end{cases}$$

(A.4b)

where $g = 9.81$ m/s^2 is the gravitational acceleration;

$$\delta_{1,3} = x_1 - x_3, \quad \text{(A.5a)}$$

$\delta_{i-1-N,i-N} = x_{i-1-N} - x_{i-N}$, for i=N+3,…,2N. (A.5b)

And $K_{i-1-N} = 1.5(1.25\pi D_m\, E_d d^{-\frac{1}{2}})x_{0,i-1-N}^{\frac{1}{2}} + 6(50\pi D_m E_d d^{-5})x_{0,i-1-N}^{5}$,

$i = N+4, \dots, 2N.$ (A.6)

The boundary conditions is:

$\dot{x}_i(\bar{x}) = 0,\ i = N, 2N.$ (A.7)

And the initial conditions corresponding to gravitationally loaded chain:

$$\begin{cases} x_N(t=0) = 0; \\ x_{N-i}(t=0) = x_{N-i+1}(t=0) + x_{0,N-i}\,, i = 1, \dots, N-3; \\ x_2(t=0) = x_3(t=0); \\ x_1(t=0) = x_3(t=0) + x_{0,1}; \end{cases} \quad \text{(A.8a)}$$

$$\begin{cases} x_{N+1}(t=0) = 0; \\ x_{N+2}(t=0) = 2.24\ m/s; \\ x_{N+i}(t=0) = 0,\ 3 \le i \le N. \end{cases} \quad \text{(A.8b)}$$

Here μ_C and μ_D are the viscosity coefficients between the precompression mass and top cylinder, and between the striker and the top cylinder.

The large discrepancy between experimental data and numerical calculations based on the Model-I in signal amplitude, demonstrates not only the need of introduction of dissipative property of O-ring in this model, but also the potential importance of the dissipative properties of the contacts between striker and the top cylinder, as well as between precompression mass and the top cylinder.

The viscosity coefficient between the precompression mass and top cylinder (μ_C), and the striker and top cylinder (μ_D) are selected to set the recoil velocity of striker in numerical calculation the same as measured in experiments by using high-speed camera (1.39 ± 0.01 m/s).

Table A.3 presents the influence of the value of μ_C and μ_D on the recoil velocity of striker. Obviously, the recoil velocity of striker and the impact duration were mainly affected by μ_D the viscosity between the striker and the top cylinder. The theoretical duration of impact is calculated using the following equations:

$$t = 2.94(\frac{5}{4nn_1})^{2/5} v^{-1/5} , \quad (A.9)$$

in which $n = \sqrt{\frac{16}{9\pi^2}\frac{R_1R_2}{(k_1+k_2)^2(R_1+R_2)}}$, $n_1 = \frac{m_1+m_2}{m_1m_2}$, $k_1 = \frac{1-\nu_1^2}{\pi E_1}$ and $k_2 = \frac{1-\nu_2^2}{\pi E_2}$, where R_1, m_1, ν_1 and E_1 represent the radius, mass, poison ratio and elastic modulus of the striker. Similarly, R_2, m_2, ν_2 and E_2 represent the radius, mass, poison ratio and elastic modulus of the the top particle of the chain. And v is the impact velocity of the striker, in experiments is was measured to be 2.24 m/s by using high-speed camera. These parameters used in numerical calculations to represent the materials properties are listed in Table A.4.

Table A.3: The influence of μ_C (the viscosity coefficient between the precompression mass and top cylinder) and μ_D (the viscosity coefficient between the striker and top cylinder) on the recoil velocity V_{recoil} of striker and the impact duration T_{imp} in the numerical calculation using Model-II. All the data were calculated with the precompression force F_0 = 193 N, and the viscosity coefficient of O-ring μ is selected to be 70 Ns/m.

μ_D = 10 Ns/m					
μ_C (Ns/m)	2	6	10	14	18
V_{recoil} (m/s)	1.387	1.388	1.389	1.39	1.392
T_{imp} (μs)	12.6	12.6	12.6	12.6	12.6
μ_C = 14 Ns/m					
μ_D (Ns/m)	2	6	10	14	18
V_{imp} (m/s)	1.638	1.494	1.389	1.283	1.184
T_{imp} (μs)	13.07	12.6	12.6	12.6	12.13

Table A.4: Parameters used in numerical calculations to represent the properties of the materials composing the strongly nonlinear media tested experimentally.

	Radius (mm)	Mass (g)	Poison ratio	Elastic modulus (GPa)
Striker	2.38	0.455	0.29	200
Top cylinder	$+\infty$	$+\infty$	0.29	200

It is interesting to know whether the viscosity coefficient μ of the O-ring will affect the impact duration and the recoil velocity of striker. From Table A.5, we can see that μ has no influence on the impact time and the recoil velocity of striker in numerical calculation in the frame of Model-II. The calculated impact duration in numerical calculation was in good agreement with the experimental measurement using high-speed camera.

Table A.5: The influence of μ (the viscosity coefficient between system particles due to O-ring) on the recoil velocity V_{recoil} of striker and the impact time T_{imp} in numerical calculation using Model-II. All the data were calculated with the precompression force F_0 = 193 N, and the viscosity coefficient between the precompression mass and top cylinder, and between the striker and top cylinder were selected to be μ_C = 14 Ns/m and μ_D = 10 Ns/m.

μ_C = 14 Ns/m, μ_D = 10 Ns/m					
μ (Ns/m)	10	20	30	40	50
V_{recoil} (m/s)	1.39	1.39	1.39	1.39	1.39
T_{imp} (μs)	12.6	12.6	12.6	12.6	12.6

The values of μ_C = 14 Ns/m and μ_D = 10 Ns/m are selected to describe the following parameters related to the impact: (1) the recoil velocity of striker measured by high-speed camera in experiments (1.39 ± 0.01 m/s) and thus a value of linear momentum transferred into the system, and (2) the impact duration being less than 18 μs in experiments and close to the 12.6 microseconds for interaction of striker with mass

0.455 g and tip radius 2.38 mm and the flat surface of the top cylinder estimated based on the Hertzian interaction law between them.

Figure A.4 shows the numerical calculation results in the frame of Model-II corresponding to two fitting constants describing viscoelastic response of O-rings in the metamaterial (E_d = 105 MPa and μ = 70 Ns/m). These constants in the frame of the Model-II provide the satisfactory results with respect to predicting the following major parameters of the system dynamic response: the pulse speed, leading pulse amplitude, its duration and attenuation. It will be seen that predictions of dynamic response based on Model-II still significantly different from experiments.

Table A.6 represents a summary of the characteristic of the positive phase of the stress pulse obtained in numerical calculation in the frame of Model-II with E_d = 105 MPa and μ = 70 Ns/m. Similarly, and Table A.7 records the negative phase of the calculated stress wave in numerical calculation.

Based on the presented results of numerical calculations it is clear that the model better predicts the values of signal speed than the Model-I at higher precompression. This is also the reason to select E_d = 105 MPa, and the signal speed in numerical calculation of Model-II was mainly effected by the selected value of E_d. But it is obvious that even optimized coefficients (E_d = 105 MPa and μ = 70 Ns/m) in the Model-II do not result in a reasonable explanation of experimental data in the pulse amplitude attenuation. The following features should be specifically mentioned:

1. The amplitude of signal in the fifth particles in the numerical calculation using model II was too high compared with the experimental data.
2. The attenuation of signal amplitude was slower than the experimental results at

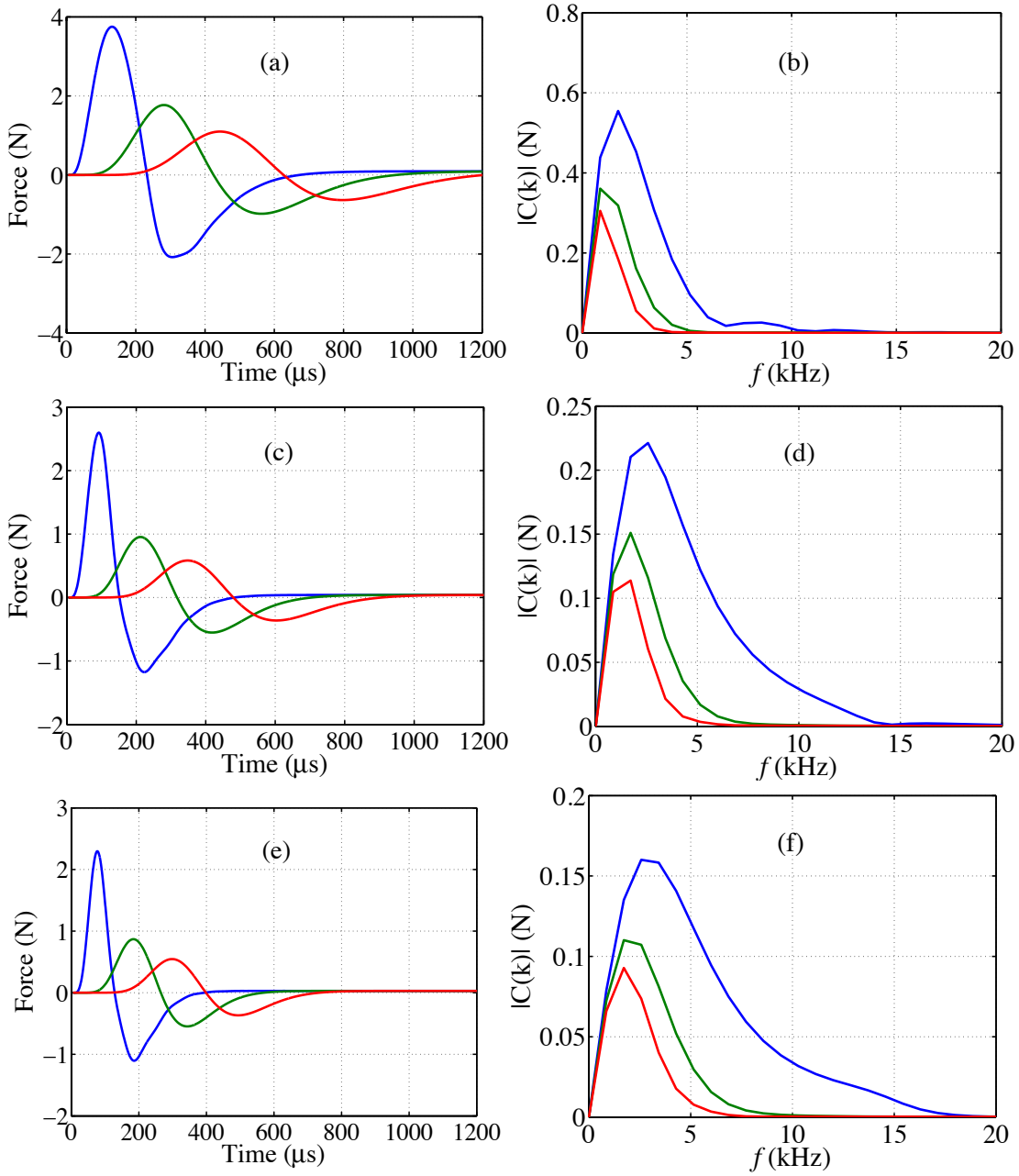

Figure A.4: Stress pulses obtained in numerical calculations using Mode-II (with linear dissipation term, and using dynamic elastic modulus E_d = 105 MPa and μ = 70 Ns/m) and their corresponding Fourier spectra in a double power-law system under various preload conditions: (a) F_0= 10 N, (c) 30 N, (e) 50 N, (g) 74 N, (i) 106 N, and (k) 193 N. Curves represent the average dynamic force in the fifth (leading curve), ninth (middle curve), and thirteenth (bottom curve) steel partial.

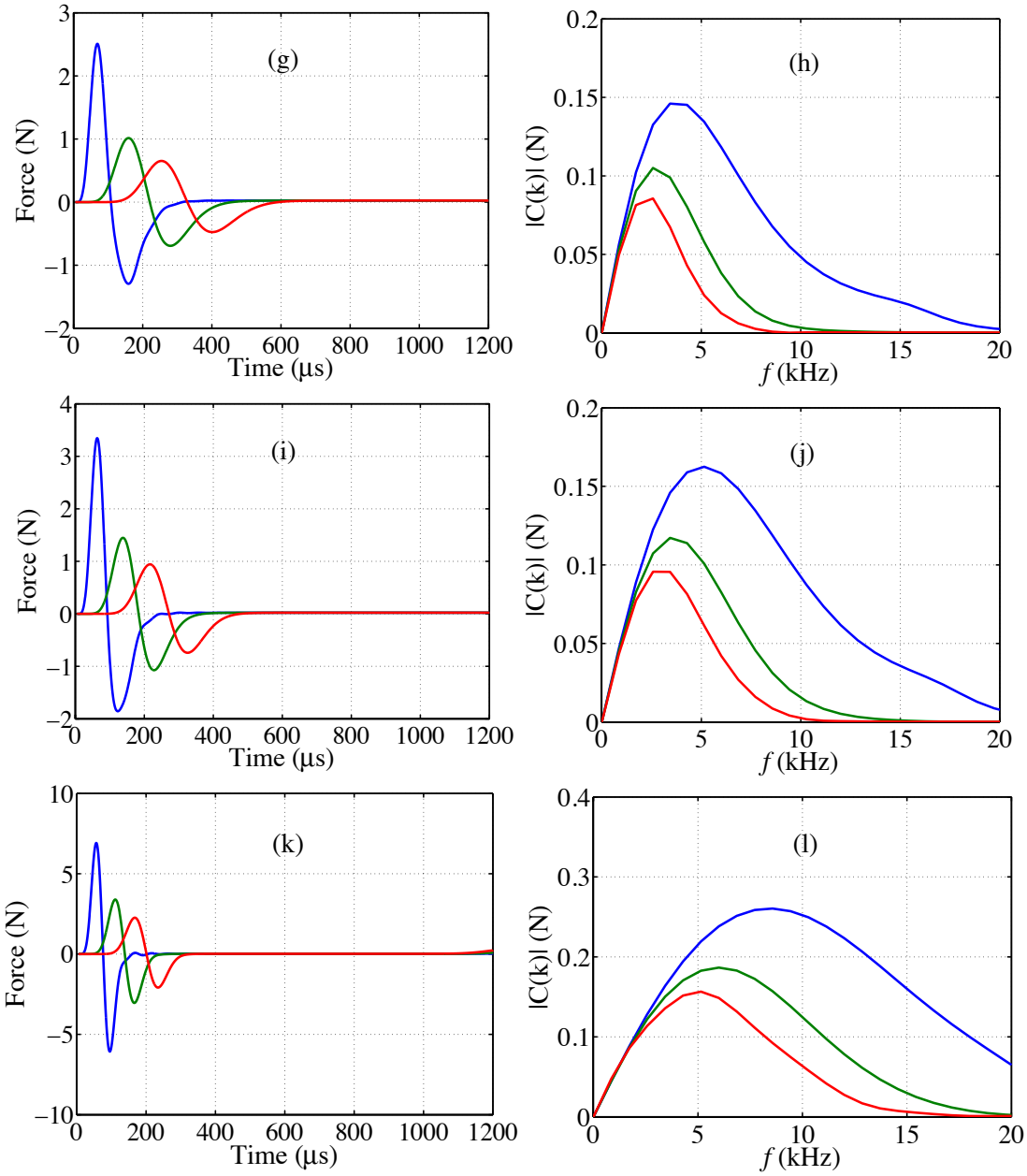

Figure A.4: Stress pulses obtained in numerical calculations using Mode-II (with linear dissipation term, and using dynamic elastic modulus E_d = 105 MPa and μ = 70 Ns/m) and their corresponding Fourier spectra in a double power-law system under various preload conditions, continued.

Table A.6: Linear dissipative numerical calculation results (Model-II) for the speeds ($V+$) and width [$L_{num,+}/(a-x_0)$] of positive pulses under different static precompression forces.

	Model-II (E_d = 105 MPa, μ = 70 Ns/m)					
F_0 (N)	10	30	50	74	106	193
$V+$ (m/s)	172	216	237	275	348	443
$L_{num,+}/(a-x_0)$	5.6	4.6	4.1	4.0	4.2	4.3
A_9/A_5	0.48	0.37	0.38	0.41	0.43	0.49
A_{13}/A_5	0.29	0.22	0.24	0.26	0.28	0.33

Table A.7: Linear dissipative numerical calculation results (Model-II) for the speeds ($V-$) and width [$L_{num,-}/(a-x_0)$] of negative pulses under different static precompression forces.

	Model-II (linear dissipation, E_d = 105 MPa, μ = 70 Ns/m)					
F_0 (N)	10	30	50	74	106	193
$V-$ (m/s)	105	132	159	207	233	337
$L_{num,-}/(a-x_0)$	7.0	6.4	6.6	6.7	5.7	5.0
A_9/A_5	0.48	0.47	0.50	0.54	0.58	0.50
A_{13}/A_5	0.31	0.31	0.33	0.37	0.40	0.34

higher precompression force (> 74N), and had almost no dependence on the system precompression, which was opposite to the phenomenon observed in the experiments.

3. The added dissipation term with the selected value of μ necessary to provide a correct pulse speed and relative attenuation completely eliminate the oscillating part of the signals at higher precompression force. There were no oscillating tails in Figs. A.4(g), A.4(i) and A.4(k), but we observed oscillating pulses in

experiments, especially at larger precompression indicating underdamped behavior of the system at these conditions.

Based on these observations, one would intuitively think that the selected fitting parameter μ is too small because it results in a less attenuation of signal amplitude at higher precompression than in the experiments and also in higher value of the leading pulse amplitude. This was carefully verified in the numerical calculations using multiple values of μ, keeping the same values of μ_C = 14 Ns/m and μ_D = 10 Ns/m to keep correct recoil velocity and the impact duration. But a broad variations of the coefficient μ, did not eliminate the significant discrepancy in the values of leading pulse amplitude and the attenuation of signal amplitude between numerical calculations and the experimental data. No single coefficient μ can provide reasonable agreement of the results of this linear dissipation Model-II with experimental data. Therefore, pure linear dissipation model cannot accurately model the strongly nonlinear dissipative system composed of alternating steel cylinders and rubber O-rings, and a nonlinear dissipative model with a nonlinear dependence on precompression force should be considered.

3. Nonlinear Dissipative Model Based on Brilliantov *et al.* Approach

Experimental data demonstrate increasing attenuation of leading pulse amplitude in the fifth particle – decay of amplitude is increasing with the increasing precompression force (see section 3.3). It is clear that to describe this phenomenon the viscous term must have a dependence on strain/precompression force.

A possible approach to the nonlinear viscoelastic deformation of the Hertzian

contact between spherical particles was proposed by Brilliantov *et al.*. I modified this approach by introducing the similar equation for the dissipative force (F_{dis}) related to the dynamic deformation of O-rings [14], then the total force due to the elastic and viscoelastic deformation of O-rings at the contact with a separated elastic (static and dynamic contributions) and viscous term is:

$$F = F_{el} + F_{dis} = \left(A_0 m {x_0}^{3/2} + B_0 m {x_0}^{6} + K_1 x_d\right) + \alpha \dot{x} \frac{\partial}{\partial x}\left(A_0 m {x_0}^{3/2} + B_0 m {x_0}^{6} + K_1 x_d\right), \quad \text{(A.10)}$$

where $K_1 = 1.5(1.25\pi D_{\text{m}}\, E_{\text{d}} d^{-1/2}) x_0^{1/2} + 6(50\pi D_{\text{m}} E_{\text{d}} d^{-5}) x_0^5$, and α is the viscosity coefficient. The elastic force F_{el} is taken from Eq. (1.1) with elastic modulus E_{d}, replacing constant E_0, to consider a possible difference in the elastic properties of O-rings in addition to their viscous behavior under the dynamic deformation.

If the linear elastic term is significantly larger than the viscous term then the pulse speed will be mostly determined by coefficient K_1 and adding a relatively small viscous term only causes dissiption. If the viscous term is comparable or larger than the linear elastic term, then the speed of attenuating signal may be significantly different than in previous case. The effective elastic modulus which combined both effects was introduced to explain speed of the small amplitude signals, the seperation of these terms will result in smaller elastic modulus K_1 than K in (chapter 3).

The first order differential equations of motion of N cylinders inside a periodic chain in the frame of the above nonlinear dissipative model (referred as Model-III) and the boundary conditions are presented in chapter 3 section 3.4.3.

For the verification of the proper initial condition used in this numerical

calculation in the frame of Model-III, the impact duration and recoil velocity of the striker with the applying of varying values of $\alpha$are calculated. The results are presented in Table A.8

Table A.8: The influence of α(the viscosity coefficient between neighboring particles in the system coming from O-rings in Model-III) on the recoil velocity V_{recoil} of the striker and the duration of the impact T_{imp} in numerical calculation using Model-III. All the data were calculated with the precompression force F_0 = 193 N, and the viscosity coefficient between the precompressing mass and the top cylinder, and between the striker and the top cylinder were selected to be μ_C = 38 μs and μ_D = 1.1 μs

Model-III (μ_C = 38 μs, μ_D = 1.1 μs)					
α(μs)	10	20	30	40	50
V_{recoil} (m/s)	1.379	1.381	1.385	1.39	1.392
T_{imp} (μs)	13.07	13.07	13.07	13.07	13.07

It is apparent that the increasing value of α only slightly increases the recoil velocity of striker, but has no influence on the duration of the impact.

Numerical calculations for the strongly nonlinear viscoelastic Model-III were conducted at the following parameters E_d = 87 MPa and α=30 μs allowing satisfactory comparison with experimental data and results are presented in chapter 3 section 3.4.3 (Tables 3.6 and 3.7, and Fig. 3.7). The reason why E_d for viscous dissipative Model-III is smaller than the effective modulus E_{eff} for purely elastic Model-I is that the viscosity term effectively contributed to the increasing rigidity of this metamaterial described by the coefficient K_1. Compared to Model-II, the dissipation term in Model-III was similar to the Model-II at low precompression forces, but significantly larger at higher precompression force. For example, at F_0 = 193 N, the net viscosity coefficient $\alpha K_1 \approx$ 312 Ns/m in Model-III was 4.4 times larger than μ = 70 Ns/m in Model-II. This resulted

in stronger attenuation of signal amplitude at higher precompression in the Model-III in comparison with the Model-II. The net coefficients in dissipation term of Model-III are shown in Table. A.9.

Table A.9: The coefficients in dissipation term of Model-III

	Model-III (E_d = 87 MPa, α = 30 μs)					
F_0 (N)	10	30	50	74	106	193
αK_1 (Ns/m)	30.07	47.03	69.27	105.48	160.28	316.99

From the comparison of numerical results obtained using the presented three models (Model-I, Model-II and Model-III) and experimental results, we can see that Model-III fits experimental data on the pulse speed, pulse width, its amplitude and the increasing attenuation with increasing precompression. The nonlinear dissipation term is essential to simulate the strong attenuation. The viscosity with nonlinear dependence on initial precompression introduced by Model-III was able to correctly explain a tendency toward higher attenuation nonlinearly dependent on the precompression force being consistent with the experimental results. Such behavior is a consequence of the dependence of effective viscosity on the precompression.

To the contrary to what is observed in experiments, the attenuation of negative pulse is slightly lower than the attenuation of positive part in both numerical models. At higher precompression force, the strongly nonlinear dissipative Model-III predicted "over damped" behavior of the pulse (similar to Model-II) completely eliminating the oscillating tail. Despite these differences, the qualitative behavior of the results of the numerical calculations based on the Model-III matches well with the experimental data.

4. Nonlinear Dissipative Models Based on Brilliantov Approach with Power-Law Strain Rate Dependence

The power-law strain rate dependence of the nonlinear dissipation term is also investigated. The Brilliantov approach is used to get strongly nonlinear dependence on the system precompression force. This approach was intended to solve a puzzle represented by the increased attenuation of stress pulse amplitude at larger precompression while the system is transformed to the underdamped behavior with increased precompression, which is evident by the oscillation tail in Fig. 3.2. This model is referred as Model-IV. The total force due to the elastic and viscoelastic deformation of O-rings at the contact is:

$$F = F_{el} + F_{dis} = A_0 m {x_0}^{3/2} + B_0 m {x_0}^{6} + K_1 x_d + \alpha K_1 \dot{x}^n. \qquad \text{(A.11)}$$

The first order differential equations of Model-IV with power-law strain rate dependence for particles of the system is similar to equations listed in chapter 3 section 3.4.1 [Eq. (3.9)—Eq. (3.16)], but with some adjustments. The expression of $\varphi_i(\bar{x})$ and $\psi_i(\bar{x})$ were adjusted using the equations presented below:

$$\varphi_i(\bar{x}) = \begin{cases} 0, \quad i = N+1, N+2\ ; \\ \frac{C}{m}(\delta^{\frac{3}{2}}_{i-2-N,i-N} + \frac{3}{2}\delta^{\frac{1}{2}}_{i-2-N,i-N}\mu_C\delta_{i-2,i})H\left(\delta_{i-2-N,i-N}\right) \\ +\frac{D}{m}(\delta^{\frac{3}{2}}_{i-1-N,i-N} + \frac{3}{2}\delta^{\frac{1}{2}}_{i-1-N,i-N}\mu_{D\delta_{i-1,i}})H\left(\delta_{i-1-N,i-N}\right), \quad i = N+3; \\ [A_0\left(x_{0,i-1-N}\right)^{\frac{3}{2}} + B_0\left(x_{0,i-1-N}\right)^{6} + \frac{K_{i-1-N}}{m}\left(\delta_{i-1-N,i-N} - x_{0,i-1-N}\right) \\ \quad +\frac{\alpha}{m}\delta^{n}_{i-1,i}]H\left(\delta_{i-1-N,i-N}\right), i = N+4, \ldots, 2N-1; \end{cases}$$

(A.12)

$$\psi_i(\bar{x}) = \begin{cases} \frac{C}{M}(\delta^{\frac{3}{2}}_{i-N,i+2-N} + \frac{3}{2}\delta^{\frac{1}{2}}_{i-N,i+2-N}\mu_C\delta_{i,i+2})H\left(\delta_{i-N,i+2-N}\right), & i = N+1; \\ \frac{D}{m_{\text{imp}}}(\delta^{\frac{3}{2}}_{i-N,i+1-N} + \frac{3}{2}\delta^{\frac{1}{2}}_{i-N,i+1-N}\mu_D\delta_{i,i+1})H\left(\delta_{i-N,i+1-N}\right), & i = N+2; \\ [A_0\left(x_{0,i-N}\right)^{\frac{3}{2}} + B_0\left(x_{0,i-N}\right)^6 + \frac{K_{i-N}}{m'}\left(\delta_{i-N,i+1-N} - x_{0,i-N}\right) \\ \quad + \frac{\alpha}{m}\delta^n_{i,i+1}]H\left(\delta_{i-N,i+1-N}\right), i = N+3, \ldots, 2N-1; \end{cases} \tag{A.13}$$

The calculation results for Model-IV with varying value of exponent *n* with precompression force 193 N are presented in Fig. A.5. All the other parameters are set as the same as Model-III, i.e. E_d = 87 MPa, α = 30 μs, μ_C = 38 μs, and μ_D = 1.1 μs.

Apparently, this model cannot correctly predicate the behavior of strongly nonlinear dissipative system because of the lower rate of attenuation [when n>1.0, Figs. A.5(d), A.5(e), and A.5(f)] and the significant larger amplitude and pulse speed [when n<1.0, Figs. A.5(a) and A.5(b)] compared with the experimental data.

From the presented analysis of above four models, we found that none of them can completely describe experimental results. The phenomenon of strong oscillations of signals under higher precompression force significantly deviate from the predictions based on the above four models. However, Model-III successfully predicted the following features of the strongly nonlinear dissipative metamaterial:

1. Provide correct relative values of amplitudes of the leading positive pulse.
2. Fit the values of the pulse speed.
3. Fit the increasing positive pulse width.
4. Qualitatively explain the increases of attenuation of leading pulse amplitude with precompression;

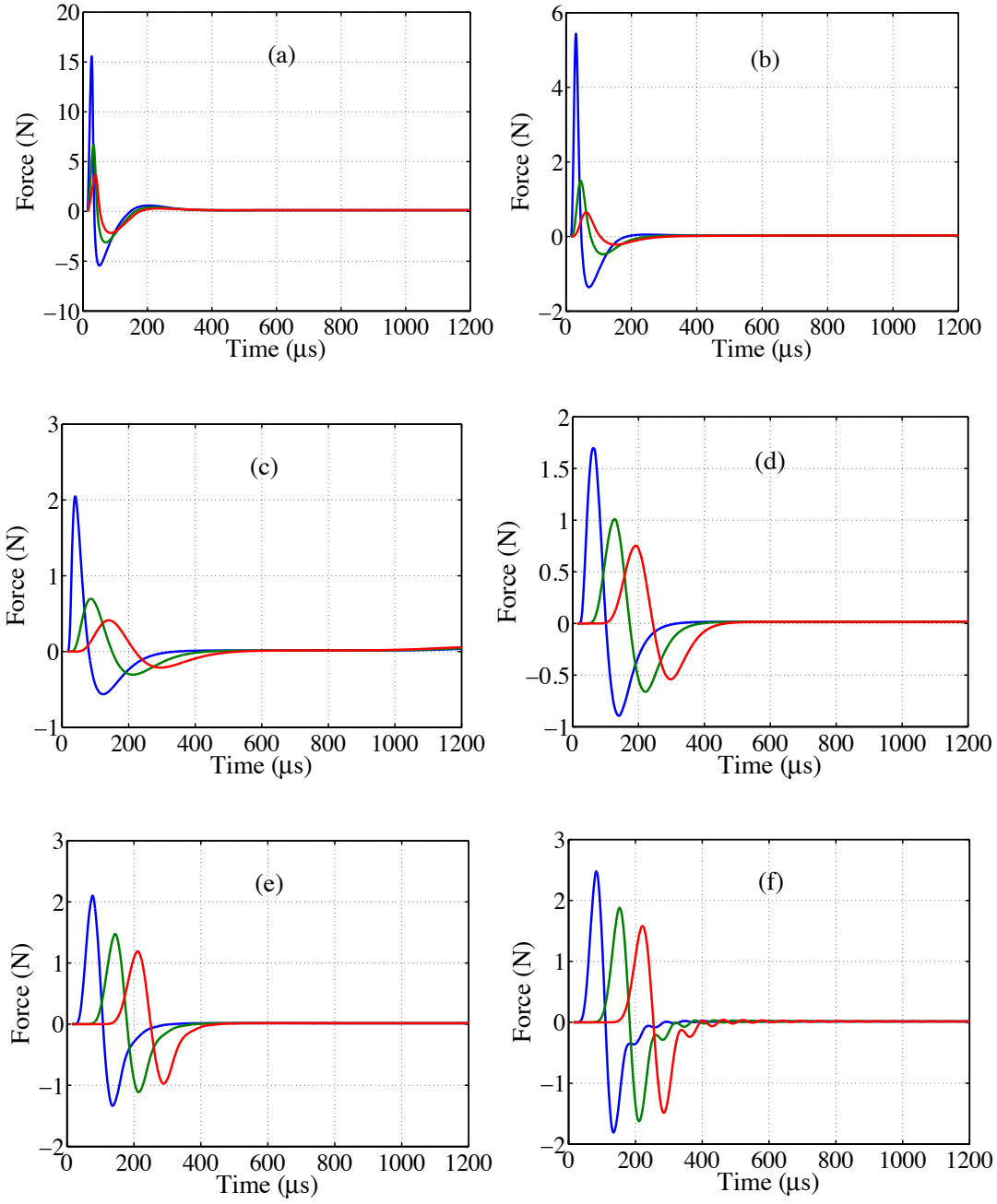

Figure A.5. Stress pulses obtained in numerical calculations using Model-IV (with dissipation term nonlinear depended on strain-rate, and using dynamic elastic modulus E_d = 87 MPa and α = 30 μs) with power-law strain-rate dependence. In (a) n = 0.6, (b) n = 0.8, (c) n = 1.0, (d) n =1.2, (e) n = 1.4 and (f) n=1.6. Curves represent the average dynamic force in the fifth (leading curve), ninth (middle curve), and thirteenth (bottom curve) steel partial. The precompression force is 193 N